Tomecki R, Drazkowska K, Kobylecki K, Tudek A. SKI complex: A multifaceted cytoplasmic RNA exosome cofactor in mRNA metabolism with links to disease, developmental processes, and antiviral responses. Wiley Interdiscip Rev RNA. 2023 Nov-Dec;14(6):e1795. doi: 10.1002/wrna.1795. Epub 2023 Jun 29. PMID: 37384835.

WILEY

SKI complex: a multifaceted cytoplasmic RNA exosome cofactor in mRNA metabolism with links to disease, developmental processes, and antiviral responses

Journal:	*WIREs RNA*
Manuscript ID	RNA-1135.R1
Wiley - Manuscript type:	Advanced Review
Date Submitted by the Author:	26-Apr-2023
Complete List of Authors:	Tomecki, Rafal ; Institute of Biochemistry and Biophysics Polish Academy of Sciences, Laboratory of RNA Processing and Decay; Warsaw University Faculty of Biology, Institute of Genetics and Biotechnology Drazkowska, Karolina; Warsaw University Faculty of Biology, Institute of Microbiology, Department of Environmental Microbiology and Biotechnology, Laboratory of Epitranscriptomics Kobylecki, Kamil; Institute of Biochemistry and Biophysics Polish Academy of Sciences Tudek, Agnieszka; Institute of Biochemistry and Biophysics Polish Academy of Sciences, Laboratory of RNA Processing and Decay
Keywords:	mRNA decay and surveillance, exosome, ribosome, SKI complex (SKIc), trichohepatoenteric syndrome (THES)
Choose 1-3 topics to categorize your article:	Turnover/Surveillance Mechanisms (RHAB) < RNA Turnover and Surveillance (RHAA), Regulation of RNA Stability (RHAC) < RNA Turnover and Surveillance (RHAA), RNA–Protein Complexes (RDAD) < RNA Interactions with Proteins and Other Molecules (RDAA)

WIREs
Wiley Interdisciplinary Reviews

Article Title: SKI complex: a multifaceted cytoplasmic RNA exosome cofactor in mRNA metabolism with links to disease, developmental processes, and antiviral responses

Article Category:

- ○ PERSPECTIVE
- ○ PRIMER
- ○ OVERVIEW
- ◉ ADVANCED REVIEW
- ○ FOCUS ARTICLE
- ○ SOFTWARE FOCUS

Authors:

Rafal Tomecki[1,2]*

[1]Laboratory of RNA Processing and Decay, Institute of Biochemistry and Biophysics, Polish Academy of Sciences, Warsaw, Poland
[2]Institute of Genetics and Biotechnology, Faculty of Biology, University of Warsaw, Warsaw, Poland

ORCID iD: 0000-0003-2473-5004

***Correspondence**
Rafal Tomecki, Laboratory of RNA Processing and Decay, Institute of Biochemistry and Biophysics Polish Academy of Sciences, Pawinskiego 5A, Warsaw, 02-106, Poland.
Email: rtomecki@ibb.waw.pl

Karolina Drazkowska[3]

[3]Laboratory of Epitranscriptomics, Department of Environmental Microbiology and

Biotechnology, Institute of Microbiology, Faculty of Biology, Biological and Chemical Research Centre, University of Warsaw, Warsaw, Poland

ORCID iD: 0000-0003-2673-7126

Kamil Kobylecki[1]

[1]Laboratory of RNA Processing and Decay, Institute of Biochemistry and Biophysics, Polish Academy of Sciences, Warsaw, Poland

ORCID iD: 0000-0003-3019-0274

Agnieszka Tudek[1]

[1]Laboratory of RNA Processing and Decay, Institute of Biochemistry and Biophysics, Polish Academy of Sciences, Warsaw, Poland

ORCID iD: 0000-0002-6085-1072

Karolina Drazkowska and Kamil Kobylecki contributed equally to this work.

Conflict of Interest

The Authors declare no conflicts of interest for this article.

Abstract

RNA stability and quality control are integral parts of gene expression regulation. A key factor shaping eukaryotic transcriptomes, mainly via 3'-5' exoribonucleolytic trimming or degradation of diverse transcripts in nuclear and cytoplasmic compartments, is the RNA exosome. Precise exosome targeting to various RNA molecules requires strict collaboration with specialized auxiliary factors, which facilitate interactions with its substrates. The predominant class of cytoplasmic RNA targeted by the exosome are protein-coding transcripts, which are carefully scrutinized for errors during translation. Normal, functional mRNAs are turned over following protein synthesis by the exosome or by Xrn1 5'-3'-exonuclease, acting in concert with Dcp1/2 decapping complex. In turn, aberrant transcripts are eliminated by dedicated surveillance pathways, triggered whenever ribosome translocation is impaired. Cytoplasmic 3'-5' mRNA decay and surveillance are dependent on the tight cooperation between the exosome and its evolutionary conserved co-factor – the SKI complex (SKIc). Here, we summarize recent findings from structural, biochemical, and functional studies of SKIc roles in controlling cytoplasmic RNA metabolism, including links to various cellular processes. Mechanism

of SKIc action is illuminated by presentation of its spatial structure and details of its interactions with exosome and ribosome. Furthermore, contribution of SKIc and exosome to various mRNA decay pathways, usually converging on recycling of ribosomal subunits, is delineated. A crucial physiological role of SKIc is emphasized by describing association between its dysfunction and devastating human disease – a trichohepatoenteric syndrome (THES). Eventually, we discuss SKIc functions in the regulation of antiviral defense systems, cell signaling and developmental transitions, emerging from interdisciplinary investigations.

KEYWORDS

mRNA decay and surveillance, exosome, ribosome, SKI complex (SKIc), trichohepatoenteric syndrome (THES)

Graphical/Visual Abstract and Caption

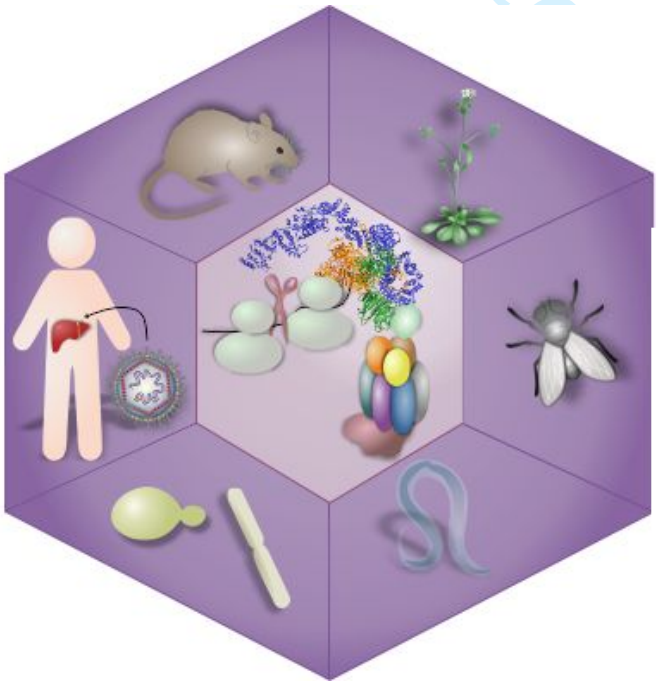

Structurally characterized SKI complex collaborates with the exosome and ribosome in translation-dependent mRNA decay and surveillance and plays versatile roles in disease, signaling pathways, antiviral responses, and developmental regulation across eukaryotic species.

1. INTRODUCTION

RNA degradation plays a pivotal role in the regulation of gene expression in Eukaryotes, not only through degradation of coding transcripts that are no longer needed, but also by removing aberrant

RNAs of all biotypes, which could be toxic and thus interfere with normal cellular metabolism. The key players controlling RNA degradation in both the nucleus and the cytoplasm are ribonucleases. Efficient transcript removal by these decay executors is strictly regulated by their co-factors. Evolutionary conserved SKI complex (SKIc) is such an accessory factor, which ubiquitously co-operates on variety of substrates with the cytoplasmic RNA exosome complex – a major eukaryotic 3′-5′ exoribonuclease.

The exosome acts both in the cytoplasmic and the nuclear compartments. Its core contains an RNase PH-like 9-subunit ring with a central channel, which is catalytically inactive in yeast *Saccharomyces cerevisiae* and humans, but retained phosphorolytic activity in plants (Dziembowski et al., 2007; Q. Liu et al., 2006; Sikorska et al., 2017). This barrel-like structure is associated with differently localized catalytic subunits. In yeast, Dis3 exo- and endonuclease is present in nuclear and cytoplasmic exosomes, while Rrp6 distributive exonuclease is restricted to the nucleus. In humans, nucleoplasmic exosome core encompasses DIS3, equivalent to yeast Dis3 in its biochemical properties, whereas cytoplasmic exosome contains DIS3L, endowed only with processive exoribonucleolytic activity (Lykke-Andersen et al., 2011; Tomecki et al., 2010). Human RRP6 is found in the cytoplasm and in the nuclei, with strong nucleolar enrichment (Lykke-Andersen et al., 2011; Tomecki et al., 2010) (Figure 1).

Ubiquitous presence of the exosome entails that it encounters a variety of coding and non-coding RNA (ncRNA) molecules, synthesized by different RNA polymerases and fulfilling their functions in distinct subcellular environments (Figure 1). An outstanding question in the field has been

how the exosome is directed to such a wide repertoire of targets and how its specific action is determined. A great deal of investigations indicate that targeting specificity is achieved via close cooperation between the exosome and various compartment- and/or species-specific adapters, co-factors or accessory complexes, including SKI complex.

Due to extreme diversity of nuclear RNA substrates, the exosome activity in this compartment is supported by several different auxiliary factors (Figure 1). Importantly, they usually share one common feature, which is the presence of MTR4(-like) ATP-dependent DExH-box RNA helicase as a central component.

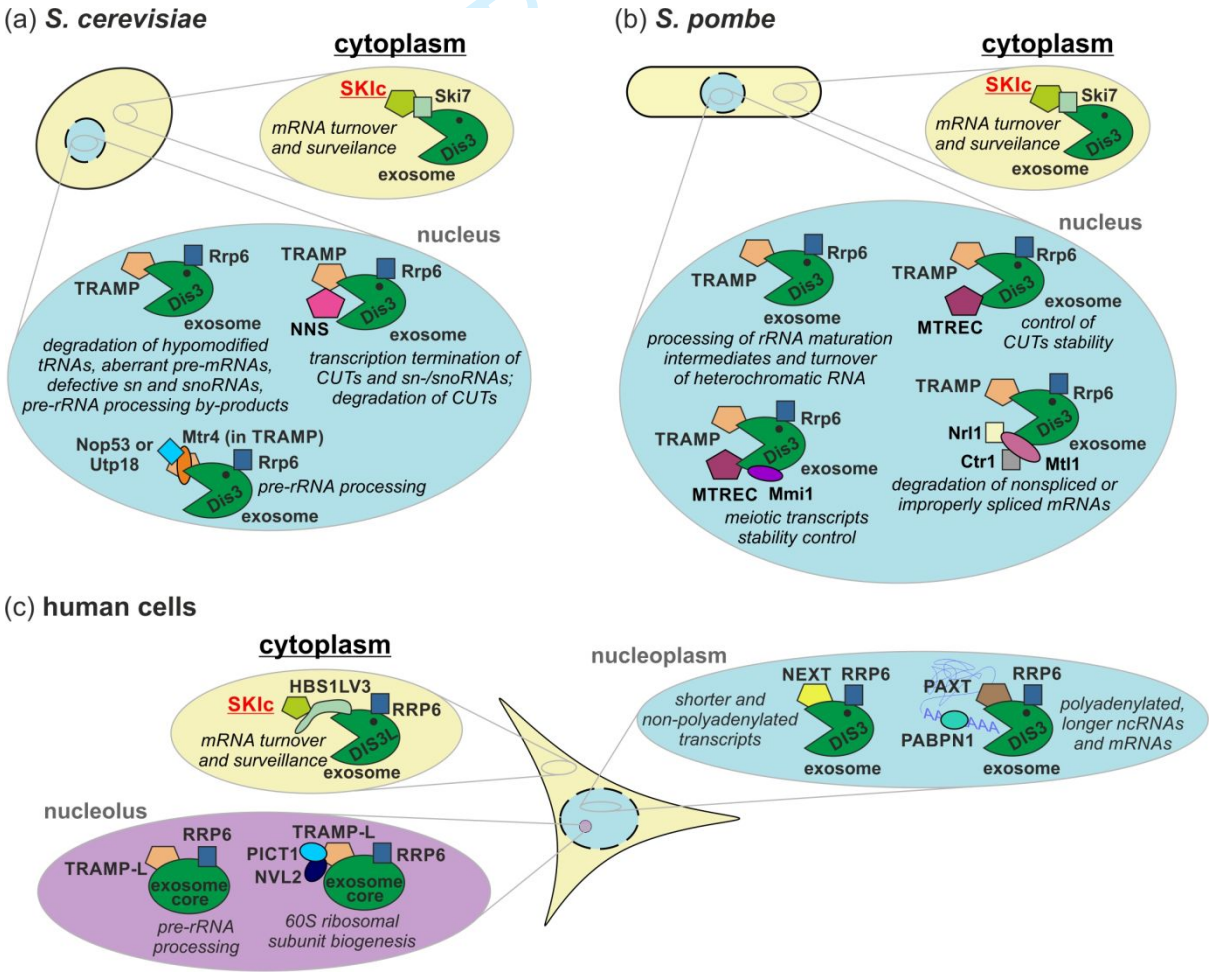

FIGURE 1 Nuclear exosome is accompanied by diverse accessory complexes containing different RNA helicases, whereas cytoplasmic exosome functions are supported exclusively by SKIc in different eukaryotic

species (a-c). (*a*) In the nucleus of *S. cerevisiae* Mtr4 provides helicase activity to the TRAMP complex, containing also Trf4/5 non-canonical poly(A) polymerase (PAP), and the zinc-knuckle RNA-binding protein Air1/2 (Das et al., 2021; Falk et al., 2014; LaCava et al., 2005; Vanacova et al., 2005); distinct TRAMP isoforms, formed by inclusion of Trf4 or Trf5 and Air1 or Air2 paralogs, enable degradation or precise trimming of ribosomal RNA precursors, pre-mRNAs, hypomodified tRNAs, sn- and snoRNAs, as well as cryptic unstable transcripts (CUTs), in the nucleolus or in the nucleoplasm (Delan-Forino et al., 2020; San Paolo et al., 2009); TRAMP-exosome recruitment to CUTs and sn-/snoRNAs is aided by interaction with Nrd1-Nab3-Sen1 (NNS) complex, which mediates transcription termination of those RNAs (Tudek et al., 2014); Mtr4 in budding yeast can also associate via its arch domain with Nop53 or Utp18 for pre-rRNA processing or degradation of its by-products (Falk et al., 2017; Thoms et al., 2015). (*b*) In *Schizosaccharomyces pombe* apart from TRAMP, encompassing Mtr4, Air1, and Cid14 (Trf4/5 ortholog), which partakes *i.a.* in the processing of rRNA maturation intermediates and heterochromatic RNA turnover (Buhler et al., 2008; Keller et al., 2010; Win et al., 2006), additional co-factors exist, either of which contains Mtr4 paralog, known as Mtl1; one of them, MTREC (or NURS), contains Red1 zinc-finger protein and controls stability of CUTs, and – together with additional partners, such as Mmi1 – meiotic transcripts (Dobrev et al., 2021; Shichino et al., 2020; Y. Zhou et al., 2015); Mtl1 can alternatively interact with Nrl1 and Ctr1 to degrade un- or misspliced mRNAs (N. N. Lee et al., 2013). (*c*) In human cell nucleolus, besides TRAMP-like complex composed of MTR4/SKIV2L2, PAPD5 or PAPD7, and ZCCHC7 Zn-knuckle protein (Lubas et al., 2011; Sudo et al., 2016), MTR4 interacts with NVL2 and with Nop53 ortholog – PICT1, to ensure proper 60S ribosomal subunit biogenesis (Lingaraju et al., 2019; Miyao et al., 2022; Yoshikatsu et al., 2015); in the nucleoplasm MTR4 forms complexes with either RBM7-ZCCHC8 or ZFC3H1, referred to as NEXT and PAXT, respectively (Gerlach et al., 2022; Lingaraju et al., 2019; Lubas et al., 2011; Meola et al., 2016; Puno & Lima, 2022; Silla et al., 2020); in addition, an important connection between the PAXT dimeric core and PABPN1 protein is mediated by RNA; significant functional specialization between NEXT and PAXT is apparent, with the former targeting shorter and non-polyadenylated transcripts, such as PROMPTs, upstream antisense RNAs, enhancer RNAs and the latter recruiting the exosome to longer ncRNAs and mRNAs, which are polyadenylated (Meola et al., 2016; Wu et al., 2020). (*a-c*) An exclusive partner of the cytoplasmic exosome in the regulation of mRNA turnover and surveillance, endowed with enzymatic activity of Ski2 RNA helicase and common for all species, is SKIc (marked in red and underlined). Interaction between SKIc and exosome is bridged by Ski7 in yeast (*a*,*b*) and HBS1LV3 in human cells (*c*).

Contrary to the multitude of nuclear targets, the major class of the cytoplasmic exosome substrates are mRNAs. Normal protein-coding transcripts are turned over by either 5'-3' Xrn1 exoribonuclease or in the parallel exosome-mediated 3'-5' decay pathway (Anderson & Parker, 1998; A. W. Johnson & Kolodner, 1995). In turn, the exosome is an indispensable constituent of several quality control pathways, eliminating aberrant mRNAs, which could potentially encode truncated or elongated proteins. Cytoplasmic exosome-dependent RNA quality mechanisms are closely linked to

sensing abnormalities in ribosome progression (D'Orazio & Green, 2021; Inada, 2020; Karamyshev & Karamysheva, 2018) and largely supported by the SKI complex.

As opposed to the situation in the nucleus, SKI complex, which contains Ski2 RNA helicase homologous to Mtr4 and two additional proteins with scaffolding and regulatory functions, is the major cofactor of the cytoplasmic exosome (Figure 1a-c). Despite overall structural, biochemical, and functional similarities of SKIc in various Eukaryotes, details of its interactions with exosome and other factors controlling cytoplasmic RNA metabolism differ. Most of the early studies on SKIc functions were done in *S. cerevisiae*, but it later turned out that not all findings based on studies in this model directly pertain to higher Eukaryotes. Moreover, details of SKIc involvement in cytoplasmic RNA turnover and surveillance pathways in metazoans and plants, some of which do not exist in yeast, have begun to emerge relatively recently. In parallel, considerable progress has been made over the last few years in mechanistic understanding of how individual SKIc components, the entire SKIc, and larger assemblies encompassing this complex work from the structural point of view. More and more attempts are currently being undertaken to translate knowledge about the molecular functions of the complex to its roles in human health and disease. All of these interdisciplinary issues deserve to be comprehensively elaborated.

Here, we summarize current structural, biochemical, and functional insights into SKIc roles in cytoplasmic mRNA metabolism and we discuss recent studies unravelling potential and sometimes unexpected new roles of SKIc in antiviral responses, signaling pathways, and developmental processes.

2. STRUCTURE OF THE SKI COMPLEX AND ITS INTERACTIONS WITH THE RIBOSOME AND EXOSOME

2.1 SKIc components and their domain architecture

Studies from the early 2000s showed that the yeast Ski2, Ski3, and Ski8 proteins co-purify, forming a tight complex coined SKIc (Brown et al., 2000). The stoichiometry of SKIc was later refined to be of 1:1:2 of Ski2:Ski3:Ski8 (Synowsky & Heck, 2008).

Ski3/TTC37 is the largest and main scaffolding subunit of the SKI complex (Figure 2a,d; Table 1). It is composed of multiple, around 34 amino acid-long tetratricopeptide repeat (TPR) motifs (Blatch & Lassle, 1999; Zeytuni & Zarivach, 2012), folding into two antiparallel α-helices, which form right-handed solenoids with approximately 8 TPRs per turn of the superhelix (Halbach et al., 2013; Kogel et al., 2022). Yeast Ski3 contains 33 TPRs, while human TTC37 is 7 repeats longer at the C-terminus (Figure 2a; Table 1).

Ski8/WDR61 is a member of the WD40-repeat protein family (Xu & Min, 2011), and folds into a doughnut-shaped seven-bladed beta-propeller structure (Figure 2b,e; Table 1). A characteristic WD (Trp-Asp) motif is present only in blades I and VI. Each blade is folded into four antiparallel β-sheets, running from inside to the outside of the propeller. Blades I-VI are formed by adjacent segments of the polypeptide chain. In the ultimate blade the most external strand originates from the N-terminal part of protein, while the three most internal strands come from the very C-terminal protein part (Cheng et al., 2004; Madrona & Wilson, 2004; Matsumoto et al., 1993).

Ski2/SKI2W catalytic subunit of SKIc is composed of three main domains: 1) N-terminal, 2) a central catalytic domain encompassing two RecA sub-domains, which contain eight conserved sequence motifs, and 3) C-terminal (Ski2C), with two winged helix (WH) segments separated by an extended Arch/insertion subdomain, and followed by helical bundle (HB) (Figure 2c; Table 1). The RecA and HB domains form a compact ring-like enzymatic core with a central RNA channel. The relative position of RecA domains is restrained by interaction with HB. The catalytic domain is roughly globular, U-shaped, with two RecA domains facing one another at the extremities (Figure 2f).

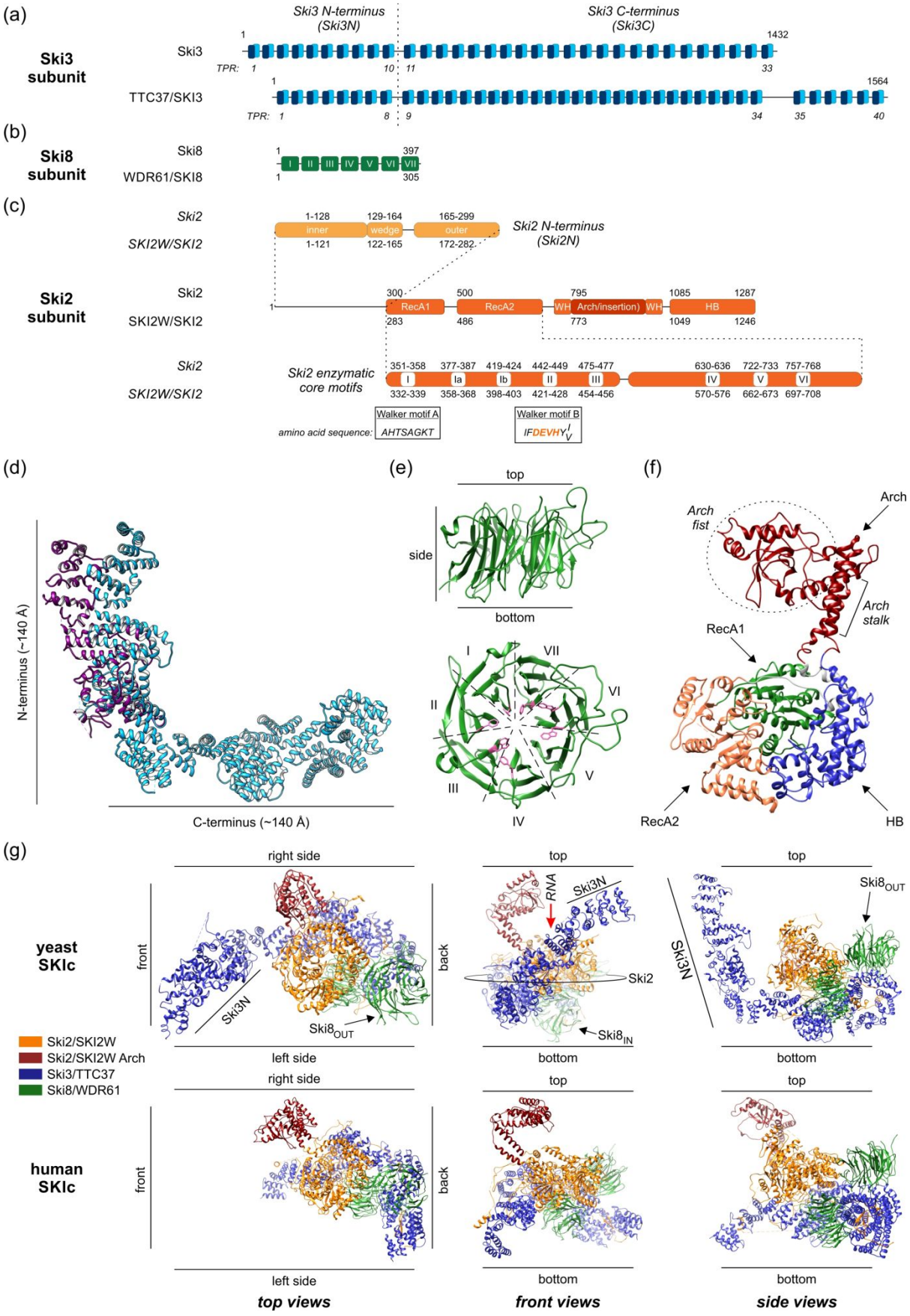
(a)
Ski3 subunit
Ski3 N-terminus (Ski3N)
Ski3 C-terminus (Ski3C)
Ski3
TTC37/SKI3
TPR:
(b)
Ski8 subunit
Ski8
WDR61/SKI8
(c)
Ski2 subunit
Ski2
SKI2W/SKI2
Ski2 N-terminus (Ski2N)
inner
wedge
outer
RecA1
RecA2
WH
Arch/insertion)
HB
Ski2 enzymatic core motifs
Walker motif A
Walker motif B
amino acid sequence:
AHTSAGKT
IFDEVHY
(d)
N-terminus (~140 Å)
C-terminus (~140 Å)
(e)
top
side
bottom
(f)
Arch
Arch fist
Arch stalk
RecA1
RecA2
HB
(g)
yeast SKIc
human SKIc
front
back
right side
left side
top
bottom
Ski3N
RNA
Ski2
Ski8OUT
Ski8IN
Ski2/SKI2W
Ski2/SKI2W Arch
Ski3/TTC37
Ski8/WDR61
top views
front views
side views

FIGURE 2 Structural features of SKIc subunits and the entire complex. (a) Comparison of TPR motifs distribution in yeast Ski3 and human TTC37; numbers above correspond to amino acids; numbering of TPR motifs is provided below, in italics; vertical dashed line indicates the boundary between TPRs building N-terminal (Ski3N) and C-terminal (Ski3C) parts of proteins. (b) Schematic presentation of Ski8/WDR61 secondary structure, with seven WD40 repeats indicated with roman numerals; numbers above and below correspond to amino acid positions in yeast Ski8 and human WDR61, respectively. (c) *middle:* domain organization of Ski2/SKI2W; WH – winged helix; HB – helical bundle; *top:* three segments of the Ski2 N-terminus (Ski2N); *bottom:* location of the eight enzymatic core motifs within Ski2 RecA domains; numbers above and below correspond to amino acid positions in yeast Ski2 and human SKI2W, respectively; amino acid sequences of motifs I and II (Walker motifs A and B) are provided in rectangular boxes; DExH signature in Walker motif B is indicated in orange. (d) Structure of the yeast Ski3 is shown in bright blue, with N- and C-terminal arms indicated. Purple ribbons visualize translocation of the N-terminal arm into position characteristic for substrate and ribosome binding. (e) Structure of the yeast Ski8 protein from the front (*top panel*) and top (*bottom panel*); dashed lines separate seven blades of the beta-propeller, indicated with roman numerals and the residues important for Ski3 binding are highlighted in pink in the bottom panel. (f) Structure of the yeast Ski2 helicase with functional domains indicated with arrows and highlighted in separate colors (red – the Arch/insertion domain with the stalk and the fist additionally marked; blue – the HB domain; orange – the RecA1 domain; green – the RecA2 domain). (g) *top:* three distinct views of the yeast SKIc structure; positions of selected structural elements are indicated; the site where RNA substrate enters the channel is marked with red arrow; *bottom:* corresponding views of the human SKIc; the N-terminal part of TTC37 is missing in the human structure; structures of both complexes were compared using MatchMaker tool of UCSF Chimera package, based on the Ski2/SKI2W helicase structure.

2.2 Interactions between SKIc subunits and overall structure of the complex

Within SKIc, Ski3/TTC37 serves as a platform and recruits Ski2/SKI2W helicase and two copies of Ski8/WDR61 to its C-terminus. The overall structure of the complex is asymmetric with the globular catalytic core being covered by two separate extended fragments formed by the Ski3/TTC37 N-terminus (Ski3N) and the Ski2/SKI2W Arch/insertion domain. This model was largely built for the yeast complex (Halbach et al., 2013), but the overall SKIc structure is conserved in humans (Kogel et al., 2022) (Figure 2g).

The Ski3/TTC37 C-terminal segment (Ski3C) has a supercoiled conformation with three-and-a-half (Ski3) or four (TTC37) superhelical turns, and binds to Ski2/SKI2W helicase and two Ski8/WDR61 subunits (Figure 2d; Table 1). The N-terminal regulatory part in yeast Ski3 (Ski3N) can

move by 20 Å and is composed of roughly 10 TPRs, wherein TPRs 4-7 are folded atypically, creating an extended structure and providing flexibility of this segment (Figure 2a,d,g; Table 1). TTC37 N-terminus had no ordered density in the human SKIc cryo-EM structure (Figure 2g), and its exact folding and position could not be determined, but it likely retained potential for mobility.

The top surface of Ski8/WDR61 doughnut binds to Ski3/TTC37 via evolutionary conserved hydrophobic residues F20, F89, W125, F188, W293, W311, and F358 (Figure 2e, bottom). Conversely, Q-R-x-x-ϕ (x – any amino acid; ϕ – an aromatic residue) motif was identified in the yeast Ski3, which strongly binds Ski8 (Table 1). Curiously, though in human TTC37 this motif is not conserved, the overall structural arrangement of the TTC37:WDR61 interaction is preserved (Halbach et al., 2013; Kogel et al., 2022). The two copies of Ski8 are positioned differently and play distinct roles in SKIc. In yeast, the first one is located more peripherally and thus designated outer ($Ski8_{OUT}$; Figure 2g; Table 1). It interacts with Ski3 TPR31 and modulates Ski2 RNA binding. The second one, termed inner ($Ski8_{IN}$; Figure 2g; Table 1), is placed closer to the center of the complex, binds Ski3 TPR 33, and plays some role in the maintenance of entire SKIc integrity (Halbach et al., 2013; Kogel et al., 2022). Those mutual interactions represent the major mode of Ski8/WDR61 recruitment to SKIc, even though both copies form some additional connections with Ski3/TTC37 and Ski2/SKI2W helicase (Table 1). This was shown by genetic studies in yeast and confirmed using biochemical assays (Halbach et al., 2013; L. Wang et al., 2005). Evolutionary conservation is highlighted by the observations that mutations in TTC37 residues responsible for WDR61 binding cause THE syndrome in humans (Fabre et al., 2011; Hartley et al., 2010; Kogel et al., 2022).

Ski2/SKI2W RecA1 and WH domains interact extensively with Ski3/TTC37 and Ski8/WDR61 (Figure 2g; Table 1). In contrast, RecA2 faces the solvent, potentially having capacity for structural rearrangement linked to catalysis, which has not yet been experimentally shown. The Arch/insertion domain extends over the RecA domains, near the RNA entrance site and is important for regulation of catalysis (see below) (Halbach et al., 2013; Halbach et al., 2012; Kogel et al., 2022) (Figure 2f,g; Table 1).

Ski2/SKI2W N-terminal domain (Ski2N) is responsible for the majority of interactions with other SKIc constituents (Table 1). It can be divided into several segments referred to as 'inner', 'wedge' and 'outer' (Figure 2c). In yeast, the inner segment is tightly wrapped by the entire Ski3 C-terminal domain, starting from TPR15. These two structural elements, derived from two different subunits form one compact structural entity. This arrangement is highly similar in humans, though more relaxed due to a higher number of TPR repeats (Figure 2g). The wedge segment, which in human was shown to have regulatory potential (Table 1), displays a well-organized globular structure, and is adjacent to Ski3 TPRs 17-25, $Ski8_{IN}$, and Ski2 enzymatic core, providing an additional surface for interaction with the RNA substrate. Those elements cooperatively form the base of the complex and an exit for the RNA 3'-end. The Ski2N outer segment is poorly characterized. Human cryo-EM structure lacks this element, while in yeast SKIc it folds into another four α-helices that groove into Ski3 TPRs, but electron density corresponding to this element is weak. A linker between Ski2N and the enzymatic core remains unresolved and is most probably unstructured (Halbach et al., 2013; Kogel et al., 2022).

2.3 Structural features important for the regulation of SKIc helicase activity

Helicases are a large collection of enzymes responsible for nucleic acid unwinding dependent mostly on ATP hydrolysis. Ski2/SKI2W is a member of a large and diverse superfamily 2 (SF2) (Byrd & Raney, 2012; Fairman-Williams et al., 2010). The SF2 helicase enzymatic core is structurally very well conserved, and comprises two RecA-like domains arranged in tandem (RecA1 and RecA2), with eight characteristic sequence motifs at defined positions (exemplified in the Figure 2c for Ski2/SKI2W). The Walker A and B motifs (or motif I and II), which are part of RecA1 (Figure 2c), provide binding sites for ATP (Sloan & Bohnsack, 2018). The SF2 family is generally divided into two classes, the DEAD- and DEAH-box helicases, based on the sequence signature within Walker motif B (De Bortoli et al., 2021; Hamann et al., 2019; Linder & Jankowsky, 2011; Tauchert et al., 2017). The latter class, apart from the canonical DEAH-box helicases, encompasses DExH-box enzymes, sometimes called Ski2-like (S. J. Johnson & Jackson, 2013). These small differences between the Walker B motifs have a substantial impact on the mechanism of catalysis, which is further deepened by the unique features of remaining RecA motifs, surrounding domains and associated proteins. The DExH-box subfamily comprises eukaryotic RNA helicases Ski2/SKI2W and Mtr4/MTR4 – important exosome co-factors in the cytoplasm and nucleus, respectively, splicing helicases Brr2 and Prp43, and archaeal Hel308 DNA helicase.

To facilitate the understanding of the mechanism of Ski2/SKI2W catalysis, we will briefly outline the mode of action of the DEAD-, DEAH-, and DExH-box enzymes. In most helicases the RecA1 and RecA2 domains are presumed to be mobile, though capturing this movement

experimentally is challenging. More specifically, they are postulated to adopt alternative 'open' and 'closed' conformations, corresponding to two stages of catalysis (Ozgur et al., 2015). Unwinding of double-stranded RNA (dsRNA) by DEAD-box helicases is mediated by an α-helix within RecA1, responsible for base-pair melting. ATP hydrolysis is required for substrate release. Closed helicase state refers to substrate binding and unwinding activation, while the open state corresponds to the disassembly of the helicase-RNA complex (Gilman et al., 2017; Hilbert et al., 2009; Sloan & Bohnsack, 2018). In contrast, in the case of DEAH-box helicases, both RecA domains bind single-stranded 3'-overhang segment of a partially double-stranded RNA substrate. ATP hydrolysis is related to open (ATP-bound) and closed (ATP-unbound) conformation. Each ATP hydrolysis cycle and switching back and forth between open and closed conformation leads to accommodation of an additional nucleotide from the RNA strand within the enzymatic core. This results in RNA movement through the helicase channel in the 3'-to-5' direction, nucleotide by nucleotide (De Bortoli et al., 2021; Gilman et al., 2017; Hamann et al., 2019; Sloan & Bohnsack, 2018; Studer et al., 2020; Tauchert et al., 2017).

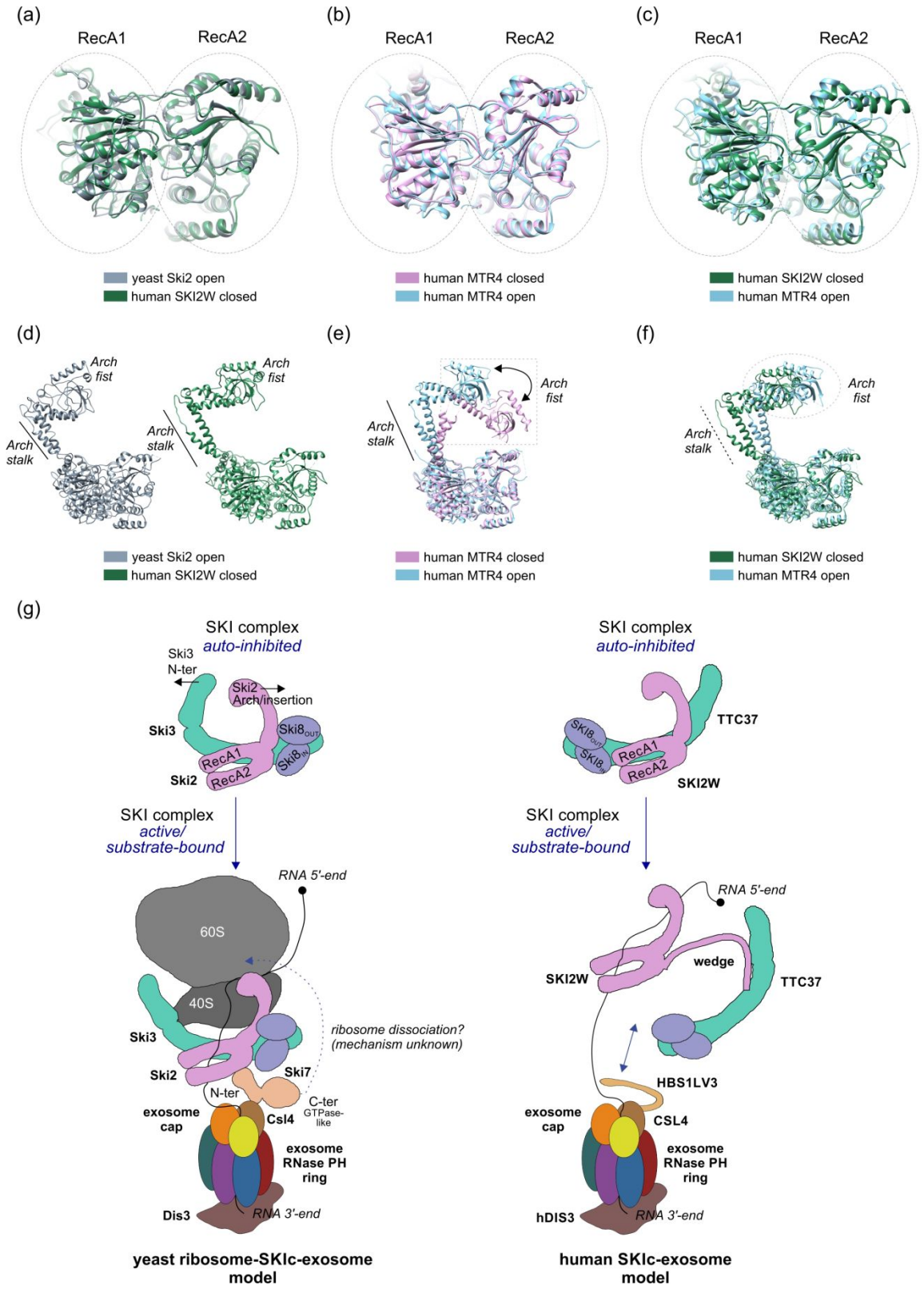

FIGURE 3 Regulation of SKIc activity is dependent on the flexibility of structural elements outside of the Ski2/SKI2W enzymatic core as well as interactions with RNA substrate and ribosome. (a-c) Superimpositions of RecA domain arrangement in Ski2 and SKI2W from yeast and humans (*a*), human MTR4 in the 'open' and 'closed' states (*b*), and human SKI2W and MTR4 in the 'open' conformation *(c)* demonstrate that they are rather

immobile. (d) Side-by-side comparison of yeast Ski2 in the 'open' state and human SKI2W in the 'closed' state, showing that positioning of the Arch domain segments ('stalk' and 'fist') is similar. (e) Relocation of the Arch 'fist' (marked with an arrow) can be readily observed in superimposed MTR structures representing 'closed' and 'open' states. In the latter the Arch domain moves further away from the helicase enzymatic core. (f) Superimposed structures of the human SKI2W and MTR4 reveal that despite different states ('closed' and 'open', respectively) the spatial location of the Arch domains is comparable. (g) Schematic illustration of changes in domain arrangement between SKIc in the auto-inhibited and active/substrate-bound states in yeast (*left*) and human (*right*) complexes. In the auto-inhibited state of yeast SKIc Ski2 Arch/insertion domain and Ski3 N-terminal fragment are close to each other and form a lid, which limits RNA access to the catalytic core. These two structural elements have to move outward (black arrows) while switching to the active/substrate-bound state. In yeast this occurs upon SKIc binding to the ribosome and the substrate and allows for RNA transfer to the exosome, linked to SKIc by the N-terminus of Ski7 protein. In the auto-inhibited state of human SKIc exit from the helicase channel is occluded, which blocks the RNA path towards exosome. This occlusion is removed by the movement of SKI2W 'wedge' segment, which induces partial dissociation of the helicase from TTC37:WDR61 scaffold.

RNA unwinding by DExH-box helicases, particularly Ski2, has not been fully characterized experimentally, but multiple available structures of the yeast and human SKI complexes as well as closely related MTR4 helicase (listed in Table 2) illuminate molecular mechanism of SKIc action to some extent. Mtr4 and Ski2 in yeast share 35% sequence identity within the catalytic core and display almost indistinguishable spatial architecture. In all available Ski2 and Mtr4 structures the RecA domains are immobile (Figure 3a-c), which precludes faithful modeling of ATP hydrolysis or RNA unwinding and therefore structural recognition of the open and closed helicase states, defined as described above. However, at least three flexible elements of SKIc outside the active site were shown to regulate enzymatic activity and/or substrate selection. Those are the Ski2 Arch/insertion domain, Ski3N, and the Ski2N wedge segment (Table 1). SKIc alternative states resulting from re-positioning of structural segments external to RecA are sometimes also referred as 'open' and 'closed', which is confusing, since these conformational changes are not directly linked to RecA domain movement. We

therefore propose that they are rather referred to as 'active/substrate-bound' and 'auto-inhibited', at least in the case of SKIc (Figure 3d-g).

Cryo-EM studies showed that the human SKI2W wedge segment of the N-terminal domain can regulate SKIc conformation, possibly by enabling the detachment of the helicase from the TTC37:WDR61 core, which was not reported in yeast (Figure 3g). Surprisingly, since SKI2W ATPase activity was not affected following loss of the wedge, the mechanism of regulation is unclear (Kogel et al., 2022).

The Ski2 Arch/insertion and the Ski3 N-terminal domains form a lid covering the helicase active site and both translocate upon substrate and ribosome binding in yeast SKIc (Figure 3g). The regulatory potential of those domains is underlined by the fact that Ski2 helicase is a more robust ATPase alone than in complex and that deletion of the Arch/insertion domain increases Ski2 ATPase activity within SKIc, but does not alter catalysis of the isolated helicase (Halbach et al., 2013). Structural information about those conformational changes in both domains in yeast and human SKIc is incomplete. The two states of Ski3N were only shown in yeast structures (Halbach et al., 2013; Schmidt et al., 2016) (Figure 2d). The Arch/insertion domain is composed of two anti-parallel coiled coils forming an L-shaped stalk (an arm) and a globular β-barrel domain (a fist) (Figures 2f and 3d-g). The stalk is rather immobile, and the base of the Arch/insertion domain is likely entirely responsible for its flexibility (Lingaraju et al., 2019; J. Wang et al., 2019). Two states of Mtr4 Arch domain were captured in structural studies (Olsen & Johnson, 2021) (Figure 3e). In the 'closed' state, the Arch domain nearly contacts the RecA2 domain, and it relocates away from the catalytic center in the

'open' state (Weick et al., 2018) (Figure 3g). The Ski2 Arch/insertion domain was modeled, however not crystalized, in the auto-inhibited state (Halbach et al., 2013), but the structure of yeast SKIc bound to the ribosome shows that the Ski2 Arch/insertion domain bends away about 30° from the entrance to the enzyme active site (Schmidt et al., 2016), which corresponds to the Mtr4 'open' state (Lingaraju et al., 2019; Olsen & Johnson, 2021; J. Wang et al., 2019; Weick et al., 2018) (Figure 3f).

The Arch/insertion domain helps the Ski2 and Mtr4 helicases in substrate selection, but does so using different mechanisms. Mtr4 substrates are often highly structured and the Arch/insertion domain is a site of recruitment of several co-factors of the nuclear exosome, such as yeast Nop58 and Utp18 or human NVL and PICT1, which are involved in pre-rRNA processing, and ZCCHC8 subunits of the NEXT complex, which mediates degradation of non-adenylated non-coding RNAs (Falk et al., 2017; Gerlach et al., 2022; Lingaraju et al., 2019; Miyao et al., 2022; Puno & Lima, 2018; Thoms et al., 2015) (Figure 1). Recruitment of structured substrates is aided by the Arch/insertion KOW (Kyrpides-Ouzounis-Woese) motif, which was suggested to also bind RNA (Weir et al., 2010). The Arch/insertion domain provides specificity to the Mtr4-containing TRAMP complex and ultimately also to the exosome, which otherwise relies on non-specific RNA binding mediated by the Air1/2 proteins within TRAMP and its own cap subunits (Falk et al., 2014; Lingaraju et al., 2019). In turn, the Ski2/SKI2W substrates are often non-structured, but even though the Arch/insertion domain does not contain a KOW motif and is dispensable for the SKIc formation and binding of other proteins, it is responsible for increasing affinity towards RNA. Yeast Ski2 devoid of Arch domain displayed lower ability to bind RNA whereas Arch domain alone efficiently bound different RNA substrates (Halbach et

al., 2013; Halbach et al., 2012). Differences between Mtr4 and Ski2 insertion domains are likely the consequence of evolutionary pressure associated with differential sub-cellular localization of the two homologous helicases, and the need to adjust biochemical properties to specific RNA substrates.

2.4 Interactions of SKI complex with the ribosome and factors linking it to the exosome

A direct SKIc-ribosome interaction is structurally well-characterized in both yeast and humans, and involves various parts of the complex, albeit does not occur in exactly the same way in both species. The greatest similarity concerns the connection of Ski2 RecA2 domain to the region of 40S small ribosomal subunit located between the shoulder of rRNA helix 16 and the head of the uS3 and eS10 ribosomal proteins (Table 1). Similar conformations are also observed for the Arch domain of Ski2, which binds the head of 40S subunit via uS3, uS10 ribosomal proteins, and rRNA helix h41 (Table 1). Yeast $Ski8_{OUT}$ is sandwiched between Ski3 and 40S, and contacts uS2, uS5, and eS21 proteins (Table 1), while in the case of human SKIc outer WDR61 is at a distance of 40 Å relative to those proteins (Kogel et al., 2022; Schmidt et al., 2016). SKIc binding to the ribosome and the substrate leads to a transition of the complex from an auto-inhibited to an active/substrate-bound state due to relocation of the Ski3N and the Ski2 Arch/insertion domains (Figure 3g).

RNase protection assays in yeast show that 35 to 42 nucleotides are protected by ribosome-bound SKIc, which is roughly a sum of regions protected by separate assemblies (28-30 nt by the ribosome and 9-10 nt by SKIc) (Schmidt et al., 2016). Human cryo-EM structure is consistent with these biochemical data (Kogel et al., 2022), suggesting that the mRNA substrate is transferred directly from the ribosome to the SKIc helicase channel (Figure 3g). The RNA path through SKIc

starts on the RecA2 domain, which is responsible for the first contact of the helicase core with RNA 3' overhang. Next, RNA is moved to the central helicase channel and interacts mainly with RecA1 domain, and – to a lesser extent – with the ratchet helix of HB domain (Kogel et al., 2022; Schmidt et al., 2016). The role of Arch/insertion domain in mRNA recognition and traversing the channel is unknown from a structural point of view.

An outstanding question in the field concerns the role of SKIc and its ATPase and helicase activity in mediating the possible mRNA transfer from the ribosome to the exosome. The connection of SKIc to the exosome is indirect and mediated in yeast and human by two proteins – Ski7 and HBS1LV3, respectively (Araki et al., 2001; Kalisiak et al., 2017; Kowalinski et al., 2016; J. J. Liu et al., 2016) (Figure 3g; Table 1).

Ski7 in yeast is encoded by a separate gene paralogous to *HBS1*. Human *HBS1L* locus encodes two proteins, HBS1LV1 and HBS1LV3, translated from alternatively spliced pre-mRNA (Brunkard & Baker, 2018; Kalisiak et al., 2017; Marshall et al., 2018; Marshall et al., 2013). Yeast Ski7 and human HBS1LV3 are structurally very different, but both have specialized domains responsible for interactions with SKI and exosome complexes. Within the N-terminal fragment of Ski7 (amino acids 1-264), both these domains are in close vicinity to each other (Figure 3g, *left*) – amino acids 1-105 interact with SKIc, while residues 116-235 are involved in association with the exosome (Table 1). The Ski7 N-terminus and both interaction domains separately are mandatory for efficient 3'-5' RNA decay (Araki et al., 2001; Kowalinski et al., 2016). In contrast, elements responsible for HBS1LV3 interactions with the SKI and exosome complexes are localized at two opposite ends of the protein

(Figure 3g, *right*). HBS1LV3 N-terminal region (amino acids 1-145) was characterized as a domain responsible only for interaction with SKIc, whereas connection with the exosome is established by HBS1LV3 fragment located in the C-terminal protein part, which encompasses two conserved motifs: RxxxFxxxL (amino acids 546-572) and PFDFxxxSPDDIVKxNQ (amino acids 609-625) (Brunkard & Baker, 2018; Kalisiak et al., 2017; Marshall et al., 2013) (Table 1). The reason and functional significance of differences in domain arrangement between Ski7 and HBS1LV3 are unknown, but they can potentially strongly impact SKIc function.

Structural analyses indicate that Ski7 forms multiple contacts with the top part of the exosome complex (including most importantly Csl4 exosome cap subunit) close to the entrance to the central channel (Kowalinski et al., 2016; J. J. Liu et al., 2016) (Figure 3g, *left*; Table 1). In turn, the precise site of Ski7 association with SKIc is uncertain, but it most likely resides at the bottom of the complex, in the area where 3' RNA strand exits the helicase channel, which would be convenient in the context of subsequent RNA substrate delivery to the exosome (Figure 3g, *left*). Neither Ski2 enzymatic activity nor the intactness of the Ski3N and Ski2 Arch/insertion domain are required for Ski7-SKIc interaction (Halbach et al., 2013; L. Wang et al., 2005). Two models for the interaction of SKIc with the exosome were proposed (Halbach et al., 2013; Kogel et al., 2022). The yeast model suggests the possible existence of a ribosome-SKIc-Ski7-exosome super-complex (Halbach et al., 2013; Schmidt et al., 2016) (Figure 3g, *left*). In contrast, in the human model interaction with HBS1LV3 could induce partial dissociation of the helicase from the SKIc structural scaffold, which is mediated by the SKI2W wedge segment (Kogel et al., 2022) (Figure 3g, *right*). This leads to unblocking the helicase channel exit and

presumably enables subsequent RNA delivery to the exosome (Figure 3g, *right*). It is not clear whether such extensive SKIc remodeling would be compatible with simultaneous ribosome binding. Elucidating the existence of super-complex biochemically and/or structurally in both species is important to comprehensively understand the SKIc mechanism of action and functions in the context of ribosome and exosome. This is because Ski7 and HBS1LV3 are components of mRNA quality control systems that rely on a larger collection of factors responsible for sensing aberrant translation events and removing paused ribosomes. Some of them induce ribosome disassembly. The SKIc enzymatic activity might be indispensable in this process to either open RNA secondary structures or to assist in the ribosome release, which has not been thoroughly investigated yet. Alternatively, SKIc might only physically connect the ribosome to the exosome, perhaps explaining its overall weak ATPase and yet poorly described helicase activity. However, since mutations in the SKI2W catalytic region are causative to the genetic disorder (see below), the SKI complex is likely not merely a courier that delivers the transcript to the exosome in a passive way.

3. SKIc FUNCTIONS IN RNA DECAY AND SURVEILLANCE

3.1 The yeast SKIc and Ski7 roles in general mRNA turnover and quality control

mRNAs undergo several rounds of translation and are then degraded to be replaced by a fresh batch of templates transcribed within and exported from the nucleus. This process, often referred to as mRNA turnover, is orchestrated by two major exoribonucleases – Xrn1 and the exosome, acting in 5'-3' and 3'-5' direction, respectively.

It is generally accepted that the major route of mRNA decay in *S. cerevisiae* begins with 5'-end decapping and is followed by 5'-3' exonucleolysis performed by Xrn1 (Labno, Tomecki, & Dziembowski, 2016). This route is tied to events occurring at the polyadenosine tail, located at the opposite transcript end (Passmore & Coller, 2022; Wurm & Sprangers, 2019). The 5'-cap and the 3'-poly(A)-tail form a loop via direct interaction of the cap-binding complex (CBC) and the poly(A)-binding protein (PABP), along with translation initiation factors, which was proposed to influence translation initiation efficiency (Vicens et al., 2018). A long-standing model postulates that a substantial poly(A)-tail shortening constitutes a signal for the Dcp1-Dcp2 complex to perform decapping, though molecular details of the process are still elusive. Deadenylation is performed by a dedicated duet of deadenylase complexes, CCR4-NOT and Pan2-Pan3 (Chen & Shyu, 2011) (Figure 4).

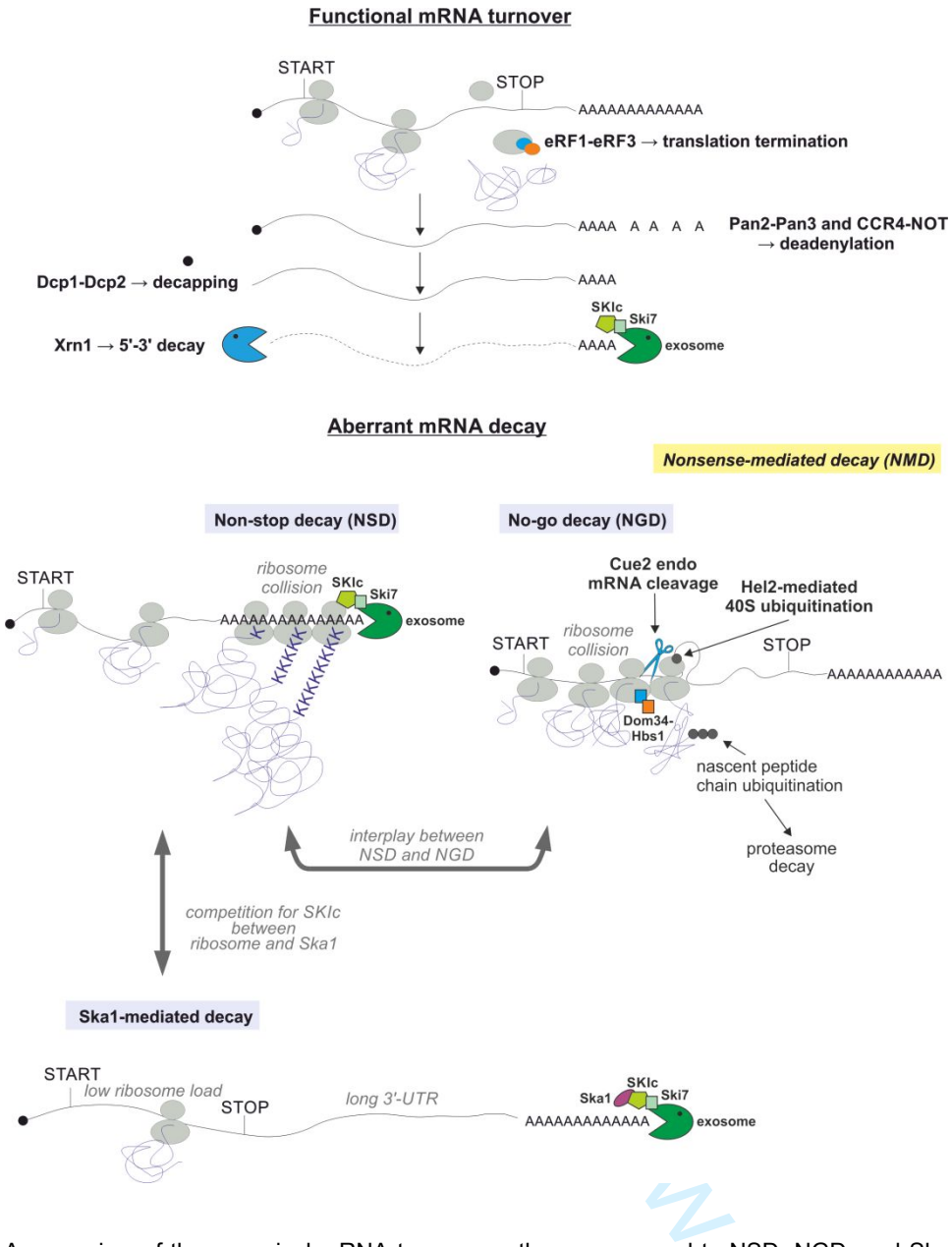

FIGURE 4 An overview of the canonical mRNA turnover pathway compared to NSD, NGD, and Ska1-mediated decay in *S. cerevisiae*. Functional mRNAs undergo several rounds of translation, which coincides with gradual 3'-end polyadenosine tail shortening, called deadenylation. This results in transcript decapping at the 5'-end by Dcp1-Dcp2, followed by degradation mediated by Xrn1 5'-3' exonuclease. Alternatively, mRNA can be degraded directly in the 3'-5' direction, by the exosome recruited to mRNAs by SKIc with Ski7. There are four cytoplasmic mRNA quality control pathways, which are functionally linked to the rate of transcript translation. Three of them rely considerably on the SKIc action, and are illustrated here. In turn, the involvement of SKIc-exosome in NMD (marked with yellow box) is less understood. NGD is triggered by ribosomes stalled within ORF; the main effector of this pathway is the Dom34-Hbs1 dimer, which structurally mimics the eRF1-eRF3 translation termination factor, and similarly interacts with the ribosomal A-site. Dom34-Hbs1 recruitment leads to endonucleolytic cleavage of the mRNA, coupled to proteolytic degradation of the defective nascent polypeptide in ribosome-associated quality control (RQC) pathway. NSD is triggered *e.g.* by the lack of a stop codon, when translation proceeds through the 3'-terminal poly(A)-tail. The third and relatively newly described pathway centers around

the Ska1 protein, which also interacts with SKIc. This pathway targets mRNAs with long 3'-UTRs, which have a low ribosome load. There is some redundancy between NSD, NGD, and Ska1-associated pathway, which ensures rapid removal of aberrant mRNAs from the cytoplasm. In particular, the line between NSD and NGD is not clear.

Following exosome purification and biochemical characterization of its 3'-5' exonucleolytic activity (Mitchell et al., 1997), it was observed that mutations in genes encoding exosome subunits and its co-factors lead to aberrant processing of nuclear sn/snoRNAs and cytoplasmic mRNAs, and postulated that two forms of the exosome operate in both cellular compartments to target distinct substrate sets, with the exosome-SKIc being dedicated to mRNA processing (van Hoof, Lennertz, & Parker, 2000). Other works posited an interdependence of the Xrn1 and exosome decay pathways (Anderson & Parker, 1998; van Hoof, Staples, et al., 2000). This was based on several observations. First, reporter mRNA containing a poly(G)-tract was trimmed from both sides, indicating that the internal poly(G) insertion impairs both 5'-3' and 3'-5' decay. Furthermore, simultaneous blocking of both pathways with mutations in *DCP1*, *DCP2* or *XRN1* combined with mutants in the genes encoding SKIc subunits, Ski7 or exosome components increased reporter mRNA half-lives and synergistically impaired growth, especially at elevated temperatures (Anderson & Parker, 1998; van Hoof, Staples, et al., 2000). Documentation of the existence of two general evolutionary conserved mRNA decay mechanisms acting in parallel and demonstration that efficient functioning of at least one of them is mandatory for viability, sparked a still ongoing debate on the relative contribution of both paths to controlling levels of different protein-coding transcripts within the same organism, as well as to global shaping of transcriptomes in evolutionary distant eukaryotic species.

While the majority of mRNA turnover in yeast is Xrn1-dependent, the exosome-associated route is essential for mRNA quality control. Seminal works from the early 2000s showed that while degradation of bulk mRNA was delayed in deadenylase or *DCP2* and *XRN1* mutants, aberrant transcripts displayed unaltered, rapid decay rates in these strains; in turn, such RNAs were stabilized upon mutations in genes corresponding to exosome-SKIc subunits and Ski7 (Frischmeyer et al., 2002; van Hoof et al., 2002). Thus, malformed transcripts and/or those that are not efficiently translated, are subjected to exosome-mediated decay, assisted by SKIc and Ski7 linking both assemblies. There are three main systems that sense faulty mRNAs, which are abundantly produced as a result of premature transcription termination, premature polyadenylation or incorrect splicing events. Nonsense-mediated decay (NMD) detects transcripts containing premature termination codons (PTCs), and thus coding for truncated proteins. Non-stop decay (NSD) targets transcripts lacking a stop codon. Finally, no-go decay (NGD) removes transcripts with features that induce ribosome stalling or are poorly translated. Detection of aberrant transcripts is performed by dedicated complexes (Karamyshev & Karamysheva, 2018).

A key and yeast-specific player in NSD is Ski7, an 84.7 kDa protein composed of two functional modules. The N-terminal domain contains a SKIc-binding region and an adjacent exosome-interacting motif (Table 1). The C-terminal part comprises a GTP-binding domain, which displays homology to translation elongation and termination factors – EF1α and eRF3, respectively – as well as to a paralogous protein, Hbs1, which all belong to a family of translational GTPases (Figure 5a) (Araki et al., 2001; Kowalinski et al., 2016; Kowalinski et al., 2015; van Hoof et al., 2002). Only the N-

terminal part of Ski7 is crucial for SKIc-assisted exosome mediated decay (Araki et al., 2001; Horikawa et al., 2016; Kowalinski et al., 2016). In turn, the Ski7 C-terminus GTPase module was suggested to play some role in ribosome dissociation (Horikawa et al., 2016). Hbs1 is a critical factor in NGD and is an active GTPase, which binds Dom34 protein. This dimer, in contrast to Ski7, is structurally and functionally well-conserved across higher Eukaryotes and cooperates with Rli1 in yeast (ABCE1 in humans) to enable recycling of stalled ribosomes (Pisareva et al., 2011; Saito et al., 2013; Shoemaker & Green, 2011) (Figure 5b).

A common feature of NSD and NGD are stalled ribosomes (Powers et al., 2020). During translation of a transcript lacking a stop codon, ribosomes enter the poly(A)-tail and synthesize a poly-lysine chain (Figure 4), which may slow down the ribosome due to electrostatic interactions with ribosomal proteins. Such transcripts are targeted by NSD (Figure 4). On the other hand, sequences present within coding regions, such as clusters of rare codons, motifs with tendencies to form strong secondary structures, or stretches of codons corresponding to *e.g.* poly-lysine tracts, may inhibit or slow down translation through interfering with ribosome progression. Such substrates are in turn eliminated by NGD (Figure 4). Ribosome stalling during translation through natural poly(A)-tails and sometimes also through internal A-stretches induces endonucleolytic cleavage of mRNA (Guydosh & Green, 2017; Szadeczky-Kardoss, Gal, et al., 2018), producing substrates for subsequent 3'-5' exonucleolysis by the exosome. Stalled ribosomes accumulate at NSD targets together with SKIc (Schmidt et al., 2016). The homology and structural similarity of Hbs1 and Ski7 to eRF3 (Figure 5a) enable these proteins to enter the ribosome A-site and induce ribosome release, probably in a

competitive manner (Horikawa et al., 2016). Hbs1 function is dependent on its interaction with Dom34, which is a paralog of eRF1 termination factor (Atkinson et al., 2008). There is a substantial difference between Hbs1 and Ski7 in the presumed mechanism of ribosome release from the mRNA template, since Hbs1 retained ability to hydrolyze GTP, while Ski7 binds GTP, but is catalytically inactive (Horikawa et al., 2016). Furthermore, it does not co-operate with an eRF1-like partner. NSD and NGD are mechanistically quite similar, and a certain interplay between Ski7, Dom34-Hbs1, and eRF1-eRF3 dependent on the translation rate, was proposed (Chiabudini et al., 2014; Horikawa et al., 2016) (Figure 4). Importantly, SKIc binding to the 40S subunit does not preclude simultaneous interaction of the ribosome with yeast Dom34-Hbs1 dimer. Therefore, it should not interfere with canonical mechanism of ribosome recycling (Schmidt et al., 2016) (Figure 5b). SKIc plays an important role in ATP-dependent mRNA extraction from the stalled ribosomes, which facilitates their dissociation and subsequent exosome-mediated transcript degradation (Zinoviev et al., 2020).

Exactly how the decay of mRNA (which is still protected at its 5'-end by the cap and at the 3'-end by the poly(A)-tail) is activated following induction of NSD and NGD is not clear and several redundant pathways may contribute to this process. In one of them, the decay of faulty transcripts is coupled to proteasomal degradation of truncated proteins via ribosome-associated quality control (RQC) (Joazeiro, 2019) (Figure 4). Collided ribosomes are sensed by E3 ligase Hel2, which polyubiquitinates 40S subunit of the trailing ribosome (Ikeuchi et al., 2018; Inada, 2020). Another ubiquitin E3 ligase – Ltn1/Listerin – marks the nascent polypeptide chain, targeting it to the proteasome (Joazeiro, 2019). Cue2 endonuclease binds to ribosome decorated with ubiquitin at 40S

and mediates mRNA cleavage between collided ribosomes (D'Orazio et al., 2019) (Figure 4), producing direct entry site for SKIc-exosome. A functional Cue2 homolog, NONU-1, was identified in *Caenorhabditis elegans* (Glover et al., 2020), and N4BP2 protein is likely their equivalent in human cells (D'Orazio et al., 2019).

Bone-fide NSD and NGD targets should be rare within the coding transcriptome, which entails that in normal growth conditions the activity of Ski7 and Dom34-Hbs1 is marginal and directed towards some ncRNAs that escape other, mostly nuclear, surveillance mechanisms. NSD and NGD targets can be also produced from normal mRNAs due to alternative 3'-end selection, which cuts off the stop codon in the open reading frame, or by intron retention, which could incorporate some structural elements slowing down translation within the open reading frame (ORF). Additionally, recent studies have shown that oxidative stress factors can also strongly modify the transcriptome. First, guanosine oxidation to 8-oxo-G within mRNAs induces ribosome stalling, which was suggested to activate NSD and NGD in yeast (Simms et al., 2014). Second, oxidative stress leads to eRF3 aggregation, increasing the likelihood of ribosomes reading through stop codons into the poly(A)-tails. SKIc-, NSD-, and NGD-deficient mutants are particularly sensitive to oxidative stress, suggesting these factors are crucial in dealing with unfavorable growth conditions. Double *hbs1Δ*/*ski7Δ* or *dom34Δ/ski7Δ* mutants exhibit exceptional susceptibility to oxidative agents, supporting the redundant nature of NSD and NGD (Jamar et al., 2017).

NMD occurs at transcripts containing PTCs, which can be mRNAs arising from alternative splicing or ncRNAs, which escape nuclear decay and are exported to the cytoplasm, like mRNAs. The

requirements for defining an NMD target are complex and are a function of the length of the 3'-UTR in yeast and/or the position of the stop codon relative to the sites of exon-junction complex (EJC) deposition in higher Eukaryotes. NMD is also dependent on a pioneer round of translation and the main NMD effector is the Upf1-Upf2-Upf3 complex, which displays ATPase activity and assembles eRF1-eRF3 (He & Jacobson, 2015). NMD substrates are decapped and degraded by both Xrn1 and the exosome (Karamyshev & Karamysheva, 2018). Ski7 and SKIc contribution to this pathway is unclear, although they were reported to be required for decay of NMD targets. Ski7 N-terminus was shown to bind directly to Upf1 with the assistance of Upf2. This interaction likely provides a mean to recruit the exosome to PTC-containing mRNAs (Mitchell & Tollervey, 2003; Takahashi et al., 2003), but was not further studied.

In conclusion, SKIc function in the translation-dependent removal of aberrant mRNAs during NSD and NGD is well-documented in yeast. Curiously, however, SKIc-exosome decay pathway might also function independently of translation, and operate instead through Ska1 (E. Zhang et al., 2019). This 33 kDa non-catalytic protein with no apparent structural motifs is a strong *in vivo* SKIc interactor (Table 1), and its loss leads to accumulation of decay intermediates mapping to transcripts with a low ribosome load, such as weakly translated mRNAs containing long 3'-UTRs (Figure 4) and ncRNA species, including XUTs and SUTs (E. Zhang et al., 2019). Thus, SKIc is apparently present in two distinct subpopulations to support exosome-mediated degradation in yeast. One fraction is linked to the ribosome and controls RNA decay in a translation-dependent manner. Conversely, when SKIc does not interact with ribosome, exosome function is facilitated by Ska1, which specifically recruits

SKIc to RNAs devoid of ribosomes. Both pathways are in apparent competition for SKIc, since Ska1 overexpression weakens SKIc interaction with the ribosome and results in a strong accumulation of NSD reporters. 3'-UTR length related to the distance between stop codon and the transcript 3'-end, which determine the presence or absence of ribosomes in the vicinity of the latter, and the ribosome density within ORF are the major determinants of mRNA sensitivity to Ska1 (E. Zhang et al., 2019). The precise mechanism of Ska1 action is unclear and it remains to be shown whether it induces conformational changes within SKIc, similar to its activation through an interaction with ribosome. Likewise, possible handover of SKIc from Ska1 to the ribosome during progressive exosome-mediated 3'-5' mRNA decay, which gradually trims 3'-UTR, thereby reducing the distance between the last ribosome and SKIc, has not been investigated. Ska1 has no homologs in higher Eukaryotes and whether any functionally similar factors exist in other organisms is unknown.

3.2 SKIc interacts with different partners in various experimental models

In human cells the exosome and SKIc are linked by HBS1LV3 protein (Kalisiak et al., 2017; Kogel et al., 2022; Kowalinski et al., 2016) (Figure 5a,c; Table 1). Transcriptomic analyses showed that SKIc and HBS1LV3 participate in general mRNA turnover and that substantial subsets of transcripts targeted by both these factors overlap (Kalisiak et al., 2017). Since HBS1LV3 lacks the eRF3-like domain (Figure 5a), it may not participate in translation-dependent mRNA surveillance pathways, contrary to Ski7 in *S. cerevisiae*. RNA-seq did not demonstrate enrichment of transcripts with features that could predispose them to entering such quality control pathways upon HBS1LV3 depletion (Kalisiak et al., 2017). On the other hand, while the levels of HBS1LV3 in HEK293 cells are rather low,

this may not be common to cells of different origin. For instance, it appears that expression of HBS1LV3 in hematopoietic cells is significantly higher than in HEK293 cell line (Kalisiak et al., 2017). Thus, the relative contribution of exosome-dependent decay to mRNA quality control may depend on the amounts of factors involved in these degradation pathways.

A sharply contrasting viewpoint on the SKIc functions in mRNA turnover and surveillance has been provided by studies in mouse embryonic stem cells (mESCs), which revealed an intense interplay between translation and mRNA decay and tremendous specialization, rather than redundancy, of different decay pathways (Tuck et al., 2020). XRN1 5'-3' exoribonuclease is predominantly responsible for bulk mRNA turnover in mESCs. It does not bind any specific sequences in mRNA targets and its activity is co-translationally supported by a direct interaction with the preceding translating ribosome, which removes obstacles that could otherwise inhibit XRN1 action. Strikingly, this is reminiscent of situation in yeast, where 5'-3' mRNA decay pathway predominates over degradation in the opposite direction in the regulation of mRNA turnover, while it contrasts with the more important role of the 3'-5' exosome-mediated degradation in controlling general mRNA stability in human cells (Kalisiak et al., 2017). Further, it was found that SKIc in mESCs participates principally in mRNA quality control – it is universally recruited by ribosomes to prevent translation errors, while it seldom affects the levels of selected transcripts, such as *e.g.* replication-dependent histone mRNAs. This is surprising taking into account that the 3'-5' decay of these transcripts in other cell types was previously shown to be dependent on 3' oligouridylation and exoribonucleolytic activity of exosome-independent DIS3L2 enzyme (Labno, Warkocki, et al., 2016).

In turn, 3' oligo(U) tails were claimed to act instead as platforms for SKIc attachment in mESCs (Tuck et al., 2020). It is thus tempting to speculate that relative contributions of XRN1, exosome-SKIc, and DIS3L2 to bulk mRNA turnover and to mRNA quality control may vary considerably between different cellular models. Therefore, any attempts to extrapolate conclusions based on investigations performed in a specific cell type to other models should be approached with due caution.

Importantly, HBS1L isoforms were not identified in mass-spectrometry analyses as proteins co-purifying with SKIc in mESCs (Tuck et al., 2020), so it is unknown how the cooperation between exosome and SKI complexes is ensured in this particular cell type (Figure 5d). Instead, the only specific SKIc partners in mESCs are AVEN and FOCAD (Focadhesin) proteins (Table 1), which were conversely not defined as relevant interactors of SKIc in human cell lines (Kalisiak et al., 2017). It was postulated that AVEN-FOCAD and SKIc in mESCs are separate complexes that both bind ribosomes, but only transiently interact with each other during translation-dependent mRNA surveillance (Tuck et al., 2020). SKI2W binding within mRNA targets was enriched at sites of ribosome collision, which often corresponded to runs of polylysine or polyproline codons and A-rich stretches in coding sequences. Treatment of mESCs with translation inhibitors caused massive SKI2W relocation, with outcomes dependent on the inhibitor's mechanism of action, such as removal from coding sequences (harringtonine treatment) or accumulation within 5'-UTRs (cycloheximide treatment), showing that SKI2W binding to sites prone to ribosome stalling was dependent on active translation. AVEN distribution on mRNAs was very similar to SKI2W and it also included GC-rich regions, which could be structured and thus preclude efficient ribosome translocation. Besides histone mRNAs, the major

targets of SKI2W and AVEN in mESCs are upstream ORFs (uORFs), small ORFs (sORFs), and RNAs with G-quadruplexes, which are likely melted by AVEN's RGG/RG domain. Rather than recruiting SKIc to its targets, AVEN counteracts ribosome arrest – when this function is compromised, SKIc promotes degradation of mRNAs with stalled ribosomes (Figure 5d). This was inferred from AVEN knock-out, which led to enhanced, rather than diminished, SKI2W binding to its target sites (Tuck et al., 2020).

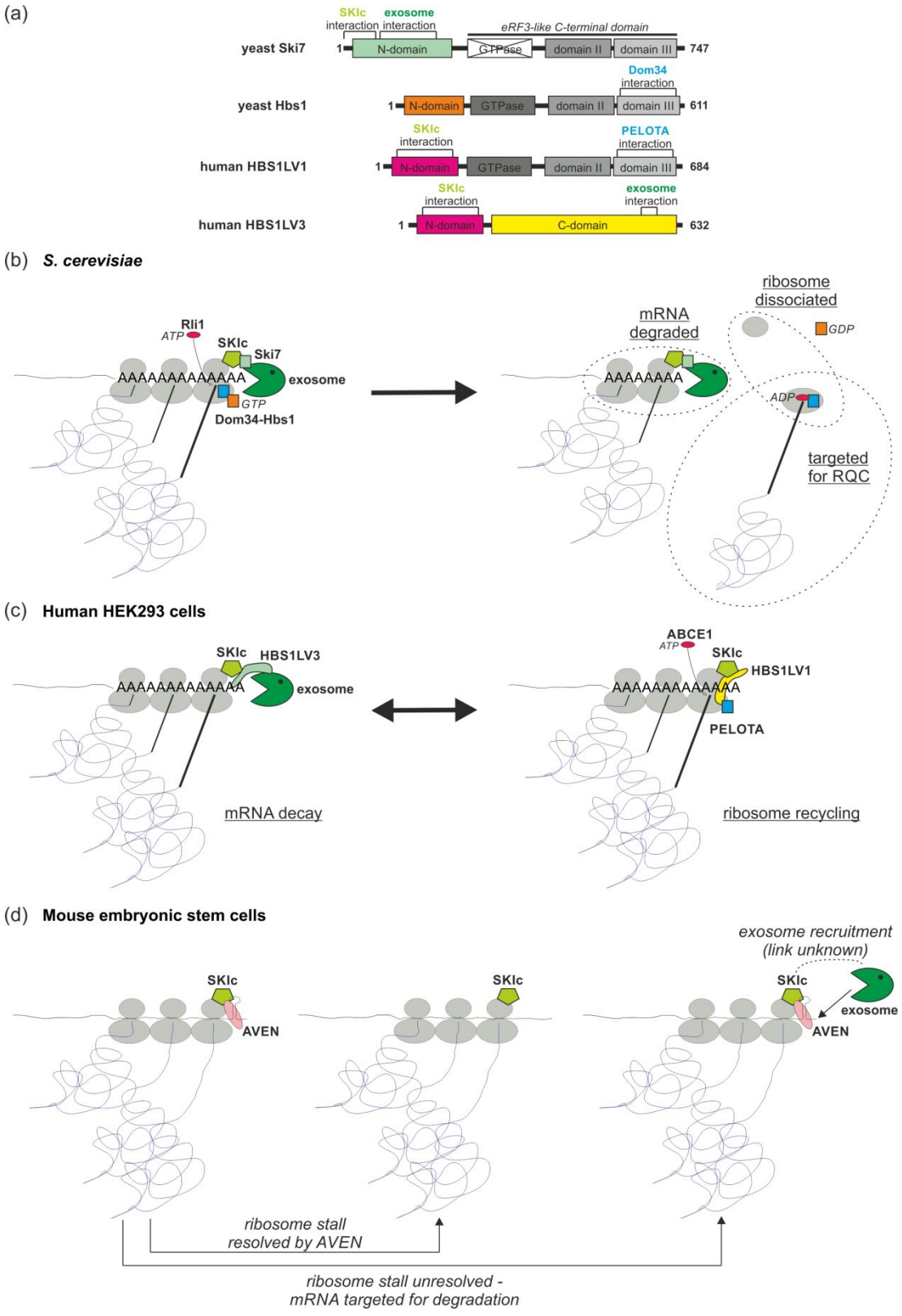

FIGURE 5 Different SKIc interactors in yeast and mammalian cells facilitate ribosome release and transcript degradation during translation-dependent mRNA surveillance. (a) Domain organization of yeast Ski7 and Hbs1 and two human HBS1L isoforms. Ski7, Hbs1, and HBS1LV1 contain conserved eRF3-like C-terminal region subdivided into segments (grey rectangles), including GTPase module, which is catalytically active only in

Hbs1/HBS1LV1. The latter are able to interact with eRF1 homolog – Dom34/DOM34 (aka PELOTA in humans). Yeast Ski7 encompasses an N-terminal domain (pale green rectangle) different from Hbs1 (orange rectangle), with SKIc- and exosome-interacting motifs. HBS1LV1 and HBS1LV3 share an identical N-terminus (magenta rectangle), responsible for their competitive interactions with SKIc. Only the unique C-terminal region of HBS1LV3 (yellow rectangle) comprises motifs connecting it to the human exosome. (b) In *S. cerevisiae*, ribosome stalling at *e.g.* internal or terminal poly(A)-tracts during NGD or NSD leads to SKIc binding to the 40S subunit and exosome recruitment via Ski7. This triggers aberrant transcript degradation, although Ski7 may be also involved in ribosome release via unknown mechanism. The major ribosome rescue factor if Dom34-Hbs1, which co-operates with Rli1 ATPase. GTP and ATP hydrolysis by Hbs1 and Rli1, respectively, are required for ribosome dissociation into 40S subunit and 60S-peptidyl-tRNA complex, subjected to RQC pathway. (c) In human cells, due to competition for SKIc between HBS1L variants, some equilibrium is probably established between SKIc functions in mRNA degradation, involving HBS1LV3 (left) and ribosome recycling (right), dependent on PELOTA-HBS1LV1 and ABCE1 (Rli1 homolog). (d) In mouse embryonic stem cells, SKIc does not interact with HBS1L isoforms, but rather with AVEN, which counteracts ribosome stalling. Otherwise, the exosome is recruited for mRNA degradation, but the physical link between SKIc and exosome in this cell-type remains elusive.

The findings from mESCs indicate that the spectrum of SKIc interactors is much broader than previously anticipated and it raises a number of questions which need to be experimentally addressed. Above all, the presence and significance of SKIc-AVEN interaction must be investigated in mammalian cells of various origin. If it is not restricted to mESCs, then contribution of SKIc-AVEN and SKIc-HBS1LV3-exosome to general mRNA turnover and specialized translation-dependent surveillance pathways should be determined and compared, also in relation to parallel cytoplasmic degradative mechanisms that may be involved into regulation of these phenomena (such as XRN1- or DIS3L2-mediated decay). If there are cells in which both SKIc-AVEN and SKIc-HBS1LV3-exosome operate, it would be interesting to check if some of their functions are redundant or whether they are responsible for entirely non-overlapping processes. It could be envisioned that HBS1LV3 bound to the SKIc targets the exosome to normal mRNA decay, while an interplay between SKIc and AVEN-FOCAD is critical for degradation of aberrant transcripts. Notwithstanding, some form of transcripts

handover between different assemblies, based on transient interactions, can be also envisaged. Moreover, it cannot be excluded that FOCAD, which has not been so thoroughly investigated yet, has other protein partner aside from AVEN, which directs SKIc (and plausibly exosome) to normal protein-transcripts instead of faulty ones.

FOCAD homolog – ARM-repeat protein RST1 (RESURRECTION1) – links the exosome and SKIc in plants and interacts with RIPR (RST1-INTERACTING PROTEIN), unrelated to mouse AVEN (Lange et al., 2019). This represents another variation on how SKIc and the exosome could be linked. RST1 associates with the exosome – preferentially with an isoform containing RRP45B (aka CER7), but not with nuclear-specific isoform encompassing RRP45A variant. The presence of an elongated C-terminus only in the former paralog is apparently crucial for interaction with RST1. What makes situation even more complicated, is the interaction between RST1 and plant Ski7 homolog, but the function of the latter in the establishment of SKIc-exosome connection has not been specified. In turn, RIPR binds RST1-Ski7 and SKIc (Lange et al., 2019).

The lack of interaction between SKIc and any of the HBS1L paralogs in mESCs is thought-provoking not only in the context of SKIc-exosome connection, but also bearing in mind that in human cells recycling of the stalled ribosomes depends on PELOTA/DOM34-HBS1LV1 rescue factor (Saito et al., 2013), and the latter component was also shown to interact with SKIc (Kalisiak et al., 2017) (Table 1). The presence of PELOTA-HBS1LV1 in mESCs was not demonstrated and it is impossible to say at this stage whether it functions in some specific ribosome splitting events or whether it was entirely replaced by AVEN-FOCAD in these cells. It should be also kept in mind that differences

between the SKIc functions and spectrum of auxiliary protein partners in various mammalian cellular models might be due to the fact that the data for human cells were obtained using immortalized cell line, contrary to the naturally pluripotent mESCs model. Obviously, much more extensive proteomic and transcriptomic analyses in distinct cell lines and organismal models must be carried out to differentiate between these and other possibilities and to shed more light on precise roles of the SKIc and HBS1L variants in mammalian mRNA metabolism.

3.3 Links between SKIc and NMD in higher Eukaryotes

One of the most significant differences between NMD and NSD/NGD is that in the former mechanism a normal, complete, albeit premature, stop codon in the ribosomal A site is recognized by canonical termination factors eRF1-eRF3, which trigger ribosome release with concomitant peptidyl-tRNA hydrolysis, while the latter pathways employ Dom34-Hbs1 recycling factors, related to eRF1-eRF3, which disassemble ribosomes stalled at transcripts devoid of stop codons or stuck on other grounds without accompanying peptidyl-tRNA breakdown (Karousis & Muhlemann, 2019).

There are multiple mechanistic dissimilarities between NMD in yeast and higher Eukaryotes. NMD targets in *S. cerevisiae* are degraded mainly by exonucleolysis, while in metazoans several parallel pathways for elimination of such transcripts exist. This is mainly because an expanded set of proteins controls NMD in evolutionary more complex Eukaryotes compared to yeast. Apart from UPF core NMD factors, universally conserved across eukaryotic lineage from yeast to humans, several SMG proteins additionally contribute to the fate of PTC-containing mRNAs in metazoans. One of them, SMG6, is responsible for endonucleolytic NMD branch and the upstream cleavage products are

degraded by the exosome, likely in concert with the SKIc (Eberle et al., 2009; Karousis & Muhlemann, 2019). However, SKIc involvement in NMD is much more enigmatic in comparison with NSD or NGD.

In *C. elegans* a substantial fraction of protein-coding transcripts with PTCs is removed by NSD pathway, which relies on the action of PELOTA and SKIc-exosome (Arribere & Fire, 2018). Similar to yeast, when the leading ribosome reaches stop codon-less mRNA 3'-end, an endonucleolytic cleavage occurs at its 5' edge. The ribosome stalled on the downstream fragment is released with the aid of PELOTA, whereas SKIc attracts the exosome to the 3'-terminus of the upstream cleavage product to induce its degradation. Subsequent stalling of trailing ribosomes leads to repetition of the entire process. Transcriptome-wide RNA-seq and ribosome profiling studies showed that several hundred endogenous mRNAs in *C. elegans* are regulated in this manner (Arribere & Fire, 2018). A distinctive common feature of SKIc and PELOTA targets observed in ribosome profiling reads was their frequent truncation after the second (UGA) or second or third (UAG, UAA) nucleotide of the termination codons. Since canonical translation termination requires contacts between the release factors and the entire stop codon as well as the downstream +1 nucleotide, such truncations triggered ribosome stalling on these substrates, since ribosomal subunits could not be dissociated by eRF1-eRF3. Most importantly, in the context of the link between SKIc and NMD, a number of such substrates contained truncated stop codons known to represent PTCs. Other lines of evidence, including dependence of the non-stop decay of PTC-containing transcripts on the key NMD factor, SMG1 kinase, prove that NMD targets cleaved endonucleolytically at or upstream of the stop codon are re-directed to NSD. This shows that SKIc participates, at least to some extent, in

the elimination of mRNAs containing PTCs (Arribere & Fire, 2018). The omnipresence of NMD suppression by NSD among higher Eukaryotes remains to be demonstrated, nevertheless it is likely conserved in *Drosophila melanogaster*, where degradation of mRNA fragments upstream NMD endonuclease cleavage site in PTC-containing reporters and natural NMD targets was reduced upon depletion of PELOTA, HBS1 or SKIc component, WDR61 (Hashimoto et al., 2017). On the contrary, no signs of coupling between NMD and NSD in *Arabidopsis thaliana* have been found yet (Szadeczky-Kardoss, Csorba, et al., 2018; Szadeczky-Kardoss, Gal, et al., 2018), which may be due to the fact that, unlike in metazoans, no SMG6 endonuclease ortholog exists in plants, reminiscent of situation in *S. cerevisiae*.

3.4 NSD and NGD in higher Eukaryotes

The crucial role of Ski7 in NSD in *S. cerevisiae*, along with long lasting inability to identify its functional homolog in higher Eukaryotes raised the question whether this mRNA quality control pathway is conserved. Experiments performed using non-stop reporters revealed that both transcript lacking termination codon and protein product of its translation are less abundant in human cells than respective controls (Saito et al., 2013). Depletion of HBS1LV1 or PELOTA and listerin E3 ubiquitin ligase, involved in RQC aberrant protein elimination pathway led to stabilization of non-stop mRNA and protein, respectively. Like in yeast, human NSD was shown to be translation-dependent (Saito et al., 2013). Importantly, treatment of the cells with siRNA against SKI2W or DIS3 nuclease also increased half-life of the non-stop mRNA, indicating that the exosome-SKIc participate in the elimination of such faulty transcripts (Saito et al., 2013). Co-immunoprecipitation experiments showed

association between PELOTA-HBS1LV1 and the exosome, confirming that they cooperate in monitoring mRNAs devoid of stop codons (Saito et al., 2013). However, at that time, these results were misinterpreted, since HBS1LV1 was proposed to be the functional equivalent of the yeast Ski7. Taking into account that HBS1LV3 isoform was later documented to act as a linker between the exosome and SKI complexes in humans (Kalisiak et al., 2017; Kogel et al., 2022), both HBS1L isoforms probably play distinct roles in human NSD – HBS1LV1 with PELOTA rescue stalled ribosome at the 3'-end of non-stop mRNA and HBS1LV3 recruits the exosome to execute degradation of aberrant transcript (Figure 5c). The role of SKIc in this pathway and its ability to interact with both HBS1LV1 and HBS1LV3 in a mutually exclusive manner (Kalisiak et al., 2017) remains to be investigated both mechanistically and functionally to decipher the exact sequence of events and to determine whether some sort of SKIc handover between the two HBS1L paralogs occurs.

Translation-dependent NSD was also demonstrated in plants. *Nicotiana benthamiana* protein-coding transcripts incised within coding sequences were prone to NSD, contrary to mRNAs cleaved in the 3'-UTR, demonstrating significance of the ribosome stalling for NSD activation. Downregulation of HBS1 or PELOTA led to accumulation of non-stop mRNAs, indicating that impairment of ribosome rescue hinders efficacious elimination of aberrant transcripts. In agreement, non-stop mRNAs amassed in the polysome fractions in PELOTA-deficient *N. benthamiana* leaves. Importantly, SKIc is also involved in the degradation of NSD targets in plants, since *SKI2* silencing caused elevated levels of stop codon-less transcripts (Szadeczky-Kardoss, Csorba, et al., 2018). Thus, NSD is an ancient mRNA surveillance mechanism, stemming from the last eukaryotic common ancestor. Taking into

account that a large fraction of plant mRNAs undergo alternative polyadenylation and are regulated by miRNAs, NSD may play particularly important role in the regulation of gene expression in this clade, because these processes are prominent source of non-stop (prematurely polyadenylated) and stop codon-less transcripts, respectively.

NSD and NGD are related pathways, converging on ribosome stalling during translation, due to different reasons. Similar to NSD, existence and mechanism of NGD in plants have been demonstrated relatively recently in *N. benthamiana*. Importantly, only mRNAs encompassing long polyadenosine stretches within ORF, but not transcripts containing stem-loop structure or run of consecutive lysine codons, were susceptible to NGD, indicating that not all types of signals triggering this quality control mechanism are conserved between yeast and plants (Szadeczky-Kardoss, Gal, et al., 2018). Interruption of poly(A)-tract with guanosines precluded NGD, demonstrating that only adenosine homopolymers induce NGD in plants. The length of poly(A)-tract and its distance from the translation initiation codon correlated positively with NGD efficiency, suggesting the demand for ribosome collision as a precondition for NGD activation in plants, much the same as in other organisms (Szadeczky-Kardoss, Gal, et al., 2018). Depletion of PELOTA or HBS1 caused accumulation of 5' endonucleolytic cleavage product, implying that the stalled ribosome recycling is mandatory for its degradation (Szadeczky-Kardoss, Gal, et al., 2018). Similar to NSD, decay of this proximal fragment was stimulated by SKI2, while the distal cleavage product was removed by the 5'-3' exoribonuclease XRN4, a plant ortholog of the yeast Xrn1 (Szadeczky-Kardoss, Gal, et al., 2018). Thus, NGD as such, as well as the SKIc function in this process, are conserved in the eukaryotic

lineage. One noticeable variation in *A. thaliana* is the presence of two PELOTA paralogs, which both are able to interact with HBS1. However, while AtPELOTA1 overexpression rescued deficiency of its homolog in *N. benthamiana*, suggesting that AtPELOTA1-HBS1 dimer fulfills ribosome splitting function, like in other model organisms, ectopic expression of AtPELOTA2 counteracted productive NGD and NSD, which indicated that it may sequester HBS1 from the interaction with AtPELOTA1.

In line with recently characterized network of interactions between the exosome and SKIc in plants (Lange et al., 2019), silencing of *RST1* or *RIPR*, encoding factors linking both multimeric assemblies inhibited degradation of 5' cleavage fragments generated during NGD, as well as non-stop reporters in *N. benthamiana* (Auth et al., 2021), demonstrating that RST1 and RIPR play pivotal roles in controlling efficiency of these two pathways, by coordinating functions of the plant exosome and its cytoplasmic adapter. Another class of events which require cooperation between the exosome, RST1, RIPR, and SKIc in plants is the degradation of 5' cleavage fragments induced by minimum uORF (AUG-stop) present in the 5'-UTR of a subset of plant genes (Auth et al., 2021).

3.5 The roles of the SKIc in RNA interference

The knowledge about SKIc functions was initially gathered mainly by studying *S. cerevisiae* model, and follow-up investigations revealed that some discoveries made using yeast can be extrapolated to higher Eukaryotes. However, specific details of some RNA metabolic pathways broadly conserved among Eukaryotes may differ between yeast and multicellular organisms, while other paths are absent in *S. cerevisiae*. The most prominent example of the latter is RNA interference (RNAi) pathway (Figure 6a-c). Therefore, SKIc functions in RNAi could be dissected only by investigating higher

Eukaryotes. While the possible outcome of RNAi in the form of mRNA endonucleolytic cleavage catalyzed by Ago2 within RNA-induced silencing complex (RISC) were deciphered already in the early 2000s (J. Liu et al., 2004; Zamore et al., 2000), the fate of upstream and downstream mRNA fragments arising after Ago2-mediated endonucleolysis remained unknown.

It was demonstrated that XRN4 in *A. thaliana* and *N. benthamiana* degrades 3' fragments resulting from RISC-mediated cleavage (Souret et al., 2004; Szadeczky-Kardoss, Csorba, et al., 2018) (Figure 6b). An independent study employing reporter constructs in *D. melanogaster* showed that the 5' fragment is in turn rapidly eliminated by the exosome (Orban & Izaurralde, 2005) (Figure 6a). Destruction of downstream and upstream products of RISC cleavage by XRN1 (aka Pacman in fruit fly) and the exosome, respectively, was shown to occur independently of deadenylation or decapping (Figure 6a). Importantly, depletion of the putative SKIc subunits precluded efficient removal of the 5' cleavage products, suggesting that SKIc is required for exosome-mediated degradation (Orban & Izaurralde, 2005) (Figure 6a). The SKIc involvement in the decay of such fragments in *D. melanogaster* was independently confirmed by others (Hashimoto et al., 2017).

Analogous to *D. melanogaster*, SKIc components were implicated in the degradation of 5' RISC cleavage fragments in *A. thaliana* and *N. benthamiana* in experiments employing miRNA- or siRNA-targeted reporters (Branscheid et al., 2015; Szadeczky-Kardoss, Csorba, et al., 2018) (Figure 6b). Furthermore, activity of the SKI and exosome complexes on such cleavage products prevented their utilization as templates for dsRNA synthesis by RNA-dependent RNA polymerase RDR6 (Figure 6b). Such dsRNA may become a source of secondary siRNA, which triggers RNAi reinforcement by

an amplification loop (L. Liu & Chen, 2016). Thereby, apart from conserved role in metabolizing mRNA cleavage fragments arising upstream RISC cleavage site, an additional crucial function of SKIc in *A. thaliana* is limitation of the RDR6-dependent RNAi transitivity. While this RNAi enhancement mechanism is advantageous in the cases of antiviral defense or transgene silencing (Figure 6b), its action on endogenous transcripts may cause significant perturbations in overall gene expression profile, rationalizing the need for tight control. Otherwise, generation of endogenous coding transcripts-derived secondary siRNA, termed ct-siRNA (coding transcript-derived siRNAs) or rqc-siRNA (RNA quality control small interfering RNA) (L. Liu & Chen, 2016) (Figure 6b), may detrimentally reprogram gene expression in a plant cell (X. Zhang et al., 2015). Thus, degradative activities of both exosome-SKIc and XRN4 cooperatively neutralize supply of RNA fragments, which could provoke siRNA transitivity, with 5'-3' decay pathway playing probably more prominent role in transgene PTGS (Yu et al., 2015). In the context of the SKIc participation in this regulation, it was demonstrated that in the absence of SKI2 secondary transitive siRNAs accumulate predominantly in close proximity to the 5' side of the cleavage site (Branscheid et al., 2015). This suggested that transitivity might be induced when the 5' fragments are still base-paired to the miRNA, which enables RDR6 recruitment, and that the preventive role of SKIc in siRNA spreading likely relies on the SKI2 helicase activity-dependent unwinding of the miRNA-mRNA duplexes (Branscheid et al., 2015) (Figure 6b).

One spectacular example of how important is the SKIc role in counteracting spurious siRNA biogenesis from endogenous loci in plants concerns regulation of *TKL1* gene expression. *TKL1*

encodes transketolase – an enzyme participating in the Calvin cycle of photosynthesis. It has been shown that combination of SKIc dysfunction with mutations in the genes coding for two major *A. thaliana* uridyltransferases, namely HESO1 and URT1, previously implicated in preventing RNAi transitivity (Scheer et al., 2021), results in massive production of illegitimate siRNAs corresponding to *TKL1* (X. Wang et al., 2022). This in turn elicits *TKL1* mRNA destabilization, decreased transketolase levels, and accumulation of various Calvin cycle intermediates, which eventually result in reduced photosynthesis efficacy and plant leaf etiolation (X. Wang et al., 2022). Notably, partial reversal of these molecular and developmental phenotypes was achieved upon loss-of-function mutation in *RDR6*.

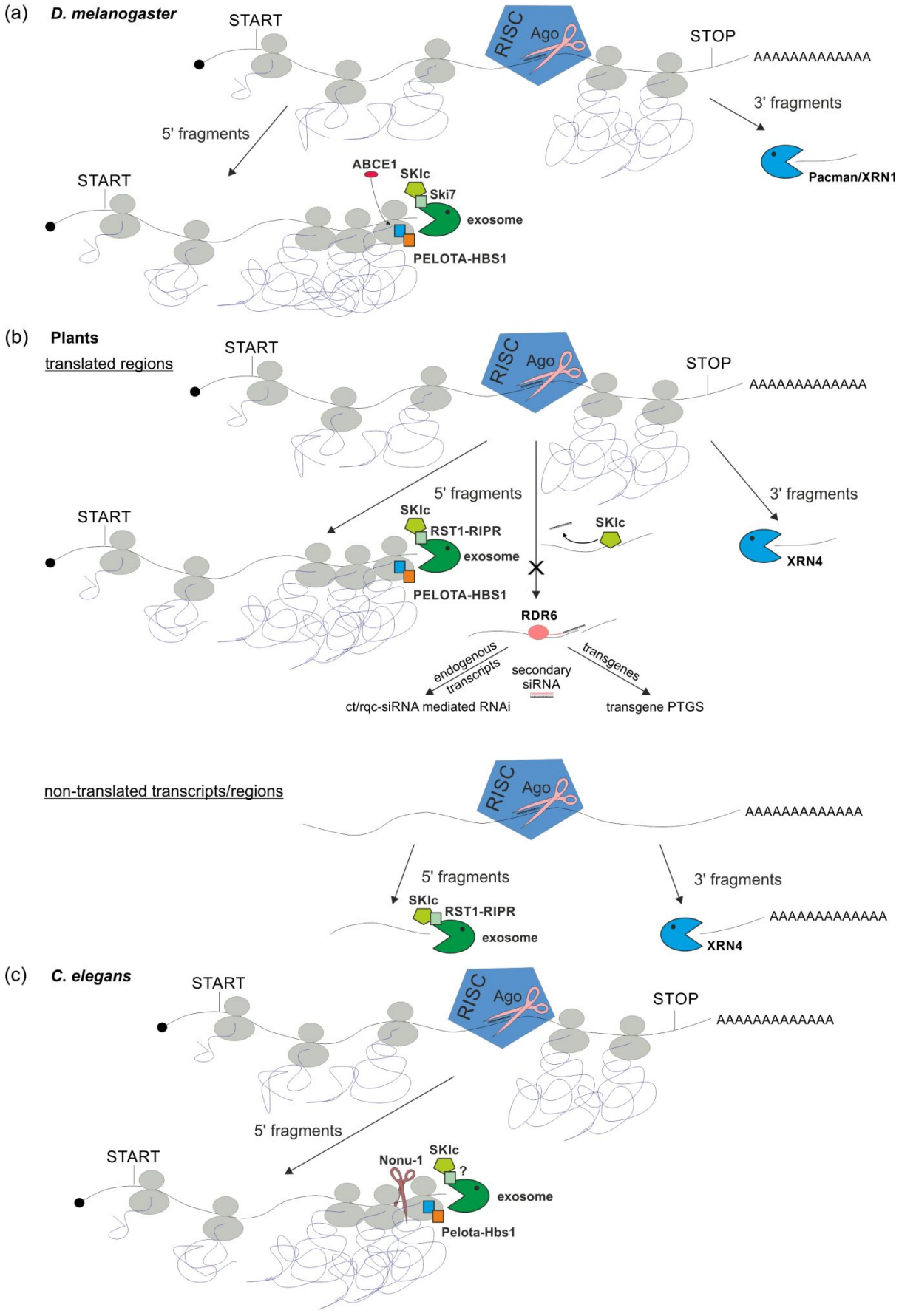
(a)
D. melanogaster
START
RISC
Ago
STOP
AAAAAAAAAAAAA
3' fragments
5' fragments
Pacman/XRN1
START
ABCE1
SKIc
Ski7
exosome
PELOTA-HBS1
(b)
Plants
translated regions
START
RISC
Ago
STOP
AAAAAAAAAAAAA
5' fragments
3' fragments
START
SKIc
RST1-RIPR
exosome
SKIc
XRN4
PELOTA-HBS1
RDR6
endogenous transcripts
secondary siRNA
transgenes
ct/rqc-siRNA mediated RNAi
transgene PTGS
non-translated transcripts/regions
RISC
Ago
AAAAAAAAAAAAA
5' fragments
3' fragments
SKIc
RST1-RIPR
exosome
XRN4
AAAAAAAAAAAAA
(c)
C. elegans
START
RISC
Ago
STOP
AAAAAAAAAAAAA
5' fragments
START
Nonu-1
SKIc
?
exosome
Pelota-Hbs1

FIGURE 6 SKIc is engaged in RNAi across eukaryotic species. (a-c) RNAi-targeted transcripts undergo RISC-mediated endonucleolytic cleavage performed by Ago2 or its counterparts, depending on the species. Cleavage generates 5' fragments and 3' fragments upstream and downstream of the Ago action site, respectively. Both fragments become available to exoribonucleases. 3' fragments are degraded from 5' to 3' end by Xrn1 homologs – Pacman in fruit fly (*a*) and XRN4 in plants (*b*). 5' fragments are digested from 3' to 5' end by the exosome (*a-c*). Degradation of 5' fragments is translation-dependent, reminiscent of NSD. Ribosomes stalled on stop codon-less transcript fragments are released by PELOTA-HBS1 and ABCE1 rescue factors, with the involvement of SKIc. Ribosome dissociation is accompanied by transcript degradation by the exosome in assistance of SKIc, linked by Ski7 in fruit fly or via RST1-RIPR in plants (*a,b*); the identity of factor bridging SKIc with exosome in *C. elegans* is unknown (*c*). Additional SKIc role in plant RNAi, which concerns coding transcripts, is preventing RDR6 polymerase action. SKIc, taking advantage of its helicase activity, unwinds miRNA-mRNA duplexes and precludes using them for RDR6-catalyzed synthesis of secondary siRNAs: ct/rqc-siRNAs arising from endogenous mRNAs and transgene-derived siRNAs acting in PTGS (*b*, *upper panel*). Furthermore, Ago cleavage of non-translated transcripts or mRNA regions devoid of ribosomes in plants generates 5' fragments with non-protected 3'-end, easily available for degradation mediated by exosome-RST1-RIPR-SKIc (*b*, *lower panel*). In *C. elegans* secondary cut between collided trailing and leading ribosomes is performed by NGD endonuclease, NONU-1 (*c*).

Regulation of silencing amplification in plants is further supported by NSD, which acts in cooperation with RNAi pathway in this group of organisms, and may facilitate SKIc recruitment (Szadeczky-Kardoss, Csorba, et al., 2018). Since RISC siRNA- or miRNA-guided cleavage usually occurs in the mRNA coding region, it generates truncated non-polyadenylated 5' proximal fragments, which are in fact stop codon-less transcripts (Figure 6b). Upon their translation, ribosomes stall at 3'-ends, so that such RNAs fulfill the criteria for entering the NSD pathway. Indeed, PELOTA-HBS1 proved to be indispensable for elimination of the 5' cleavage products generated by viral siRNA- (vsiRISC) or miRNA-programmed RISC (miRISC) (Figure 6b), and this was observed for reporter transcripts as well as for endogenous miRNA targets, in both *N. benthamiana* and *A. thaliana* models (Szadeczky-Kardoss, Csorba, et al., 2018). Importantly, protein-coding transcripts cleaved within 3'-UTRs or non-coding (*i.e.* non-translated) RNAs targeted with miRNAs evaded NSD-mediated removal of the 5' RISC cleavage products, indicating that the ongoing protein synthesis is a prerequisite for

NSD to occur, similar to other organisms. It should be emphasized, however, that SKIc, probably in conjunction with the exosome, participates in the decay of transcripts cleaved by vsi- or miRISC within 3'-UTR, independently of NSD, and thus plays broader role in RNAi than ribosome rescue factors (Szadeczky-Kardoss, Csorba, et al., 2018) (Figure 6b).

Silencing of *RST1* or *RIPR* encoding SKIc-exosome bridging factors resulted in the accumulation of vsiRISC- or miRISC-generated 5' cleavage products (Auth et al., 2021). Furthermore, *RST1* mutations suppressed transgene silencing, and RST1 restricted production of transgene-derived siRNAs and ct/rqc-siRNAs originating from endogenous PTGS-prone mRNAs, together with RIPR and the exosome (Lange et al., 2019). A substantial overlap between ct-/rqc-siRNAs accumulating in *cer7*, *rst1*, and *ripr* mutants emerged from sequencing of small RNA libraries. These findings collectively indicate that the interaction network involving exosome, RST1-RIPR, and SKIc maintains homeostasis of small regulatory RNAs and mRNAs, warranting balance between RNA silencing and degradation mechanisms to prevent synthesis of deleterious rqc-siRNAs and to counteract illegitimate RNAi amplification at silencing-prone endogenous targets (Figure 6b).

A fate of ribosomes stuck at the 3'-terminus of mRNA fragments generated during RNAi was recently illuminated by studies in *C. elegans* (Pule et al., 2019). This experimental model was advantageous compared to *D. melanogaster* or mammalian cells, in which mutations of genes coding for PELOTA-HBS1 led to inviability. Similar to fruit fly and plants, elimination of the 5' products of RISC cleavage in *C. elegans* relied on the SKIc action (Figure 6c). Interestingly, ribosome density on RNAi targets was several-fold lower in dsRNA-treated animals than would be expected from reduction

of RNA levels alone, indicating that some additional layer of regulation resulting from coupling RNAi to ongoing translation exists. Indeed, introduction of mutations in *pelo-1* and *skih-2* genes simultaneously did not abolish RNAi competence of the nematode, and resulted in ribosome stalling at and upstream mRNA cleavage sites (Figure 6c). These findings documented that messengers are prone to RNAi during protein synthesis and that ribosomes are actively dissociated by SKIc and PELO during or following transcript cleavage. Moreover, secondary mRNA cuts could be executed further upstream initial cleavage site by NONU-1 endonuclease, which breaks the transcript in-between collided trailing and leading ribosomes (Glover et al., 2020) (Figure 6c). Ribosomes, which accumulate at the 3'-ends of fragments arising from such re-iterated cuts, are also released by PELO with the help of SKIc (Figure 6c). On the whole, RNA interference could be considered as yet another co-translational mRNA decay pathway, closely related to NSD and NGD, in which collaborative action of the SKIc and PELOTA-HBS1 is indispensable for efficient rescue of the stalled ribosomes.

3.6 Involvement of SKIc in the unfolded protein response in *S. pombe*

Among processes leading to generation of stop codon-less transcripts is regulated Ire1-dependent mRNA decay (RIDD), representing one of the branches of the unfolded protein response (UPR) characteristic to *S. pombe* and higher Eukaryotes, but absent in *S. cerevisiae*. UPR is activated when the folding capacity of the endoplasmic reticulum (ER) is insufficient to deal properly with protein overload, and it involves three major interdependent mechanisms, which prevent further supply of proteins: translational inhibition, transcription reprogramming towards synthesis of ER chaperones, and dedicated degradation of ER-associated mRNAs via RIDD (Hetz et al., 2020; Maurel et al., 2014).

The latter involves incision of ER-associated protein-coding transcripts by Ire1 endoribonuclease, followed by exoribonucleolytic elimination of the cleavage fragments (Maurel et al., 2014) (Figure 7). Since such transcripts serve as templates for translation, ribosomes stall at the 3'-ends of fragments upstream cleavage site and must be disassembled, analogous to NGD or NSD. Genetic screen revealed that mutations in genes coding for Dom34, Hbs1, Ski2, and Ski7 sensitized fission yeast to ER stress (Guydosh, Kimmig, et al., 2017). Accordingly, ribosome profiling experiments showed accumulation of short, 15-18 nt reads in *dom34Δ/ski2Δ*, indicative of ribosome stalling, and this applied to approximately ¼ of *S. pombe* mRNAs, meaning that a subset of mRNAs subjected to RIDD is much more abundant than previously assumed (Guydosh, Kimmig, et al., 2017). A significant fraction of ribosome footprints terminated at guanosine within short UGC motifs, known to represent Ire1 cleavage sites, which are sliced between G and C (Figure 7). Most of Ire1 targets containing UGC sites coded for proteins with transmembrane domains, likely anchored in the ER membrane (Guydosh, Kimmig, et al., 2017). Among the remaining Ire1-targeted mRNAs, nearly a quarter was cleaved at sites deviating from UGC consensus by only 1 nucleotide. Non-UGC motifs represented mostly secondary cleavage sites, exerted by Cue2 at the 5' side of the stalled ribosome (Guydosh, Kimmig, et al., 2017) (Figure 7). Closer inspection of ribosome positioning in *S. pombe* strains deleted for *SKI2* and *DOM34* genes individually or in combination showed that ribosome rescue by Dom34-Hbs1 and degradation of mRNA fragment upstream cleavage site with the involvement of the SKIc both contribute to coupling RIDD with NGD pathway (Guydosh, Kimmig, et al., 2017). These discoveries have broader implications for NGD mechanism, indicating that ribosomes act as rulers

that precisely space iterative secondary cleavages upstream primary cleavage site and that stacking of collided ribosomes commonly occurs in the course of this process.

FIGURE 7 SKIc involvement in *S. pombe* UPR. ER overload with proteins entails incorrect protein folding and activates UPR. One of the UPR pathways is RIDD, which leads to dedicated degradation of ER-associated mRNAs. Transmembrane endonuclease Ire1 cleaves RIDD targets, usually within UGC motifs. Most transcripts targeted by RIDD encode proteins with ER membrane-anchoring domains. mRNA incision by Ire1 results in ribosome stalling at newly generated 3'-end of transcripts, which are reminiscent of NGD substrates. No-go endonuclease Cue2 cleaves mRNAs upstream of the initial Ire1 cut, at the 5' side of leading stalled ribosome, and this process could be re-iterated. Eventually, SKIc and exosome linked by Ski7, as well as Dom34-Hbs1 cooperatively lead to mRNA degradation and release of stalled ribosomes, similar to NGD.

Collectively, *S. pombe* RIDD converges in NGD-like mechanism, wherein the action of the SKIc followed by exosome-mediated degradation ensures that truncated transcripts with ribosomes detained at their 3'-termini are eradicated to prevent synthesis of shortened proteins. Whether SKIc and exosome functions in RIDD are evolutionary conserved among higher Eukaryotes remains to be examined.

4. TRICHOHEPATOENTERIC SYNDROME (THES) – A MAJOR CLINICAL MANIFESTATION OF THE SKIc DYSFUNCTION IN HUMANS

Mutations in *SKIV2L* and *TTC37* (see Figures 11a and 12a for respective gene structures), encoding two out of three SKIc subunits, are the genetic cause underlying severe human disease – the

trichohepatoenteric syndrome (THES). Such association underscores a fundamental physiological SKIc role in humans.

THES is a rare disease (<140 cases identified worldwide; an estimated prevalence of <1/1,000,000) (Fabre et al., 2013; Goulet et al., 2008), inherited in an autosomal recessive manner (Fabre et al., 2014; Fabre et al., 2013), with probably the first case described in 1982 (Stankler et al., 1982) and subsequent ones reported in the 90s of the last century (Girault et al., 1994; Verloes et al., 1997). The name originates from some clinical symptoms observed in affected individuals. Sometimes, an alternative term SD (syndromic diarrhea) can be encountered, however it is rather uncommon nowadays.

THES molecular basis remained unexplored until the second decade of the current century, when SKIc dysfunction was indicated as the likely genetic cause by genome-wide linkage screens, followed by sequencing of the candidate genes – first by identification of THES patients with mutations in *TTC37* (Fabre et al., 2011; Hartley et al., 2010), and then by finding the presence of mutations within *SKIV2L* in other affected individuals, for which *TTC37* sequencing revealed wild-type status (Fabre et al., 2012). Due to two different molecular etiologies, two THES entries are present in the OMIM database, namely THES1 (MIM #222470; *TTC37* mutations) and THES2 (MIM #614602; *SKIV2L* mutations). While this differentiation emphasizes THES genetic heterogeneity, from the functional and clinical viewpoints the condition can be considered as one disease, irrespective of the affected gene.

Identification of mutations in two genes encoding SKIc subunits unequivocally confirmed the link between molecular functions of the SKIc-exosome network and THES as a Mendelian disorder (Fabre & Badens, 2014). Nonetheless, the exact mechanisms underlying this connection still remain largely unexplored.

Apart from THES, potential impact of *SKIV2L* and/or *TTC37* mutations has been suggested in other disorders, *e.g.* age-related macular degeneration (McKay et al., 2009), inflammatory bowel disease (Kammermeier et al., 2014), and common variable immunodeficiency disorders (van Schouwenburg et al., 2015). However, due to low incidence, lack of follow-up studies, and possible failure to identify full spectrum of characteristic THES symptoms, particularly in the two latter cases, it is uncertain whether they indeed represent disease entities distinct from THES. Furthermore, *SKIV2L* mutation was recently identified in a pediatric patient suffering from mitochondrial disease (Riley et al., 2020). This issue deserves further in-depth investigation, taking into account that mitochondrial dysfunction was demonstrated at approximately the same time in *Drosophila* model with disrupted *ski3/TTC37* gene (Ohnuma et al., 2020).

4.1 THES symptoms and disease management

THES is homogenous at the level of clinical signs. According to its name, THES involves impairment of functions of many organs and systems. There are 7-9 typical THES symptoms (Figure 8). Three of them are present in the vast majority of cases: 1) intractable chronic diarrhea, usually with early onset, leading to malabsorption and failure to thrive; 2) facial dysmorphism (coarse features, hypertelorism, broad flat nasal bridge, prominent forehead and cheeks, low-set ears, large mouth);

and 3) hair abnormalities (fragile/brittle, sparse, coarse, woolly, patchy, uncombable, easily removable, and poorly pigmented hair with *trichorrhexis nodosa*) (Fabre et al., 2014; Fabre et al., 2012; Fabre et al., 2013; Fabre et al., 2011). Another two symptoms are very frequent: 4) intrauterine growth restriction (IUGR); and 5) immunodeficiency (reflected by *e.g.* hypogammaglobulinemia in IgG; monoclonal hyper IgA; T and NK cell lymphopenia; hyper IgM; reduced number of memory B cells and low counts of switched memory B lymphocytes; impaired IFN-γ production by T and NK cells, associated with a reduced degranulation of NK cells, which indicates problem with their activation following *e.g.* pharmacological stimulation; defects in antibody production after vaccination – decreased or absent response; increased vulnerability to frequent opportunistic viral and bacterial infections) (Chong et al., 2015; Fabre et al., 2014; Fabre et al., 2012; Fabre et al., 2013; Fabre et al., 2011; Kinnear et al., 2017; Kristal et al., 2022; Vely et al., 2018). The next two symptoms are frequent and include: 6) skin abnormalities (xerosis; rubbery skin; lentigines; *café-au-lait* spots – sometimes hyperpigmentation is limited to specific body parts, such as pelvic girdle and lower limb in a cohort of patients from Saudi Arabia; one extreme case of *pyoderma gangrenosum*-like skin lesions was also described) (Chong et al., 2015; Fabre et al., 2014; Fabre et al., 2012; Fabre et al., 2013; Karaca Edeer et al., 2019; Monies et al., 2015); and 7) liver disease (mildly elevated liver enzymes, hepatic hemangiomas, siderosis, fibrosis, cirrhosis) (Fabre et al., 2014; Fabre et al., 2012; Fabre et al., 2013). Some authors expand this spectrum of clinical signs by two less frequent symptoms, *i.e.*: 8) congenital cardiac defects (particularly in the Asian population) (Fabre et al., 2017; Fabre et al., 2014; Fabre et al., 2012; Fabre et al., 2013; W. I. Lee et al., 2016); and 9) platelet abnormalities (Fabre et

al., 2017; Fabre et al., 2014; Fabre et al., 2012; Fabre et al., 2013; Hartley et al., 2010). Other anomalies detected in THES patients include: enteric symptoms (colitis, intestinal villous atrophy; abnormal sorting and/or decreased expression of several brush-border transport proteins, such as: Na^+/H^+ exchangers, aquaporin 7, Na^+/I^- symporter and the H^+/K^+ ATPase, on the apical surface of jejunal enterocytes, was demonstrated by immunohistochemistry (Hartley et al., 2010), hypoglycemia (Gao et al., 2022; Xinias et al., 2018), dental abnormalities (Karaca Edeer et al., 2019), premature birth with low birth weight (Fabre et al., 2012; Fabre et al., 2013), short stature (below 3rd percentile in 50% of individuals) (Fabre et al., 2014; M. Yang et al., 2022), and mild mental retardation (Fabre et al., 2014). Due to such a wide spectrum of symptoms, the prognosis is poor and one of THES characteristics is high mortality rate (up to 50%) – many patients die before the age of 5-10 and just a few affected individuals survived up to the third decade (Fabre et al., 2014).

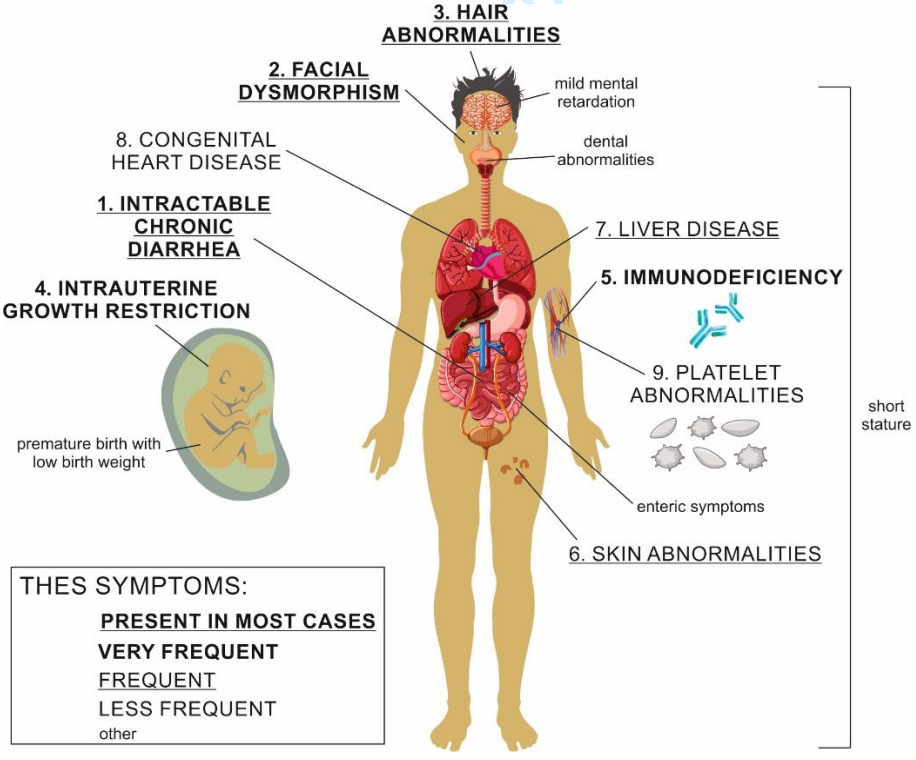

FIGURE 8 Broad spectrum of clinical symptoms, which affect multiple tissues and organs, is observed in THES patients. 9 major symptoms are numbered and highlighted with different fonts (see rectangular inset box for explanations) to illustrate the differences in the frequency, with which they are identified in different cases of the disease. Minor, less recurring symptoms are marked with lowercase. Assets freely available at freepik.com (human body and fetus images) were used for the preparation of this illustration.

In line with the major symptoms, THES management involves mainly parenteral nutrition/feeding support (essential in >80% of patients; can last from several months to several years; even in rare cases with no diarrhea, problems with oral feeding may exist, due to *e.g.* abdominal distension), and temporary or long-term immunoglobulin supplementation, provided that the immune defects are observed (Fabre et al., 2017; Fabre et al., 2014). The latter treatment led to efficient diminution of infection and/or reduction of diarrhea (Fabre et al., 2017; Rider et al., 2015). The data on the maintenance of diet regime are inconclusive. In turn, the use of antibiotics, steroids, immunosuppressive agents, and hematopoietic stem cell transplantation (HSCT) are not recommended, since there is no clear evidence of efficacy, and some of them can have adverse effects, such as HSCT, which is associated with increased mortality (Fabre et al., 2017; Fabre et al., 2013). The cases presenting with serious hepatic dysfunction require liver transplantation (Fabre et al., 2014; Fabre et al., 2013).

Immunological THES phenotypes are particularly significant. It was suggested that THES could be classified as a primary immunodeficiency within the class of 'combined immunodeficiencies with associated or syndromic features' (Bousfiha et al., 2018; W. I. Lee et al., 2016). In several THES cases, recurring bacterial infections despite continuous antibiotic prophylaxis, and rapidly declining titers of antibodies specifically targeting causative pathogen upon immunization, were documented

(Rider et al., 2015). Specific antibody deficiencies with impairment of humoral memory suggest a possible SKIc role in adaptive immune function. This entails the need for immunoglobulin replacement therapy, which allows to reduce the use of antibiotics and increase resistance to infection. In addition, severe viral infections were reported, caused mainly by herpesviruses, such as Epstein-Barr virus (EBV) in 50% of *TTC37*-mutated patients in a French cohort (Vely et al., 2018) or cytomegalovirus (CMV), leading to fulminant pneumonitis in a patient of Somalian descent (Kinnear et al., 2017). In all these cases, the low natural killer (NK) cell count was noted. Since NKs play a role in recognizing and eliminating virus-infected cells, this defect potentially makes the cells extraordinarily susceptible to viral infections. Moreover, strong elevation in the interferon-stimulated genes (ISGs) expression, suggestive of type I interferon overproduction, was found in the peripheral blood samples from two individuals with severe THES symptoms, harboring mutations in *SKIV2L* (Eckard et al., 2014), but not in another patient with *SKIV2L* dysfunction, in whom the clinical symptoms were considerably milder (Hiejima et al., 2017). This allowed to speculate that the disease severity and type I interferon production might be correlated, and that ISGs expression levels may represent THES marker with prognostic value. These latter examples imply that immune defects in THES patients could be somehow linked to SKIc antiviral functions, which we discuss in one of the following sections of this review.

4.2 An overview of THES-associated mutations in *SKIV2L* and *TTC37*

Although THES symptoms are nowadays well-described and understood, reliable genetic testing is indispensable to confirm that they are due to mutations in the genes encoding SKIc components.

SKIV2L or *TTC37* mutations are generally the only ones identified in THES patients. One reported exception was the case with homozygous *AKR1D1* mutation apart from *SKIV2L* mutation (Morgan et al., 2013). While most of the phenotypic features characteristic for THES were due to SKIc dysfunction, mutation in *AKR1D1*, encoding an enzyme from bile acid biosynthesis pathway, could additionally contribute to liver disease (Morgan et al., 2013). Another report revealed the case with overlapping features of THES and a mild form of multiple intestinal atresia with combined immunodeficiency (MIA-CID); however, no mutations in *SKIV2L* and *TTC37* were identified; instead, compound heterozygous mutations in *TTC7A*, unrelated to SKIc, encoding a TPR protein involved in the RhoA signaling pathway, were found (Neves et al., 2018). Both these cases illustrate the need for broad-ranging genetic analysis, particularly when overlapping phenotypes or unobvious disease manifestation are observed.

4.2.1 General mutation statistics, worldwide distribution and occurrence

The advent and rapid progress of the whole-exome next-generation sequencing, along with reduction of its costs, greatly facilitated identification of mutations. Therefore, a number of patients diagnosed with THES has increased substantially over the last dozen years. We have been able to collect information on 138 THES cases (Tables 3 and 4; Figures 9-12) due to mutations, which could be either homozygous, compound heterozygous or affect only one allele (heterozygous state, although THES is generally an autosomal recessive disorder, as stated above) in both *SKIV2L* or *TTC37*. Numerical data on the distribution of mutations between the two genes are presented in the Figure 9a-d.

Most mutation sets were found uniquely in different single families, irrespective of the gene affected. For *SKIV2L* only 6 mutation sets (5 homozygous and 1 compound heterozygous) were observed in at most 2 unrelated families (***mut 3***, ***mut 7***, ***mut 8***, ***mut 20***, ***mut 22***, and ***mut10/mut41***; Table 3). One mutation – c.3561_3581del, p.Ser1189_Leu1195del (***mut 32***, Table 3) – was exceptionally recurrent, and noted in 21 families, mainly from Saudi Arabia (Figure 10) (Alsaleem et al., 2022). This is due to high rate of consanguineous marriages in this world region, and thus the incidence of THES in the Middle East is much higher than in the global population (~1/200,000). Another mutation reported for several cases was c.3187 C>T, p.Arg1063* (***mut 10***), found in one homozygous, one heterozygous, and two different compound heterozygous sets in 5 unrelated families (6 cases in total), representing various geographical locations (Europe, Asia, North America; Table 3 and Figure 10). Yet another mutation – c.1891 G>A, p.Gly631Ser (***mut 26***) was identified in homozygous set in one family from Middle East and in two different compound heterozygous sets in two Chinese families (Table 3 and Figure 10) (W. S. Lee et al., 2016; Vardi et al., 2018; B. Zheng et al., 2016). Moreover, each of the following three mutations – c.2479 C>T, p.Arg827* (***mut 5***), c.2662_2663 delAG, p.Arg888Gly fs*12 (***mut 7***), and c.1452 delC, p.Val485Cys fs*45 (***mut 15***) – was found in two different mutation sets, in at least two unrelated families (Table 3 and Figure 10).

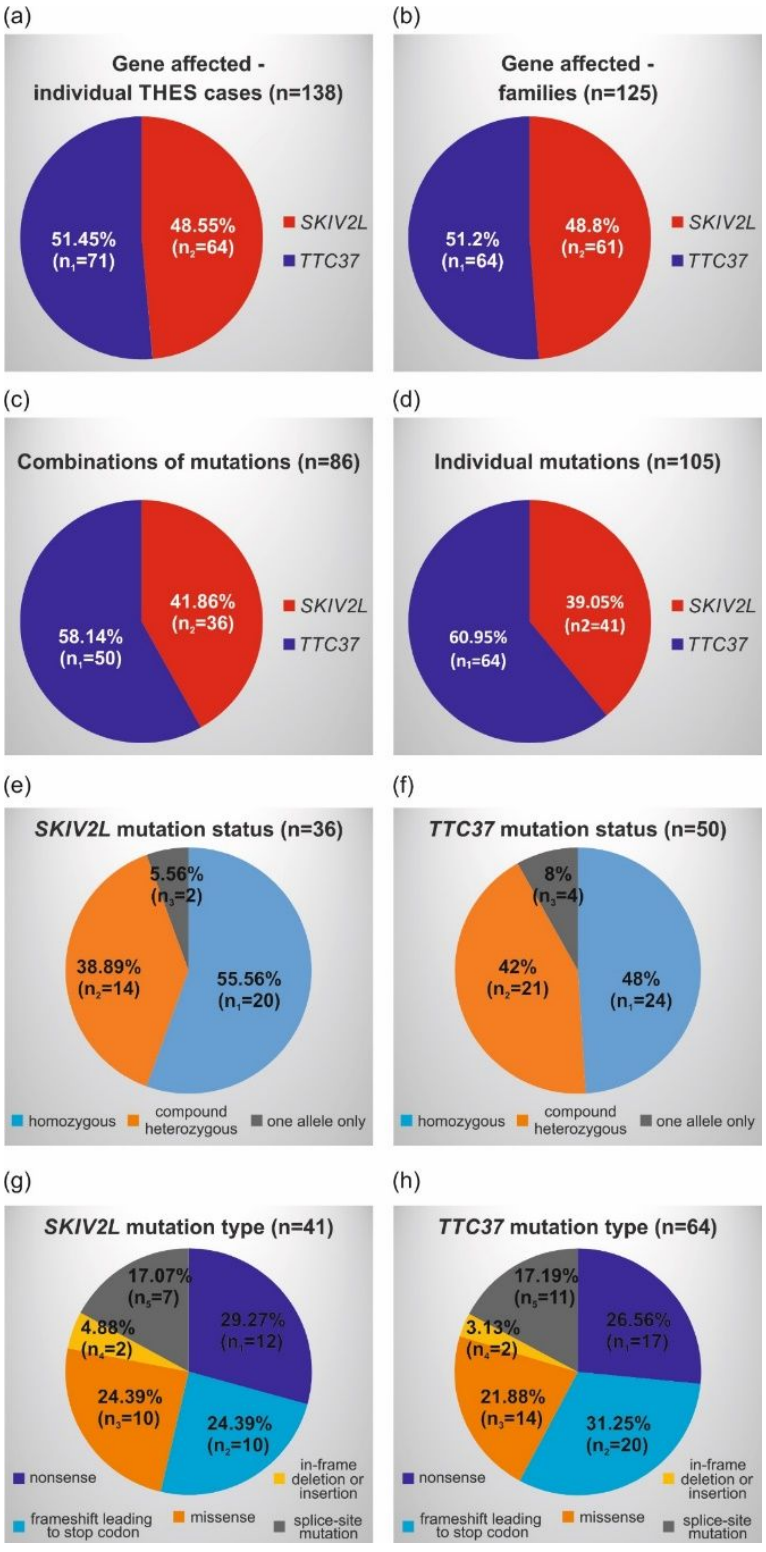

FIGURE 9 General THES-associated mutations statistics. (a-d) Percentage and number (in parentheses) of: (*a*) mutations in *SKIV2L* (red) and *TTC37* (dark blue), identified in 138 individual THES cases; (*b*) mutations in *SKIV2L* and *TTC37* in 125 families, where THES cases were identified; (*c*) different combinations of mutations in *SKIV2L* and *TTC37* among 86 sets detected in total; (*d*) individual mutations in *SKIV2L* and *TTC37* among 105 detected in total. (e-f) Percentage and number (in parentheses) of mutation sets identified as homozygous (blue), compound heterozygous (orange) or affecting one allele only (grey) in THES patients with impaired *SKIV2L* (*e*) or

TTC37 (*f*) gene function. (g-h) Percentage and number (in parentheses) of mutation types (nonsense – dark blue; frameshift leading to the immediate appearance of the termination codon – blue; missense – orange; in-frame deletion/insertion – yellow; splice site mutation – grey) identified in THES patients with *SKIV2L* (*g*) or *TTC37* (*h*) mutations.

Regarding *TTC37*, 5 mutation sets were identified in at most 2 unrelated families (***mut G***, ***mut I***, ***mut AP***, ***mut AZ***, and ***mut BA***; Table 4). In addition, mutation 2808 G>A, p.Trp936* (***mut J***) was found in homozygous state in 6 families (5 South Asian and 1 North American – 7 cases in total; Table 4 and Figure 10). Its recurrent character in conjunction with geographical occurrence suggested that it may be a founder mutation in the Gujarat state in India and adjoining areas in Pakistan (Kotecha et al., 2012; W. I. Lee et al., 2016) (Figure 10). Further, c.3507 T>G, p.Tyr1169* (***mut T***), found in three distinct compound heterozygous sets in 3 families from China, Cambodia, and Taiwan (Table 4 and Figure 10), is apparently a founder mutation amongst the East Asians (Chong et al., 2015; W. I. Lee et al., 2016). These two nonsense mutations, along with 2779-2G>A, p.Glu974Gly fs*19 (***mut I***) frameshift/nonsense discovered in two Pakistani families (Hartley et al., 2010) (Table 4 and Figure 10), in combination with overall higher incidence of nonsense mutations and heart anomalies, are features that seemingly differentiate Asian from non-Asian THES patients (W. I. Lee et al., 2016). On the other hand, c.4572 G>A, p.Trp1524* mutation (***mut P***), reported as usually homozygous in 6 families (9 individuals in total), mainly from Middle East (Table 4 and Figure 10), was defined as recurrent one in patients of Turkish origin living in different countries. In several cases, the mother and father were first cousins, documenting that consanguinity contributes to increased incidence of mutations, as expected for autosomal recessive disorders (Fabre et al., 2018). Finally,

c.4514 T>C p.Leu1505Ser mutation (***mut AQ***) was identified in three different families of European origin, albeit in distinct mutation sets (Table 4 and Figure 10).

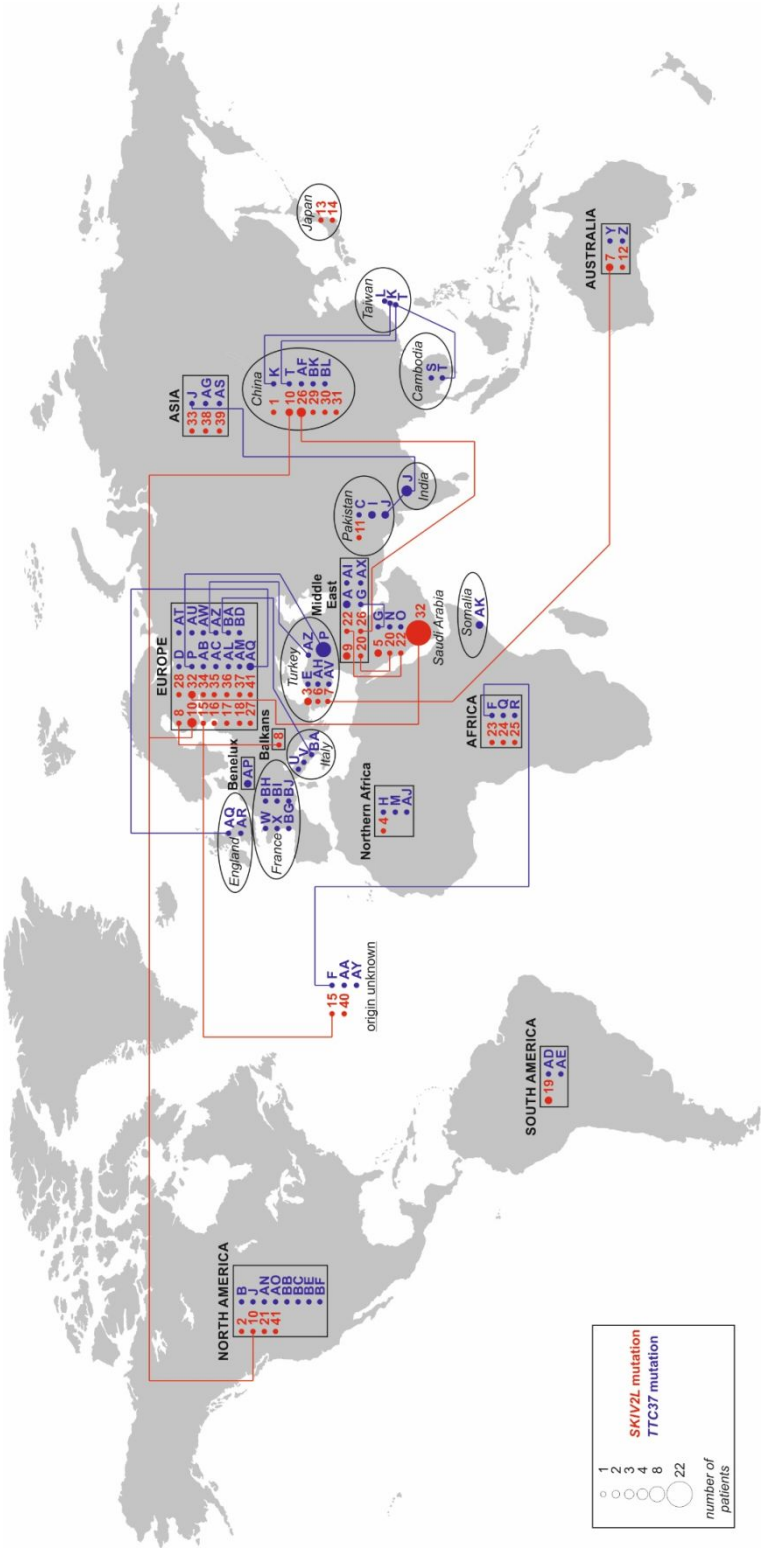

FIGURE 10 Global distribution of individual THES-associated mutations in *SKIV2L* (red) and *TTC37* (dark blue). Unless precise information about the country (italicized), in which a given THES case was identified, was

provided in the original publication (instances marked with ovals), mutations are categorized under the names of world regions (bolded capitalized case) or continents (bolded upper case) within rectangular boxes. Size of the filled circle next to the mutation name corresponds to the number of patients carrying the same mutation (see inset box in the bottom left corner). Red (*SKIV2L*) and dark blue (*TTC37*) lines connect identical mutations found in different world locations. Names of mutations (numerical symbols 1-41 for *SKIV2L*; letter symbols A-BL for *TTC37*) match the data presented in Tables 3 and 4. World contour freely available at freepik.com was used for the preparation of this illustration.

4.2.2 Types, genetic location and possible consequences of mutations for SKI2 and TTC37 protein functions

In the case of *SKIV2L* homozygous mutations are the most prevalent, followed by compound heterozygous status and mutations of the single allele (Table 3 and Figure 9e). The most numerous class includes nonsense substitutions and frameshift mutations (mainly caused by out-of-frame deletions) leading to an immediate stop codon appearance, resulting in SKI2W truncations (Table 3 and Figure 9g). These mutations are uniformly spread along the sequence, and no clear hot-spot can be indicated (Figure 11b). 6 of them principally lead to the removal of only the C-terminal HB domain or its fragments (Figure 11b). The other 6 result in the production of protein variants lacking both HB and an entire Arch/insertion domain or at least the C-terminal half of the latter (Figure 11b). Another 5 mutations of this type further truncate SKI2W towards its N-terminus, so that the protein is devoid of HB, Arch, and – either completely or partly – RecA2 domain (Figure 11b). 3 variants represent proteins encompassing only SKI2W N-terminus, optionally with a half of the RecA1 domain, and the 2 most extreme truncations terminate within the N-terminal inner segment (Figure 11b). Biochemical and functional characterization of truncated SKI2W variants is missing, except for a recent report which demonstrated that in four cases equivalent mutations in the simple yeast model led to growth defect at elevated temperature in the background of temperature-sensitive *dcp2* allele (Orlando et al.,

2022). Based on the structural insights, it can be hypothesized that most of causative mutations are loss-of-function (LOF), and that such proteins are unable to support normal SKIc function, either due to lack of enzymatic activity and/or inability to mediate proper interactions with remaining SKIc subunits. Furthermore, PTC-containing transcripts may be targeted to NMD, which would result in decreased levels of aberrant mRNA and encoded protein. Indeed, nonsense mutations led to diminished SKI2W synthesis, detected by flow cytometry and western blot analysis in peripheral blood mononuclear cells (PBMCs), in which the physiological levels of SKI2W (and TTC37) are high. Thus, these methods could be used for rapid screening for SKI2W (and TTC37) deficiency (Hiejima et al., 2017).

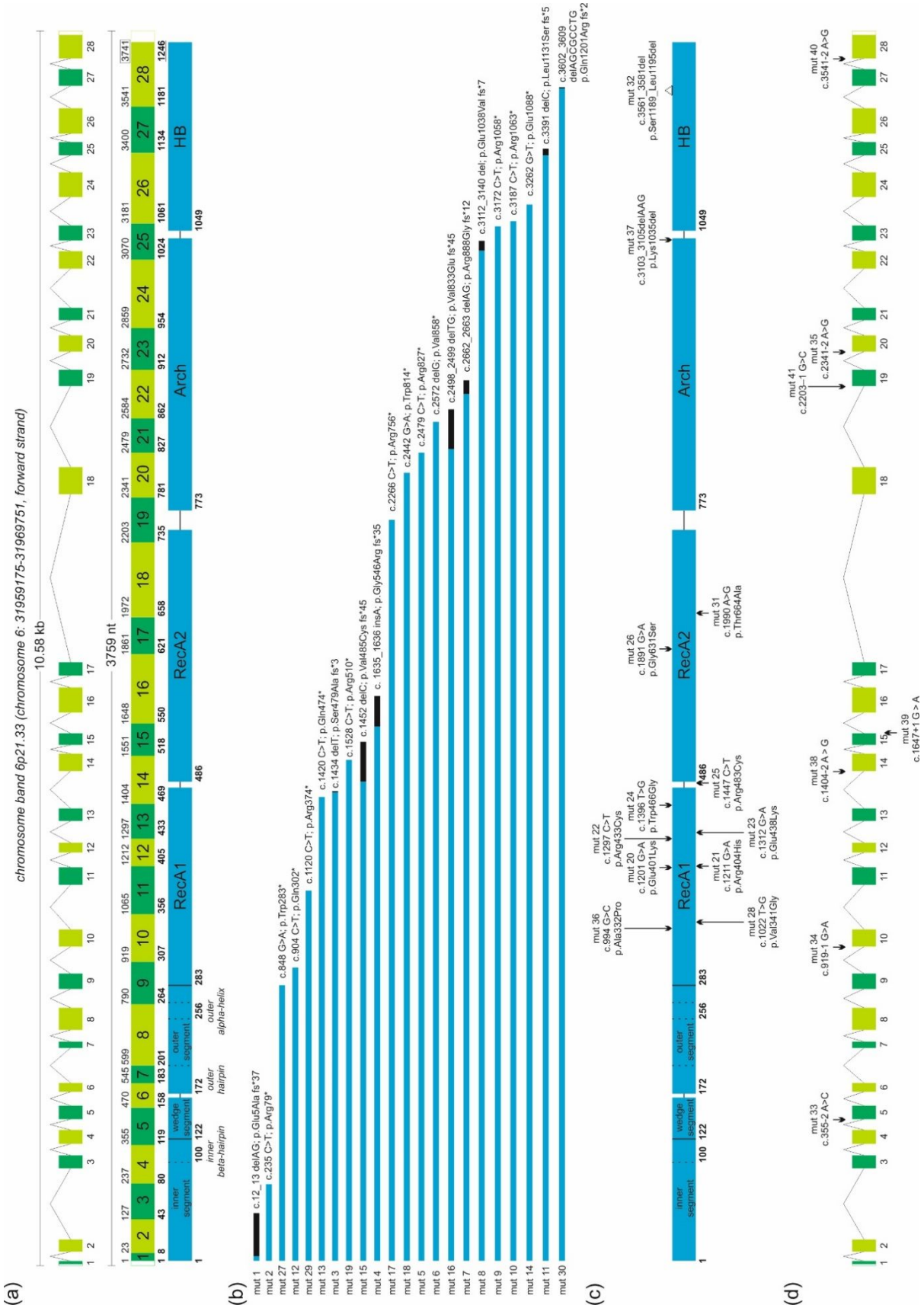
(a)
chromosome band 6p21.33 (chromosome 6: 31959175-31969751, forward strand)
10.58 kb
3759 nt
inner segment
wedge segment
outer segment
RecA1
RecA2
Arch
HB
inner beta-hairpin
outer hairpin
outer alpha-helix
(b)
mut 1 c.12_13 delAG; p.Glu5Ala fs*37
mut 2 c.235 C>T; p.Arg79*
mut 27 c.848 G>A; p.Trp283*
mut 12 c.904 C>T; p.Gln302*
mut 29 c.1120 C>T; p.Arg374*
mut 13 c.1420 C>T; p.Gln474*
mut 3 c.1434 delT; p.Ser479Ala fs*3
mut 19 c.1528 C>T; p.Arg510*
mut 15 c.1452 delC; p.Val485Cys fs*45
mut 4 c. 1635_1636 insA; p.Gly546Arg fs*35
mut 17 c.2266 C>T; p.Arg756*
mut 18 c.2442 G>A; p.Trp814*
mut 5 c.2479 C>T; p.Arg827*
mut 6 c.2572 delG; p.Val858*
mut 16 c.2498_2499 delTG; p.Val833Glu fs*45
mut 7 c.2662_2663 delAG; p.Arg888Gly fs*12
mut 8 c.3112_3140 del; p.Glu1038Val fs*7
mut 9 c.3172 C>T; p.Arg1058*
mut 10 c.3187 C>T; p.Arg1063*
mut 14 c.3262 G>T; p.Glu1088*
mut 11 c.3391 delC; p.Leu1131Ser fs*5
mut 30 c.3602_3609 delAGCGCCTG p.Gln1201Arg fs*2
(c)
mut 36 c.994 G>C p.Ala332Pro
mut 22 c.1297 C>T p.Arg433Cys
mut 20 c.1201 G>A p.Glu401Lys
mut 24 c.1396 T>G p.Trp466Gly
mut 26 c.1891 G>A p.Gly631Ser
mut 21 c.1211 G>A p.Arg404His
mut 25 c.1447 C>T p.Arg483Cys
mut 31 c.1990 A>G p.Thr664Ala
mut 28 c.1022 T>G p.Val341Gly
mut 23 c.1312 G>A p.Glu438Lys
mut 37 c.3103_3105delAAG p.Lys1035del
mut 32 c.3561_3581del p.Ser1189_Leu1195del
(d)
mut 33 c.355-2 A>C
mut 34 c.919-1 G>A
mut 38 c.1404-2 A > G
mut 39 c.1647+1 G > A
mut 41 c.2203–1 G>C
mut 35 c.2341-2 A>G
mut 40 c.3541-2 A>G

FIGURE 11 Distribution of THES-associated mutation in *SKIV2L* with regard to gene structure and protein domains. (a) *Upper part*: *SKIV2L* gene spans the region of 10.58 kb and comprises 28 exons (numbered 1-28 and marked as dark and light green rectangles) and 27 introns (represented by polylines); *middle part*: resulting transcript is 3759 nt-long and encodes SKI2W containing 1246 amino acids; larger numbers inside green rectangles indicate exons; small numbers above indicate positions of the exon-exon boundaries in mature *SKIV2L* transcript and are based on the numbering of the coding sequence; bolded numbers below indicate corresponding amino acid positions in SKI2W protein; *bottom part* (in blue): location of structural domains, crucial for SKI2W activity and interactions with other SKIc subunits; SKI2W N-terminal subdomains are further specified; numbers below indicate positions of the first amino acids in particular segments. (b) Schematic representation of truncated SKI2W variants, arising as a result of 22 mutations introducing PTC (13 nonsense and 9 frameshift), lined up from the most extreme at the top to the most benign at the bottom; blue segments correspond to natural SKI2W amino acid sequence; black segments represent divergent C-terminal extensions, generated due to out-of-frame insertions or deletions. (c) Location of 10 missense mutations and 2 in-frame deletions, with respect to protein domains. (d) Location of 7 splice site mutations with respect to the gene structure (6 mutations affecting 3'ss are indicated above, and 1 mutation affecting 5'ss is shown below). Arbitrary names of *SKIV2L* mutations (numerical symbols 1-41) match the data presented in Table 3.

Notwithstanding, LOF is not a pre-requisite for disease manifestation, since the second most numerous class of THES *SKIV2L* mutations are missense ones (Figure 9g). 7 and 2 of them lead to amino acid substitutions within RecA1 and RecA2 domains, respectively, and the remaining one affects residue located between RecA domains (Figure 11c). Contrary to truncating mutations, the outcomes of amino acid changes within SKI2W are more difficult to predict. Most web-based *in silico* pathogenicity prediction tools, such as PolyPhen-2, SIFT, MutationTaster, UMD-Predictor, LRT, Provean or MutationAssessor, indicate that all *SKIV2L* missense mutations affect highly evolutionary conserved amino acids and are deleterious, with a high degree of probability. However, these assumptions await biochemical and functional validation, exemplified by a study of Val341Gly mutation, located next to the Walker motif A (***mut 28***; Table 3 and Figure 11c), which showed loss of SKI2W ATPase activity (Kogel et al., 2022). Further, corresponding substitution in Ski2, like three other mutations within RecA enzymatic core, compromised growth of yeast strain bearing *dcp2* mutation at restrictive temperature (Orlando et al., 2022). If similar experimental approaches prove to

be unsuccessful, structural modeling would be desirable for missense mutations which could help to elucidate whether and how they alter SKIc activity, integrity or interactions with partners. Such modeling was described for Gly631Ser substitution in RecA2 domain (***mut 26***; Table 3 and Figure 11c), and underscored important differences between glycine and serine in terms of side chain size, polarity and flexibility, implying that this mutation may cause structural destabilization, affecting the entire area surrounding respective residue (Vardi et al., 2018).

Another class of THES-associated *SKIV2L* mutations encompass splice site (ss) mutations (Figure 9g) – 6 and 1 of them affect 3' (acceptor) and 5' (donor) ss, respectively (Figure 11d). The impact at the protein level is unknown, since no investigation of splicing pattern in affected individuals was performed. Presumably, such mutations lead to exon skipping or intron retention, resulting in PTC occurrence.

Two remaining *SKIV2L* mutations are in-frame deletions (Figure 9g): one leading to a single amino acid deletion (p.Lys1035del; ***mut 37***; Table 3 and Figure 11c) within the Arch domain C-terminus, and the second to elimination of several amino acids from the HB domain (p.Ser1189_Leu1195del; ***mut 32***; Table 3 and Figure 11c).

Compared to *SKIV2L*, the fraction of homozygous *TTC37* mutations is slightly lower, but still the most prevalent, followed by compound heterozygous status and mutations of the single allele (Figure 9f). At the level of individual mutations, the most numerous class includes nonsense substitutions and frameshift mutations leading to a rapid appearance of the stop codon (Figure 9h). The repertoire of events entailing frameshift mutations in *TTC37* is broader than for *SKIV2L* and

includes: out-of-frame deletions, insertions and duplications (10, 3 and 1, respectively), two 5' and two 3' splice site mutations, for which exon skipping and changes of the reading frame were confirmed, one indel, and one seemingly missense mutation in the vicinity of splice site, which in fact results in exon skipping and frameshift (Table 4 and Figure 12b). All these mutations result in the synthesis of truncated TTC37, missing a different number of TPRs, and are rather evenly distributed along the sequence, with no apparent hot-spot (Figure 12b). 8 of the truncations lacked TPRs 9-40 (Figure 12b), warranting proper interactions with SKI2W and WDR61 (Kogel et al., 2022), suggesting that corresponding mutations probably result in the impaired SKIc assembly. Further 22 truncated variants encompassed variable number of consecutive TPRs from 1 to 32, which may ensure most of the interactions with SKI2W N-term, but lacked the eight most C-terminal repeats including the region within TPRs 33-34 (Figure 12b), responsible for interaction with at least one WDR61 copy (Kogel et al., 2022), indicating that such TTC37 variants probably also fail to support correct formation of the functional SKIc. The remaining 7 truncations lacked TPRs 35-40 (entirely or partially), and two among them (p.Trp1524*; ***mut P*** and p.Tyr1525*; ***mut AE***) were only devoid of TPR40 (~last 40 amino acids of the protein) (Figure 12b).

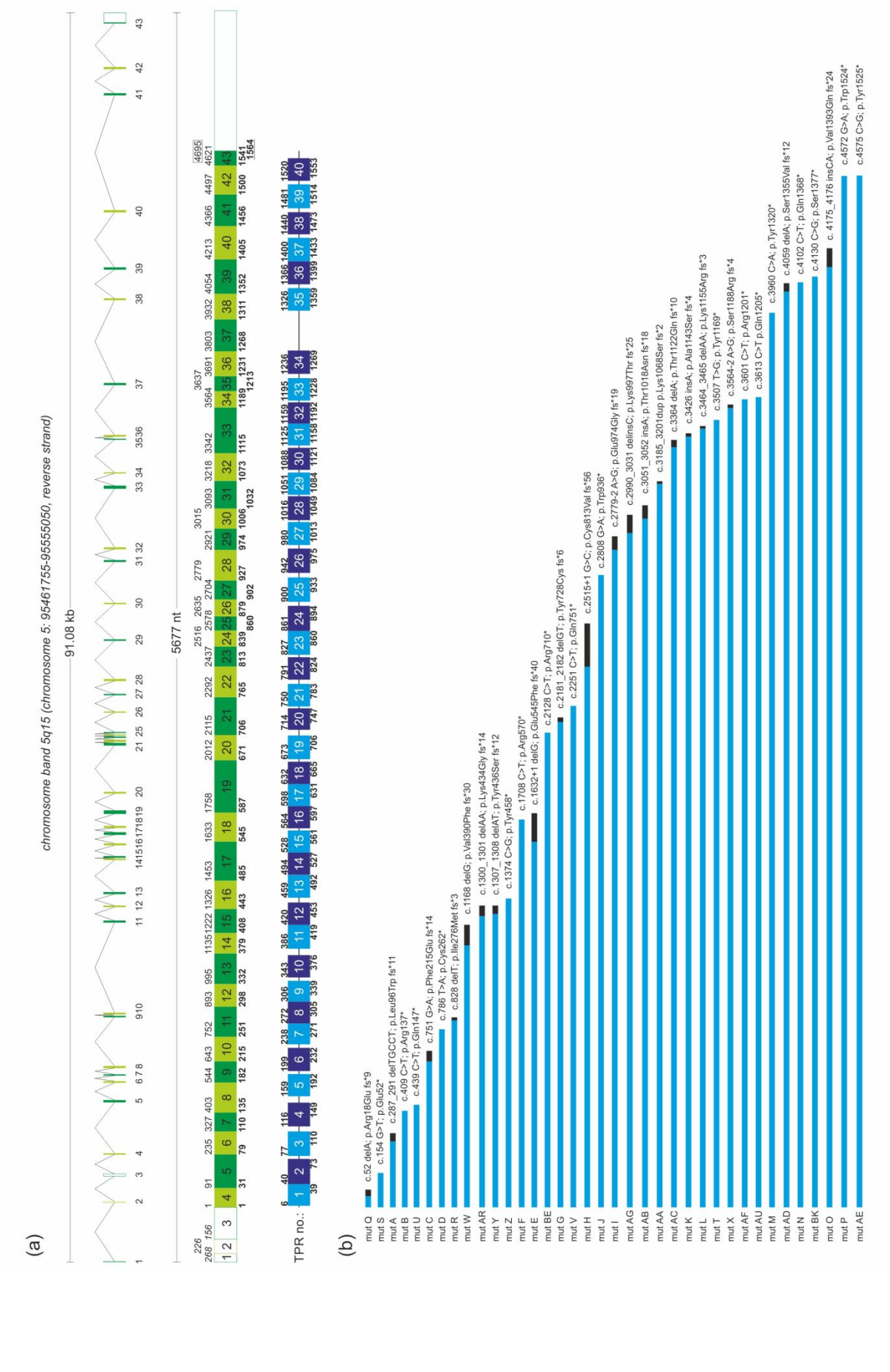
(a)
chromosome band 5q15 (chromosome 5: 95461755-95555050, reverse strand)
91.08 kb
5677 nt
TPR no.:
(b)
mut Q c.52 delA; p.Arg18Glu fs*9
mut S c.154 G>T; p.Glu52*
mut A c.287_291 delTGCCT; p.Leu96Trp fs*11
mut B c.409 C>T; p.Arg137*
mut U c.439 C>T; p.Gln147*
mut C c.751 G>A; p.Phe215Glu fs*14
mut D c.786 T>A; p.Cys262*
mut R c.828 delT; p.Ile276Met fs*3
mut W c.1168 delG; p.Val390Phe fs*30
mut AR c.1300_1301 delAA; p.Lys434Gly fs*14
mut Y c.1307_1308 delAT; p.Tyr436Ser fs*12
mut Z c.1374 C>G; p.Tyr458*
mut F c.1708 C>T; p.Arg570*
mut E c.1632+1 delG; p.Glu545Phe fs*40
mut BE c.2128 C>T; p.Arg710*
mut G c.2181_2182 delGT; p.Tyr728Cys fs*6
mut V c.2251 C>T; p.Gln751*
mut H c.2515+1 G>C; p.Cys813Val fs*56
mut J c.2808 G>A; p.Trp936*
mut I c.2779-2 A>G; p.Glu974Gly fs*19
mut AG c.2990_3031 delinsC; p.Lys997Thr fs*25
mut AB c.3051_3052 insA; p.Thr1018Asn fs*18
mut AA c.3185_3201dup p.Lys1068Ser fs*2
mut AC c.3364 delA; p.Thr1122Gln fs*10
mut K c.3426 insA; p.Ala1143Ser fs*4
mut L c.3464_3465 delAA; p.Lys1155Arg fs*3
mut T c.3507 T>G; p.Tyr1169*
mut X c.3564-2 A>G; p.Ser1188Arg fs*4
mut AF c.3601 C>T; p.Arg1201*
mut AU c.3613 C>T p.Gln1205*
mut M c.3960 C>A; p.Tyr1320*
mut AD c.4059 delA; p.Ser1355Val fs*12
mut N c.4102 C>T; p.Gln1368*
mut BK c.4130 C>G; p.Ser1377*
mut O c. 4175_4176 insCA; p.Val1393Gln fs*24
mut P c.4572 G>A; p.Trp1524*
mut AE c.4575 C>G; p.Tyr1525*

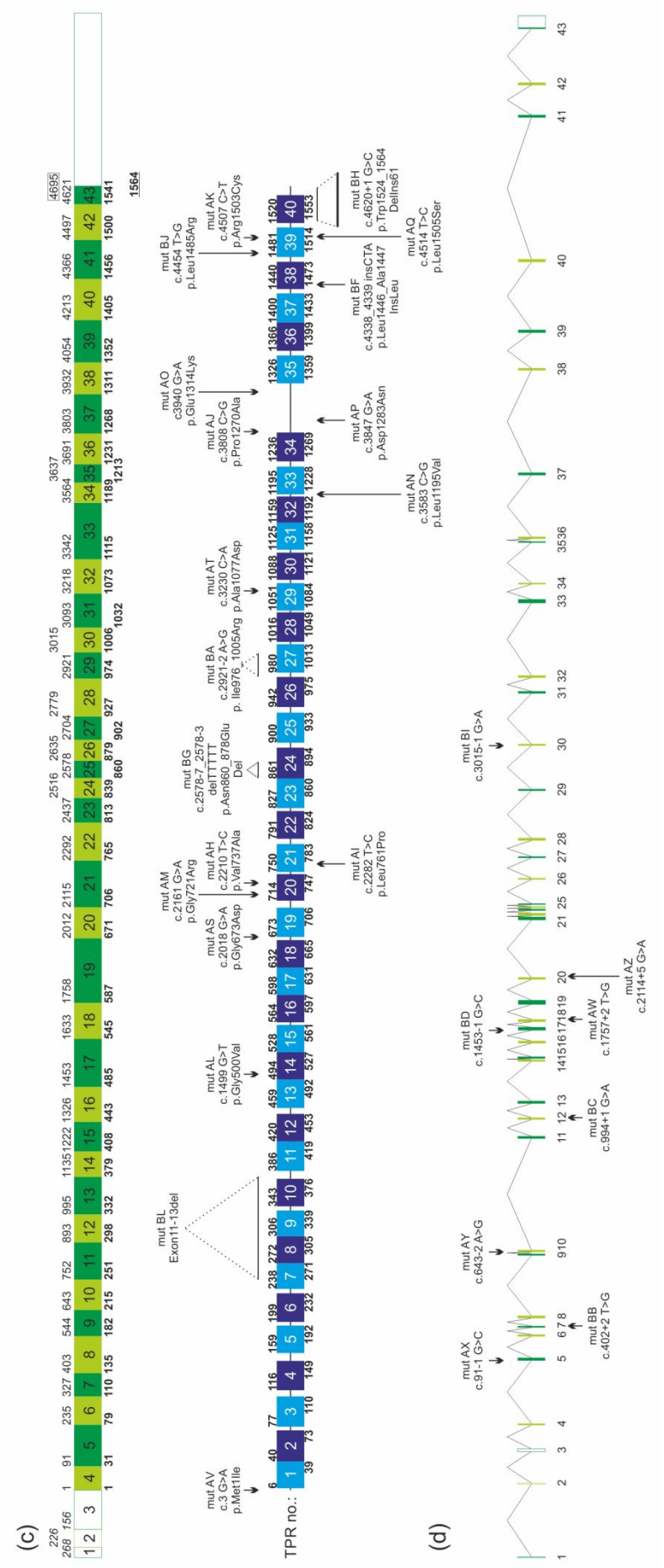
(c)
TPR no.:
mut AV c.3 G>A p.Met1Ile
mut BL Exon11-13del
mut AL c.1499 G>T p.Gly500Val
mut AM c.2161 G>A p.Gly721Arg
mut AS c.2018 G>A p.Gly673Asp
mut AH c.2210 T>C p.Val737Ala
mut AI c.2282 T>C p.Leu761Pro
mut BG c.2578-7_2578-3 delTTTTT p.Asn860_878Glu Del
mut BA c.2921-2 A>G p. Ile976_1005Arg
mut AT c.3230 C>A p.Ala1077Asp
mut AN c.3583 C>G p.Leu1195Val
mut AP c.3847 G>A p.Asp1283Asn
mut AJ c.3808 C>G p.Pro1270Ala
mut AO c.3940 G>A p.Glu1314Lys
mut BJ c.4454 T>G p.Leu1485Arg
mut AK c.4507 C>T p.Arg1503Cys
mut AQ c.4514 T>C p.Leu1505Ser
mut BF c.4338_4339 insCTA p.Leu1446_Ala1447 InsLeu
mut BH c.4620+1 G>C p.Trp1524_1564 DelIns61
(d)
mut AX c.91-1 G>C
mut BB c.402+2 T>G
mut AY c.643-2 A>G
mut BD c.1453-1 G>C
mut BC c.994+1 G>A
mut AW c.1757+2 T>G
mut BI c.3015-1 G>A
mut AZ c.2114+5 G>A

FIGURE 12 Distribution of THES-associated mutations in *TTC37* with regard to gene structure and TTC37 TPRs. (a) *Upper part*: *TTC37* gene spans the region of 91.08 kb and comprises 43 exons (numbered 1-43 and marked as dark and light green rectangles, except for exons 1-3, which are non-coding and thus marked as white rectangles) and 42 introns (represented by polylines); *middle part*: resulting transcript is 5677 nt-long and encodes TTC37 protein containing 1564 amino acids; larger numbers inside dark and light green rectangles indicate exons; small numbers above coding exons indicate positions of the exon-exon boundaries in mature *TTC37* transcript and are based on the numbering of the coding sequence; italicized small numbers above non-coding exons 1-3 indicate the distance between their 5'-end and translation initiation codon present in exon 4; bolded numbers below indicate corresponding amino acid positions in TTC37 protein; *bottom part:* location of 40 TPR motifs (marked as light and dark blue rectangles), crucial for TTC37 scaffolding functions; numbers above and below each TPR indicate their boundaries. (b) Schematic representation of truncated TTC37 variants, arising as a result of 37 mutations introducing PTC (17 nonsense, 16 frameshift, and 4 splice site mutations), lined up from the most extreme at the top to the most benign at the bottom; blue segments correspond to natural TTC37 amino acid sequence; black segments represent divergent C-terminal extensions, generated due to out-of-frame insertions, deletions or splice site mutations. (c) Location of 14 missense mutations, and 5 other mutations: insertion, deletion, and 3 splice site mutations, which result in the in-frame changes at the protein level, with respect to TPRs. (d) Location of the remaining 8 splice site mutations with respect to the gene structure (4 mutations affecting 3'ss are indicated above and 4 other mutations, affecting 5'ss are shown below). Arbitrary names of *TTC37* mutations (letter symbols A-BL) match the data presented in Table 4.

The other groups of *TTC37* mutations ranked by frequency are: missense mutations, splice site mutations, small in-frame deletions, small in-frame insertion, large in-frame deletion, and large in-del (Figure 9h). Some splice site mutations (***mut E***, ***mut H***, ***mut I***, ***mut X***; Table 4 and Figure 12b) are known to result in frameshift and generation of PTC, and are classified herein within *'nonsense and frameshift mutations resulting in the rapid emergence of stop codon'*, based on the same eventual outcome. The 8 remaining splice site mutations constituting a separate group include four 3'ss (acceptor) and four 5'ss (donor) changes, the impact of which at the protein level remains unexplained (Figure 12d).

Analyzing the location of mutations within TTC37 primary structure, several interesting observations can be made. One of the missense mutations (c.3 G>A, p.Met1Ile; ***mut AV***; Table 4) leads to the loss of initiation codon. Considering that no other in-frame AUG is present in the vicinity

of natural *TTC37* start triplet, and assuming that no non-AUG initiation is possible, this mutation potentially results in the lack of protein production. Furthermore, at least two sequence regions presumably represent mutational hot-spots. One of them encompasses TPRs 19-21, where 4 missense mutations were identified, namely p.Gly673Asp (***mut AS***), p.Gly721Arg (***mut AM***), p.Val737Ala (***mut AH***), and p.Leu761Pro (***mut AI***) (Table 4 and Figure 12c). Structural inspection suggested that they may adversely affect folding of one of the TTC37 superhelices, which wraps around the SKI2W N-terminal inner segment (Kogel et al., 2022). The second hot-spot comprises fragment downstream TPR34, where 8 mutations leading to different amino acid sequence changes (Figure 12c). This region has no equivalent in the several repeats shorter yeast Ski3. Furthermore, while TTC37 TPRs 1-34 are densely packed, the distance between TPR34 and TPR35 is nearly 60 amino acids (Figure 12c), suggesting that the 6 most C-terminal TPRs could have been acquired later in evolution. Three of the 8 mutations (p.Pro1270Ala; ***mut AJ***, p.Asp1283Asn; ***mut AP***, and p.Glu1314Lys; ***mut AO***; Table 4) affect amino acids in the linker between TPRs 34 and 35 (Figure 12c). Notably, Pro1270 and Asp1283 are situated in the WDR61-binding site (Kogel et al., 2022). Three other substitutions in this hot-spot are located in TPR39 (p.Leu1485Arg; ***mut BJ***, p.Arg1503Cys; ***mut AK***, and p.Leu1505Ser; ***mut AQ***; Table 4), and the two remaining mutations include: a single amino acid insertion in TPR38 (***mut BF***; Table 4), and a large indel (deletion of ~40 amino acids with concomitant insertion of 61 residues; ***mut BH***; Table 4) in TPR40 (Figure 12c). Structural organization of the extended C-terminus into further TPRs, and the presence of THES-associated mutations in this region implicates that it is functionally relevant. Indeed, one of the

substitutions in TPR39, changing hydrophilic, positively charged Arg1503 into hydrophobic, uncharged cysteine able to form disulfide bridges (***mut AK***; Table 4), was suggested to interfere with proper TTC37 folding (Kinnear et al., 2017), most probably with the formation of the fourth superhelical turn (Kogel et al., 2022). Although this mutation is located close to C-terminus, it had fatal outcome in the patient suffering from immunodeficiency, leading to severe CMV pneumonitis and death at 3 months of age (Kinnear et al., 2017).

4.2.3 Less typical THES cases argue against the existence of genotype-phenotype correlation

The association between severity of THES manifestation and location of *SKIV2L* or *TTC37* mutations is unclear. Individuals with *SKIV2L* dysfunction were shown to suffer from more severe liver disease and had significantly lower growth parameters at birth than patients with *TTC37* deficiency (Bourgeois et al., 2018). Several case reports seem to confirm that *TTC37* mutations might indeed result in slightly milder disease presentation than *SKIV2L* mutations. For instance, no hepatic symptoms, immunodeficiency, or less frequent THES features including cardiac, cutaneous, and platelet abnormalities were observed in a patient bearing homozygous *TTC37* mutation c.2282 T>C, p.Leu761Pro (***mut AI***; Table 4 and Figure 12c), who had only certain facial dysmorphism, minor hair abnormalities, and mild congenital diarrhea (Oz-Levi et al., 2015). Similarly, no chronic diarrhea and liver disease was described in an individual with homozygous *TTC37* mutation c.2210 T>C, p.Val737Ala (***mut AH***; Table 4 and Figure 12c), affecting neighboring TPR (Karaca Edeer et al., 2019) or in the patient with *TTC37* allele encoding severely truncated protein (c.2128 C>T, p.Arg710*; ***mut BD***; Table 4 and Figure 12c) (Rider et al., 2015). However, the two latter cases presented with

immunodeficiency and recurring infections. The most C-terminal *TTC37* mutation described to date in a homozygous state (c.4572 G>A, p.Trp1524*; ***mut P***, Table 4 and Figure 12c) resulted in clearly milder THES symptoms – approximately half of the patients displayed better growth rate and higher survival age than the majority of affected individuals; most of them did not have IUGR and did not require parenteral nutrition; no cardiac defects were noted and only one patient had skin abnormalities; moreover, normal values of immunoglobulins were reported, only mild elevation of liver enzymes and low frequency of hepatomegaly was observed; finally, all patients tended to improve with increased age (Fabre et al., 2018). Since the site of truncation in the mutant variant is localized only forty amino acids upstream normal TTC37 C-terminus (Figure 12c), it is possible that despite being slightly shortened, the protein is still able to fulfill most of its functions within SKIc, which suggests that at least part of the additional TTC37 C-terminal extension might not be critical for interaction with WDR61 subunits (Fabre et al., 2018). On the other hand, contradictory reports on the effects of amino acid substitutions in this region (see above) indicate that such interpretation should be treated with caution.

Diarrhea is present in the vast majority of disease cases, but is not absolutely an intrinsic symptom, even in individuals with *SKIV2L* mutations, which argues against using the term 'syndromic diarrhea' as an alternative name for THES. For instance, no diarrhea was described in the patient bearing two different *SKIV2L* variants, both likely resulting in detrimental SKI2W truncations: c.904 C>T, p.Gln302* (***mut 12***; Table 3 and Figure 11b) and c.2662_2663 delAG, p.Arg888Gly fs*12 (***mut 7***; Table 3 and Figure 11b) (Poulton et al., 2019). Furthermore, no IgG replacement therapy was

required in this patient. Curiously though, theoretically less harmful ***mut 7*** in the homozygous state was associated with later onset diarrhea and severe combined immunodeficiency in a patient, who additionally presented with *Pneumocystis jirovicii* pneumonia (PJP) and postnatally acquired CMV infection (Hosking et al., 2018). On the other hand, the female patient with homozygous mutation leading to production of the most severely truncated SKI2W among all cases studied (c.12_13 delAG, p.Glu5Ala fs*37; ***mut 1***; Table 3 and Figure 11b), who suffered from mild diarrhea in the neonatal period, was able to survive until the age of >30 years, which allowed to observe novel symptoms, *i.e.* premature menopause and osteoporosis (M. Yang et al., 2022). All these examples show that it is virtually impossible to capture any logical correlation between specific genotypes and phenotypes of THES patients.

5. MISCELLANEOUS SKIc FUNCTIONS IN THE REGULATION OF ANTIVIRAL DEFENSE SYSTEMS, CELL SIGNALING, AND DEVELOPMENTAL TRANSITIONS

5.1 SKIc and antiviral responses

5.1.1 SKIc subunits and Ski7 as components of the antiviral system in yeast

SKIc constituents and some associated factors were identified in the two last decades of the 20th century as central components of the antiviral system in *S. cerevisiae* during genetic screens and collectively named *superkiller* (alias suppressor of killer). Those screens were related to studies of toxin production by yeast encoding the L-A dsRNA virus, belonging to *Totivirus* genus, and its satellites. The L-A virus propagates exclusively via mitosis and during yeast mating. Toxin production and secretion is associated with infection with a satellite virus M and provides a selective advantage

over uninfected yeast cells due to associated toxin resistance (McBride et al., 2013; Wickner, 1992, 1996a, 1996b). Protein products of *ski* genes are components of the dedicated yeast antiviral system, which decreases copy number of L-A dsRNA virus and its satellites. The characteristic features of the *superkiller 1-2-3-4-5-6-7-8* yeast mutants phenotype were an increased copy number of M satellite virus and elevated M toxin production (Toh-E et al., 1978; Wickner, 1996b). Respective proteins were later functionally characterized to play roles related mostly to RNA degradation. Of all the Ski proteins in yeast only Ski2, Ski3, Ski8, and Ski7 retained their names, while Ski1 (Xrn1 5'-3' exoribonuclease), Ski4, and Ski6 (Csl4 and Rrp41 subunits of the exosome) were renamed upon later characterization.

The L-A and M satellite dsRNA viruses produce decapped and non-polyadenylated RNAs, whose translation efficiency should be expected to be very low, if not for the L-A-encoded major coat protein Gag, which binds to 5' cap and removes this protective structure from cellular mRNAs. The increased number of decapped endogenous transcripts in the presence of the virus was proposed to attract Xrn1, and thus 'hide' the viral RNAs from the major cellular decay system by titration of this predominant degradative exonuclease (Wickner, 1996a) (Figure 13). Such 'decoy' mechanism is reminiscent of the function of structured non-capped RNAs produced by viruses infecting higher Eukaryotes (MacFadden et al., 2018; Markiewicz et al., 2021; Masison et al., 1995). Importantly, caps eliminated from host cellular messengers during such process are not 'stolen' by the virus, *i.e.* they are not subsequently transferred onto viral transcripts. Importantly, an undisturbed Gag-mediated decapping is essential for the expression of viral information only in the wild-type yeast strain, but not in the *xrn1Δ* background.

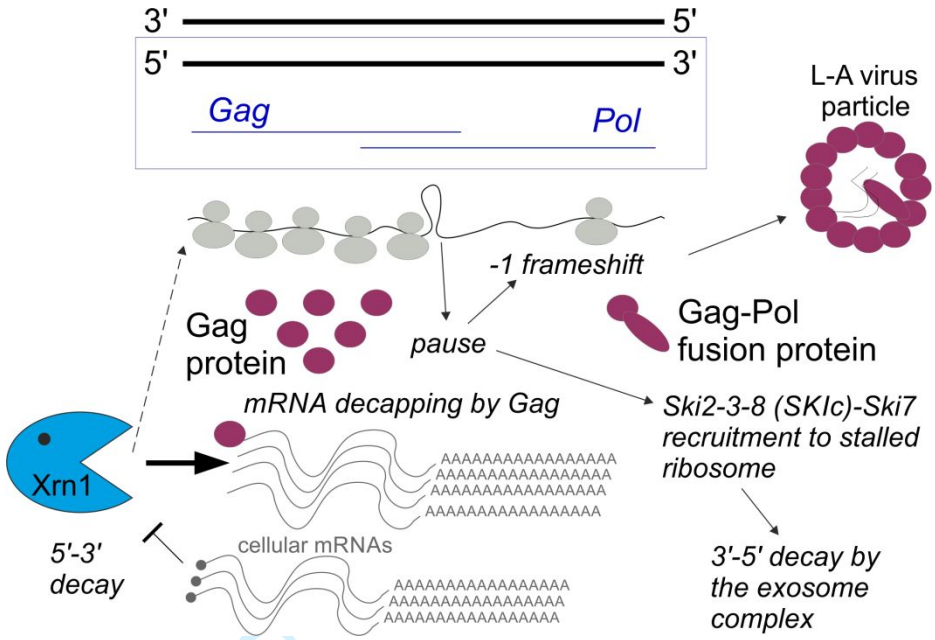

FIGURE 13 An overview of *S. cerevisiae* dsRNA L-A virus biogenesis, showing the role of cellular factors involved in RNA degradation in curbing virus propagation, and mechanisms used by the virus to counteract their activity. The double-stranded L-A RNA virus contains two ORFs under a single translation initiation signal. The first ORF serves as a template for the synthesis of the coat protein (Gag), the second encodes the RNA-dependent RNA polymerase (Pol). Production of Pol protein fused to Gag requires a -1 frameshift, which is facilitated by ribosome pausing at a strong secondary structure. Gag protein, aside from its structural role, triggers decapping of cellular mRNAs. This diverts Xrn1 5'-3' exonuclease activity from targeting viral transcripts, which are less effectively delivered to the major cytoplasmic decay pathway. However, the virus RNA levels are also controlled by the SKI and exosome complexes, which are effectors of mRNA quality control pathways triggered by ribosome stalling: NSD and NGD.

Works on *ski2-3-7-8* mutants pointed towards a strong function in curbing translation of de-capped and non-polyadenylated viral RNAs, in addition to reducing the dsRNA viruses copy number, which is characteristic for all *superkiller* mutations (Masison et al., 1995; Widner & Wickner, 1993). Moreover, the *ski2-3-7-8* network was at least comparably effective in blocking translation from capped and non-polyadenylated reporter transcripts, which provided the first hint towards the physiological role of those genes (Benard et al., 1999; Masison et al., 1995; Wickner, 1996a, 1996b). Additional data shedding light on the SKIc function came from studies in human cells, where the Ski2 ortholog – SKI2W (encoded by *SKIV2L*) – co-purified with the 40S ribosomal subunit (Qu et al., 1998),

indicating that some Ski proteins functions might be translation-dependent. These early investigations revealed that co- and posttranscriptional modifications of mRNA termini are key elements of the race between the virus and the host RNA degradation systems. Despite the former evades Xrn1 activity by hiding the lack of the 5' cap structure on its transcripts, SKI antiviral system ensures translational repression of non-polyadenylated RNAs. Thus, 5'-terminal 7-methylguanosine cap and 3'-terminal poly(A)-tail serve as marks, allowing to differentiate between 'self' and 'non-self' RNAs. It was also assumed that Ski proteins may eliminate fragmented cellular RNAs devoid of the poly(A)-tail, in addition to viral RNAs, and this was later experimentally confirmed.

In light of current knowledge, the impact of *ski2-3-7-8* network on virus propagation can be interpreted more accurately. The L-A virus plus (+) strand contains two ORFs; the first one codes for Gag protein with decapping activity, and the second encodes the RNA-dependent RNA polymerase (Pol), both of which overlap by 130 nt. Gag and Pol are encoded in different frames. Pol is only expressed in fusion with Gag, upon -1 ribosomal frameshift occurring in 1.9% of translation events. The frameshifting segment is adjacent to a secondary structure that induces ribosome pausing (Wickner, 1996a) (Figure 13). Later works documented the *ski2-3-7-8* network involvement in endogenous mRNA quality control mechanisms induced by ribosome pausing, namely NSD and NGD, which have been described in previous sections of this review. Other mutations affecting L-A virus propagation were identified in the genes encoding 60S ribosome protein subunits (Wickner, 1996a), and might impact ribosome assembly or translation efficiency.

While Ski7 is not an integral SKIc component, it displayed antiviral properties analogous to SKIc subunits within the same regulatory system, including inhibition of non-polyadenylated mRNA expression, irrespective of the cap presence (Benard et al., 1999). High similarity of Ski7 to translational GTPases, such as EF1α, eRF3, and Hbs1, playing roles in translation elongation, termination, and mRNA surveillance, respectively, combined with an increased sensitivity of *ski7* mutant to hygromycin B and cycloheximide protein synthesis inhibitors, suggested that Ski7 and SKIc functions are linked to translation (Benard et al., 1999), which was later well-documented, as discussed in details above.

5.1.2 Antiviral SKIc functions in humans

The antiviral SKIc functions are not limited to yeast, although mechanistic details of its roles in counteracting viral infections are obviously different in budding yeast and humans, due to the higher organismal complexity, intricacy of signaling pathways, and disparate nature of infectious agents in the latter species.

A prominent example from human cells, wherein SKIc function in the regulation of NSD is utilized for restriction of viral infection, pertains to Hepatitis B virus (HBV) (Aly et al., 2016). Transcription of HBV genome gives rise to several mRNAs, all having identical polyadenylation signal and sharing the same 3'-end (Figure 14a). HBV mRNAs contain overlapping ORFs, encoding polymerase as well as surface (HBsAg), core (HBcAg), and envelope (HBeAg) antigens, the latter of which results from proteolytic processing of the pre-core protein (Figure 14a). Translation initiation codons for pre-core (upstream AUG) and core (downstream AUG) proteins are in frame. Three start

codons of HBsAg, subdividing the ORF into three parts referred to as pre-S1, pre-S2, and S, are located much further downstream pre-core/core AUGs, in the same frame. Since any of the three HBsAg initiation codon may be used first, protein variants of variable length, namely large (L: pre-S1+pre-S2+S), medium (M: pre-S2+S) or small (S: only S), are produced (Figure 14a). The smallest ORF codes for HBV X (HBx) protein (Figure 14a), which acts as a transcriptional activator. HBx-mediated induction of HBV mRNA synthesis promotes replication of the virus. In all HBV transcripts, except the shortest one, translation initiation codon for HBx lies downstream HBsAg AUGs in an alternative reading frame (Doitsh & Shaul, 2004; Gonzalez et al., 2018; Stadelmayer et al., 2020) (Figure 14a).

SKI2W emerged as a hit in a screening assay aimed at identification of helicases that regulate HBV replication. Manipulating SKI2W levels via silencing or overexpression resulted in increased or decreased HBV DNA/RNA levels, respectively. Further studies based on RNA-IP revealed that this is due to post-transcriptional regulation, and that SKI2W specifically binds HBV mRNAs, including particularly X mRNA. X mRNA-SKI2W interaction proved to be indispensable for X mRNA binding to the exosome, indicating that SKIc-assisted targeting RNA substrates to the exosome is crucial for its antiviral function in the context of HBV infection. Moreover, *HBS1L* silencing suppressed the effects of *SKIV2L* overexpression on X mRNA titers, although it remains unexplained whether it was due to weakened interaction between the SKI and exosome complexes (HBS1LV3 function) or because of disturbance of downstream events in the possible degradation pathway (HBS1LV1 function). Nevertheless, involvement of SKIc, exosome and HBS1L variants in the adjustment of X mRNA levels

allowed to conclude that it might be targeted by some cytoplasmic mRNA quality control mechanism (Aly et al., 2016). The (pre)-core initiation codons out-of-frame with regard to HBx AUG, present in the vicinity of the HBV transcripts' 3'-end, are translationally active only in the case of X mRNA (Figure 14b). Their utilization in longer HBV transcripts is precluded by the presence of upstream in-frame HBsAg start codons (Figure 14b). On the other hand, the frame containing (pre)-core AUGs in X mRNA lacks a functional termination codon (Doitsh & Shaul, 2004; Gonzalez et al., 2018; Stadelmayer et al., 2020) (Figure 14b). Therefore, if the ribosome skips the first AUG (HBx initiation site) of X mRNA, subsequent scanning of this transcript in the frame encompassing (pre)-core AUGs will eventually result in ribosome stalling at the 3'-end of message and launch NSD (Figure 14b). Introduction of stop codon in-frame with (pre)-core AUGs increased X mRNA stability and patients infected with HBV variant bearing such termination codon displayed elevated HBV DNA levels in serum (Aly et al., 2016). Altogether, an inherent X mRNA vulnerability to SKIc-dependent NSD limits HBV infectivity.

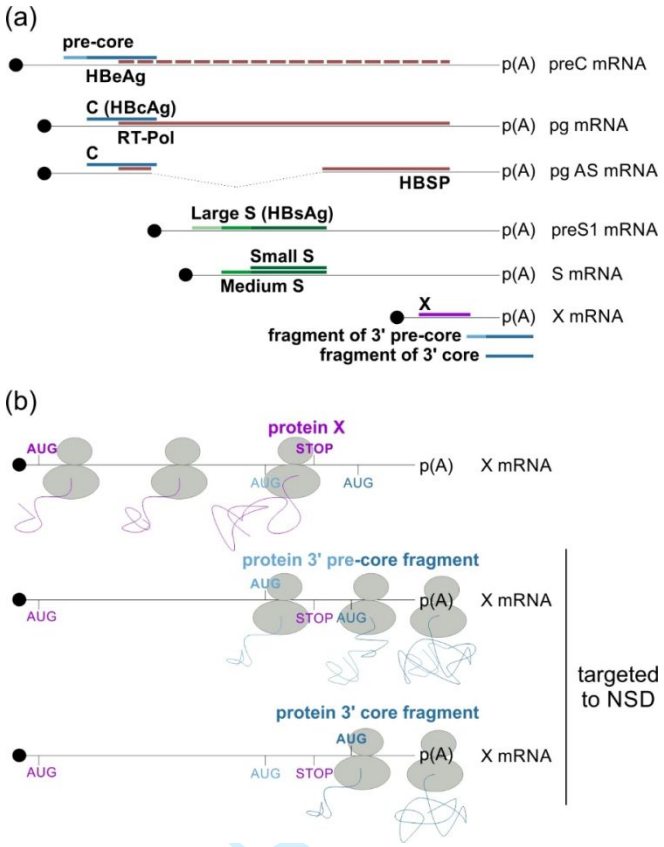

FIGURE 14 NSD helps to restrict HBV infection in human cells. (a) Six mRNAs, with the same polyadenylation signal and 3'-end, arise from HBV genome. **preC** mRNA encodes pre-core protein (light+dark blue), which undergoes proteolytic cleavages at N- and C-termini to generate envelope antigen HBeAg (dark blue); an overlapping ORF corresponds to RT-polymerase (burgundy, dashed line), which is not expressed from this transcript; **pg** mRNA gives rise to the core protein – HBcAg antigen (dark blue), and RT-polymerase (burgundy, solid line) from overlapping ORFs; **pg AS** (alternatively spliced) mRNA encodes core protein (dark blue) and HBSP (burgundy) in overlapping ORFs; **preS1** and **S** (also named preS2) mRNAs encode three surface antigens (HBsAg), translated from overlapping ORFs: the former gives rise to large S (light+mid+dark green), and the latter – to medium (mid+dark green) and small (dark green) S proteins; **X** mRNA encodes transcriptional activator, protein X (purple), which is expressed only from this transcript due to its AUG situated in an ORF alternate to frame shared by all remaining HBV transcripts; likewise, exclusively X mRNA gives rise to fragmentary 3' pre-core and 3' core proteins (see panel *b* for further details). (b) *Upper part:* Protein X (purple) is synthesized in a standard manner, *i.e.* the first AUG (bolded purple) present at the X mRNA 5'-end and STOP codon (bolded purple) are used. Instead, one of two downstream out-of-frame AUGs (light and dark blue) can be used for synthesis of fragmentary 3' (pre)-core proteins; *middle part:* when translation begins at the first of additional AUGs (bolded light blue), 3' pre-core protein fragment is synthesized; *bottom part:* alternatively, ribosomes start synthesis of the 3' core fragment (dark blue) from the downstream AUG (bolded dark blue). 3' pre-core and 3' core ORFs lack termination codon, which results in ribosome stalling during translation. In such case, X mRNAs are targeted to NSD. This in turn leads to decreased levels of HBV transcriptional activator and attenuation of protein X ability to promote replication of the virus in the cells.

Another layer of SKIc involvement in the HBV replication control is provided by the regulatory circuit of *SKIV2L* expression in the host cells. *SKIV2L* promoter activity responds to interleukin-1β (IL-1β), a key mediator of the inflammatory response. Treatment of HepG2 cells with IL-1β decreased X mRNA stability. *SKIV2L* promoter contains a cyclic AMP-responsive element (CRE), specifically bound by ATF3 transcription factor. *SKIV2L* activation and induction of X mRNA decay is dependent on *ATF3*, the expression of which is positively regulated by IL-1β. Interestingly, viral HBx augments *SKIV2L* expression synergistically with IL-1β. Such a complex network of interdependencies and feedback loops ensures that HBV replication is efficiently suppressed by the host. Induction of SKI2W production by HBx suggests that maintaining protein X levels low might be also beneficial for the virus for some reason (Shiromoto et al., 2018).

One of the key elements of host antiviral defense is associated with the potentiation of the immune response by type I interferons (IFN) (Haller et al., 2006). The link between SKIc antiviral properties and interferon response has been inspected in several recent studies. During HBV infection, SKI2W involvement in restriction of virus replication via NSD-mediated regulation of X mRNA decay was IFN-independent – *SKIV2L* expression in HepG2 cells was not prone to IFN stimulation and, conversely, no interferon induction occurred upon *SKIV2L* overexpression (Aly et al., 2016). In contrast, IFN response to uncapped, 5'-triphosphorylated RNA ligand of retinoic acid-inducible gene I (RIG-I) receptor, and to poly(I:C) dsRNA, recognized by both RIG-I and MDA5 receptors, was more robust in mouse bone marrow-derived macrophages (BMDM) subjected to *SKIV2L* silencing than in control cells (Eckard et al., 2014). RIG-I-like receptors (RLRs) detect viral

RNAs and are involved in differentiation between self and non-self transcripts (Lassig & Hopfner, 2017). SKI2W may assist in RLRs discriminatory function by specifically counteracting their illegitimate activation. In relation with this phenomenon, it was demonstrated that IRE1, which cleaves multiple protein-coding transcripts localized in the ER vicinity during UPR, may generate endogenous RNAs able to activate RLRs, particularly in SKI2W-depleted cells. The entire process was accompanied by a substantial production of IFN-β, provided that MAVS adaptor, linking RLR signaling with interferon response stimulation, was intact (Eckard et al., 2014). A potential key role of SKI2W as a negative regulator of IFN-mediated antiviral response in metazoan was supported by detection of a strong type I interferon signature in the peripheral blood of THES patients with *SKIV2L* mutations, as revealed by significant upregulation of several ISGs. Intriguingly, *TTC37* downregulation in BMDMs or mutations in THES patients did not exert similar effects, which led to an assumption that SKI2W role in the regulation of RLR-interferon axis might be unique and distinct from functions that it fulfills within SKIc in RNA metabolism. It was hypothesized that the observed difference may arise due to unique interactions of SKI2W, but not TTC37, with yet-to-be-identified protein partners outside SKIc (Eckard et al., 2014). It would be worth studying whether and how the catalytic activity of SKI2W, which – like RLRs – is an RNA-dependent ATPase/helicase, contributes to the mechanism limiting activation of RLRs (Rehwinkel & Gack, 2020). Since SKI2W should restrict RLR signaling in response to endogenous immunostimulatory transcripts, its malfunction may potentially contribute to the autoimmune disorders, but no obvious signs of autoimmunity have been reported for majority of THES patients with *SKIV2L* mutations. On the other hand, some variants of the *SKIV2L* gene, which

is localized in the central part of the major histocompatibility complex (MHC) cluster (D. Zhou et al., 2019), may predispose to an increased risk of developing an autoimmune disease, such as systemic lupus erythematosus (SLE) or inflammatory bowel disease (IBD) (Ashton et al., 2016; Fernando et al., 2007; D. Zhou et al., 2019). Furthermore, as described in more details in the subsequent section, *SKIV2L* deficiency in a transgenic mice model, was associated with skin autoinflammation (K. Yang, Han, Asada, et al., 2022).

The SARS-CoV-2 pandemic has provided the incentive to search for novel therapeutics. A suppressor screen in yeast uncovered that the influenza A virus (IAV) NS1 and a related ORF4a proteins of the Middle East respiratory syndrome coronavirus (MERS-CoV), which bind dsRNA and dampen RLR signaling and interferon response, interact genetically with SKIc subunits (Weston et al., 2020). The ability of these viral proteins to physically bind SKIc components was confirmed by co-immunoprecipitation. *SKIV2L*, *TTC37* or *WDR61* silencing with siRNA resulted in considerable decrease of IAV and MERS-CoV replication in human cell lines. Therefore, SKIc was considered as a potential novel antiviral target (Weston et al., 2020). Based on the yeast SKIc structural data and modeling, a putative binding pocket at the WDR61:TTC37 interface was proposed, and an extensive *in silico* screening of ligands that could potentially dock into this site was performed. The inhibitory effect of almost forty different potential ligands on IAV replication was assessed, and at least four compounds were identified as promising antiviral agents targeting SKIc. The two lead compounds elicited minimal cytotoxicity, and one of them displayed broad spectrum of activity – apart from IAV and MERS-CoV, it was able to inhibit infection with two other coronaviruses, namely SARS-CoV and

SARS-CoV2, as well as two filoviruses, *i.e.* Marburg and Ebola. The antiviral properties of SKIc-targeting drugs were the consequence of the repression of viral RNA synthesis (Weston et al., 2020). The exact role of the host SKIc in the regulation of viral gene expression, and the prevalence as well as importance of interactions between viral proteins with the SKIc subunits remain to be examined. Moreover, the link between SKIc disruption by the novel therapeutics and activation of the interferon response awaits more careful investigation, taking into account the role of SKI2W catalytic subunit in limiting activation of this antiviral mechanism. Nevertheless, further development of compounds interfering with SKIc catalytic properties or assembly could be expected. A recently published structure of the human SKIc (Kogel et al., 2022) can prove very useful in achieving this goal.

5.2 Mouse models of the SKIc dysfunction as tools towards understanding of its physiological role at the organismal level

The majority of knowledge about SKIc functions in higher eukaryotic organisms comes from studies in cell lines of different origin. Further, as described above, functional investigations often focused on the SKIc roles in cells exposed to some kind of extra- or intracellular stress, *e.g.* viral infection or ER stress, leading to UPR activation. As also exemplified above, such conditions may activate a potent interferon response. Nevertheless, whether this outcome of SKIc malfunction is widespread under more physiologically relevant circumstances is doubtful, taking into account contradictory data that one comes across in literature on THES individuals with different *SKIV2L* mutations (Eckard et al., 2014; Hiejima et al., 2017). These arguments, together with scarcity of THES patients and broad

spectrum of clinical phenotypes, urge the need to develop proper animal models that would enable more comprehensive examination of SKIc physiological functions.

Several mouse models of *SKIV2L* gene deficiency have been recently constructed and investigated, disclosing novel and largely unexpected links between RNA degradation and quality control, general pathways regulating cellular metabolism, and phenotypic THES manifestations (K. Yang, Han, Asada, et al., 2022; K. Yang, Han, Gill, et al., 2022). However, an appropriate caution should be taken prior to attempts to extrapolate results of these important studies to the entire SKIc and its functions in humans, considering that the networks of interactions between SKIc components and other factors involved in RNA metabolism, as well as their contribution to either normal mRNA turnover or specialized mRNA surveillance might differ even between so evolutionary close species as mice and humans (Kalisiak et al., 2017; Tuck et al., 2020). Furthermore, taking into account technical problems with efficient and time-coordinated gene deletion in every single cell of a multicellular organism, it is not surprising that some *SKIV2L* knock-out mice mimic only some aspects of SKI2W dysfunction in THES patients.

Since *SKIV2L* deletion in the germline led to embryonic lethality, the initial model was a postnatal whole-body Cre-LoxP conditional knock-out induced in 4-weeks-old mice by tamoxifen treatment (K. Yang, Han, Asada, et al., 2022). The most striking phenotypes were skin lesions and progressive hair loss. At the tissue level, abnormal epidermis stratification was observed, including hyperplasia and the presence of immune infiltrates in the dermis, suggestive of skin inflammation (Figure 15a). This is largely in concordance with skin and hair abnormalities reported in THES

patients. On the other hand, no signs of inflammation in the liver or in the intestines (duodenum, colon) were noted in the animal model. Thus, although SKI2W was absent in every mouse cell, phenotypic manifestation appeared to be limited only to the skin. More detailed analysis revealed hyperproliferation of keratinocytes, resulting in the loss of skin barrier function (Figure 15a). Additional *SKIV2L* knock-outs, including one specific to keratinocytes, demonstrated that more local SKI2W absence leads to increased keratinocyte proliferation in the basal epidermal layer and its thickening, lymphocyte infiltration, abnormal hair morphogenesis, and impaired epidermal permeability (Figure 15a). Interestingly, skin autoinflammation due to an impairment of SKIc-mediated regulation did not trigger IFN signaling. Targeted *SKIV2L* deletion in the bone marrow did not lead to skin abnormalities and inflammation. Altogether, these results point towards the cell-intrinsic role of SKI2W in keratinocytes in the tight regulation of their proliferative potential (K. Yang, Han, Asada, et al., 2022).

Conspicuously, immune infiltrates in the dermis and hair follicles were rich in T lymphocytes. *SKIV2L*-deficient mice displayed lymphadenopathy and evidence was found that T cell homeostasis in these animals was perturbed, since more effector and central memory T cells, and concomitantly less naïve T lymphocytes were observed in their spleens compared to control mice. Apparently, naïve T cells from mice with SKI2W dysfunction had a tendency to exit from quiescence due to chronic activation, resulting in an enhanced and faster proliferation (K. Yang, Han, Asada, et al., 2022) (Figure 15a).

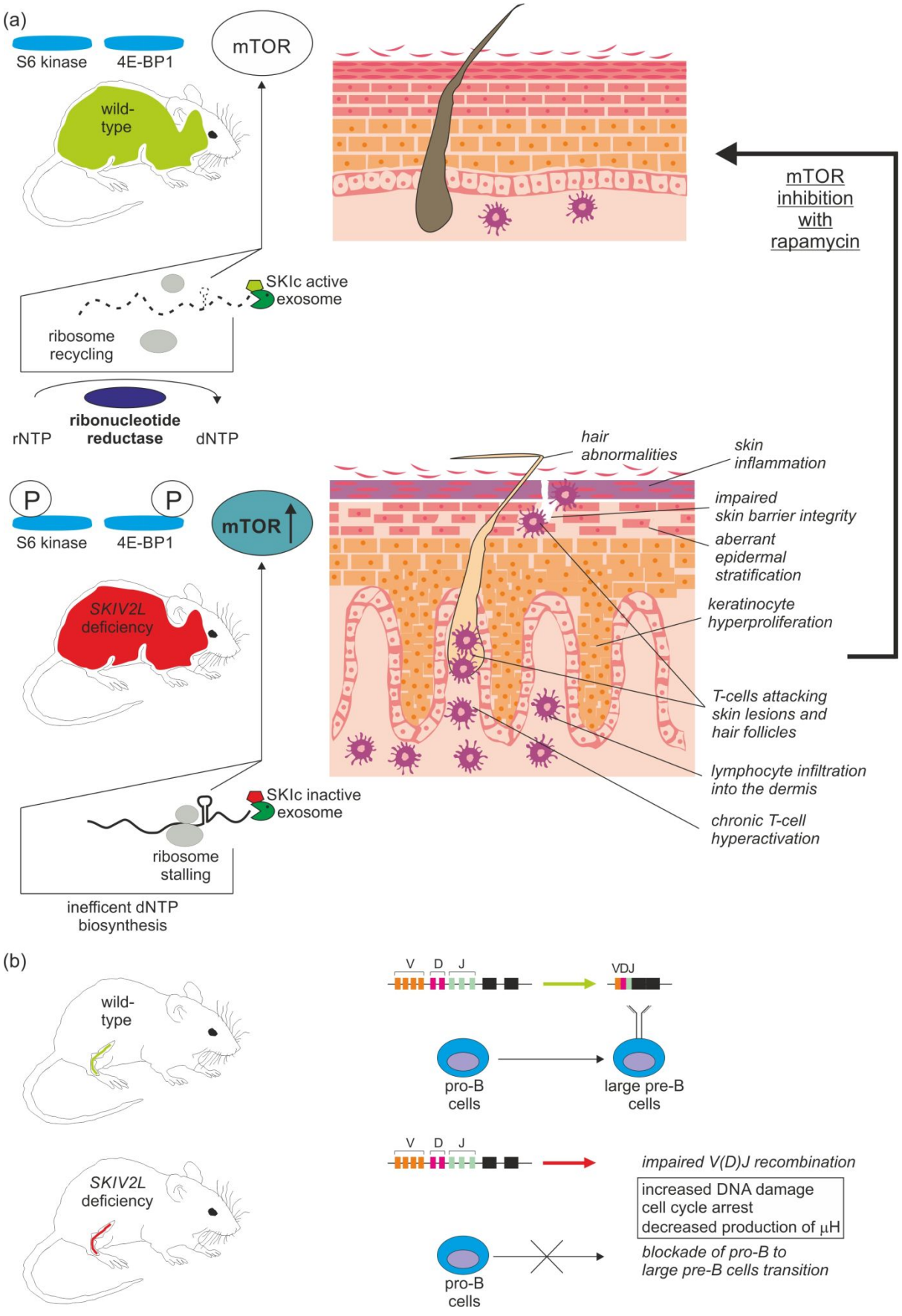
(a)
S6 kinase
4E-BP1
mTOR
wild-type
SKIc active exosome
ribosome recycling
ribonucleotide reductase
rNTP
dNTP
mTOR inhibition with rapamycin
hair abnormalities
skin inflammation
impaired skin barrier integrity
aberrant epidermal stratification
keratinocyte hyperproliferation
T-cells attacking skin lesions and hair follicles
lymphocyte infiltration into the dermis
chronic T-cell hyperactivation
P
P
S6 kinase
4E-BP1
mTOR
SKIV2L deficiency
SKIc inactive exosome
ribosome stalling
inefficent dNTP biosynthesis
(b)
wild-type
SKIV2L deficiency
V D J
VDJ
pro-B cells
large pre-B cells
V D J
impaired V(D)J recombination
increased DNA damage
cell cycle arrest
decreased production of μH
blockade of pro-B to large pre-B cells transition
pro-B cells

FIGURE 15 *SKIV2L*-deficient murine models reveal consequences of SKIc dysfunction at the organismal level. (a) Whole-body conditional *SKIV2L* knock-out resulted in skin inflammation and lesions due to aberrant stratification of the epidermis, hyperproliferation of keratinocytes, and loss of skin barrier function. In addition, T lymphocytes were chronically hyperactivated, infiltrated into the dermis, and attacked skin lesions and hair follicles, leading to hair abnormalities and progressive hair loss. These phenotypes likely stemmed from enhanced mTOR signaling, as documented by increased phosphorylation of S6 kinase and 4E-BP1. This might be due to *e.g.* reduced supply of dNTPs, produced by RNR from ribonucleotides, the pool of which is diminished upon SKIc inactivation resulting in inefficient RNA turnover. (b) *SKIV2L* knock-out specific to B cells precludes efficient transition from pro-B to large pre-B cell stage in the bone marrow, which is caused by impaired V(D)J recombination, leading to diminished synthesis of μ heavy chain (μH), and accompanied by elevated DNA damage response and cell cycle defects.

Molecular mechanism linking *SKIV2L* deficiency with keratinocyte and T cell hyperproliferation was illuminated by the results of RNA-seq, which, apart from genes involved *e.g.* in keratinization and associated with inflammatory skin disorders, showed enrichment of metabolic pathways linked to lipids, glucose, steroids or vitamins (K. Yang, Han, Asada, et al., 2022). This suggested engagement of some principal regulator of metabolism. Indeed, mTOR signaling pathway activation in both keratinocytes and T lymphocytes was demonstrated in mice devoid of functional SKI2W by increased phosphorylation of S6 ribosomal protein and 4E-BP1 factor (Figure 15a). Accordingly, global protein synthesis was increased, and *SKIV2L*-deficient keratinocytes were larger than their counterparts from control mice. It remains to be shown which events or metabolites directly activate mTOR signaling, be that inefficient disassembly of stalled ribosomes during RNA quality control or reduced supply of deoxyribonucleotides due to less efficient RNA degradation to ribonucleotides, which are substrates for dNTP production via ribonucleotide reductase (RNR) (Greene et al., 2020; Lee-Kirsch, 2022; K. Yang, Han, Asada, et al., 2022) (Figure 15a). Regardless of the identity of the trigger, both systemic or topical mTOR pathway inhibition with rapamycin substantially reversed morphological and molecular phenotypes arising from *SKIV2L* deficiency (K. Yang, Han, Asada, et al., 2022) (Figure

15a). Detection of lymphocyte infiltration in the dermis of THES patient with *SKIV2L* mutations, along with observed mTOR activation, which recapitulate major conclusions from the murine models, indicates that mTOR inhibitors deserve consideration as potential therapeutics, which may help to cope with at least a subset of THES symptoms, in at least some patients.

Independent reports suggest that the SKIc plays a pivotal role in limitation of the activation of various signaling pathways. Under physiological conditions, SKIc may act mainly to prevent mTOR signaling (Lee-Kirsch, 2022; K. Yang, Han, Asada, et al., 2022). In specific circumstances, *e.g.* during viral infection, SKIc functions may in turn switch to inhibition of the interferon response, particularly when the latter could be elicited by endogenous immunostimulatory RNAs (Eckard et al., 2014). The exact molecular links between SKIc involvement in different nucleic acid metabolic processes and these signaling paths remain to be deciphered.

Another model was generated to address the molecular basis of immunological defects in the reported THES patient, including primary B cell immunodeficiency, hypogammaglobulinemia, hyper IgA, and kappa-restricted plasma cell dyscrasia (K. Yang, Han, Gill, et al., 2022). This mouse model consisted in knocking out *SKIV2L* specifically in B cells, and revealed that SKI2W is indispensable during early stage of B cell development in the bone marrow, namely for transition from pro-B to large pre-B cells (K. Yang, Han, Gill, et al., 2022). This developmental block is mainly due to increased DNA damage and cell cycle arrest, and is associated with decreased production of μ heavy chain (μH), suggestive of V(D)J recombination impairment (K. Yang, Han, Gill, et al., 2022) (Figure 15b). Largely in line with these findings, an independent report documented inefficient elimination of

ncRNAs overlapping with DNA double strand breaks (DSBs) at *Igh* loci in pro-B cells of transgenic mice devoid of structural (RRP40) or catalytic (DIS3, RRP6) subunits of the exosome complex, which resulted in the activation of p53 pathway-associated genes, compromised V(D)J recombination leading to unproductive rearrangements at *Igh*, and ultimately to equivalent blockage of pro- to pre-B transition during early phase of B cell development (Laffleur et al., 2022). These seminal discoveries expand previously identified mechanisms, by which the exosome and its co-factors regulate various stages of B cell maturation, through controlling efficiency of somatic hypermutation (SHM) and class-switch recombination (CSR), which also contribute to diversification of immunoglobulin genes (Basu et al., 2011; Laffleur et al., 2021; Lim et al., 2017; Pefanis et al., 2014).

5.3 SKIc as a regulator of wax biosynthesis in plants

A. thaliana mutants, including those in genes encoding proteins involved in RNA metabolic processes, often display easily observable morphological phenotypes. One of the most striking examples is the cuticular wax biosynthesis defect in plants with non-functional exosome or some of its cytoplasmic interactors.

Cuticle membrane formation is a multi-stage biochemical path. One of the steps in wax production is the conversion of very long chain (VLC) acyl-CoA to VLC alkanes, controlled, by CER3 (ECERIFERUM3) protein involved in aldehyde decarbonylation (Bernard et al., 2012) (Figure 16a). Wax production was reduced in *A. thaliana* mutant in *CER7* gene, coding for AtRRP45B subunit of the core exosome RNase PH-like ring, and accompanied by decreased levels of *CER3* transcript (Hooker et al., 2007) (Figure 16b). It was proposed that CER7/AtRRP45B is involved in the

degradation of transcript encoding proteinaceous repressor of *CER3* expression (Hooker et al., 2007), but follow-up studies showed that *CER3* mRNA is a subject of PTGS, and its levels are controlled by siRNAs (P. Lam et al., 2012) (Figure 16a,b). Indeed, 21-24 nt-long siRNAs complementary to *CER3* accumulated in plants with non-functional CER7/AtRRP45B, demonstrating that in wild-type *A. thaliana* the exosome plays a key role in the elimination of such molecules, which otherwise silence *CER3* expression via PTGS and interfere with proper cuticular wax deposition (P. Lam et al., 2015) (Figure 16b). Loss of functions of RST1 and RIPR, likely linking plant exosome and SKI complexes, caused morphological, biochemical, and molecular phenotypes analogous to *cer7* mutation, *i.e.* glossy green inflorescence stems indicative of wax biosynthesis defect, decreased levels of chemical compounds required for wax production, and reduction of *CER3* transcript with concurrent accumulation of its siRNA derivatives (Lange et al., 2019) (Figure 16c). Consistently with the conserved auxiliary role of SKIc in cytoplasmic exosome targeting to its RNA substrates, all three SKIc subunits also proved to partake in wax biosynthesis (Zhao & Kunst, 2016). Unexpectedly, mutations in genes encoding SKIc constituents reversed wax-deficient *cer7* phenotype, restoring *CER3* transcript and VLC alkane production to near-wild-type levels, which occurred through regulation of *CER3*-derived siRNAs (Zhao & Kunst, 2016) (Figure 16d). The exact reason why *rst1* and *ripr* mutations phenocopy *cer7* (Figure 16b,c), and dysfunction of SKIc subunits on the contrary suppresses *cer7* phenotype (Figure 16d) is unknown, but might be associated with the fact that in the former cases SKIc is functional, albeit unable to interact with the exosome, while in the latter situation the exosome is still tethered to its inoperative co-factor. Association of *CER3* transcript with wild-type

SKIc in *cer7*, *rst1* or *ripr* implies that it is inefficiently degraded due to two reasons: first – the 3'-5' decay pathway is inhibited, and second – mRNA binding by SKIc limits its accessibility for XRN4-mediated 5'-3' degradation (Figure 16b,c). On the contrary, when SKIc is unable to interact with *CER3* transcript, availability of mRNA excess to XRN4 increases, which explains suppression of *cer7* by *ski* mutations (Daszkowska-Golec, 2020; Zhao & Kunst, 2016) (Figure 16d). All above-described data provided some insights into the intriguingly complex molecular mechanism linking functions of the multiprotein network controlling RNA metabolism and silencing with plant-specific wax biosynthesis process.

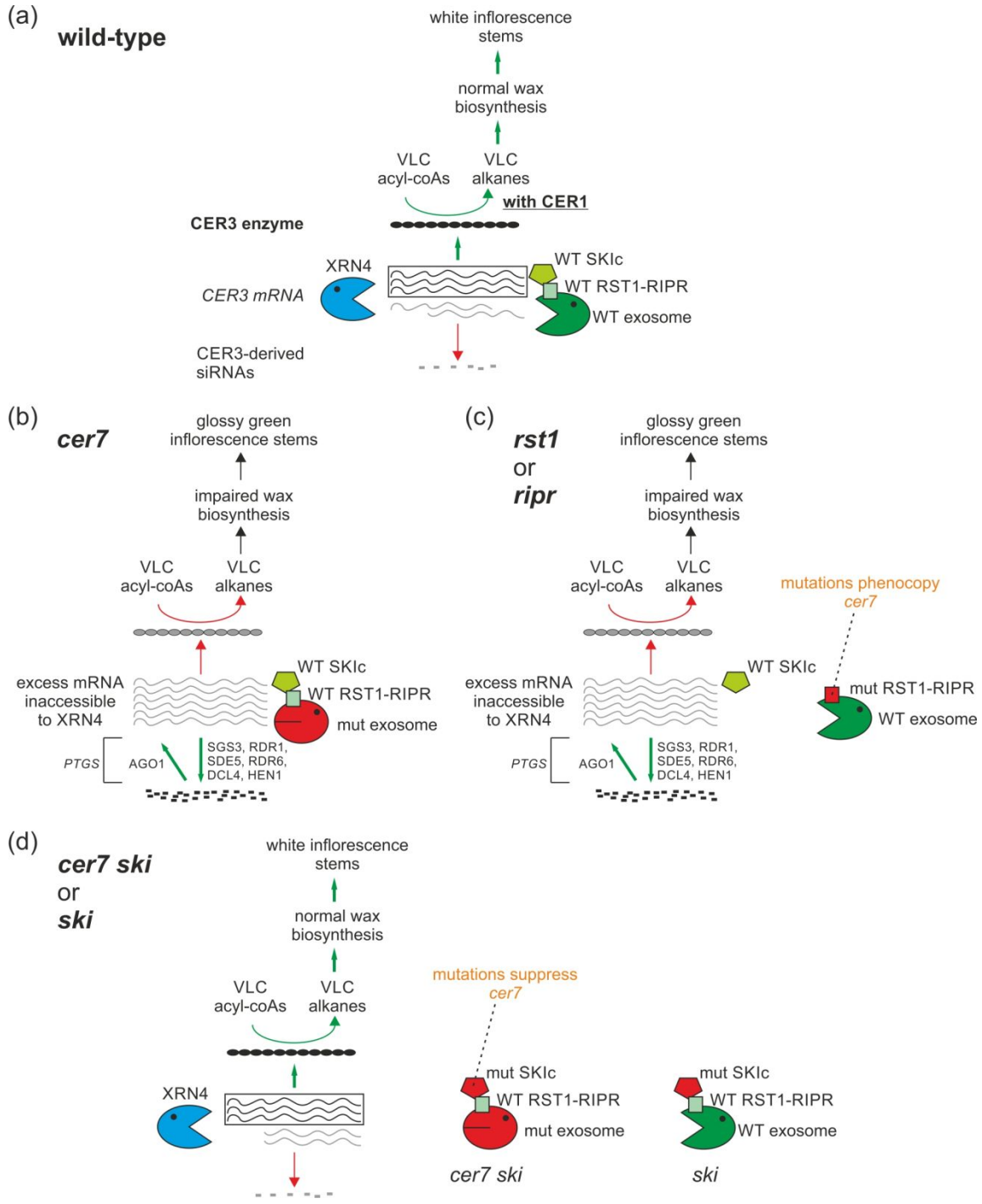

FIGURE 16 SKIc co-regulates wax biosynthesis in *A. thaliana*. (a) In wild-type plants the levels of *CER3* mRNA are fine-tuned by both XRN4-mediated 5'-3' decay and 3'-5' degradation, carried out by the exosome in collaboration with SKIc and RST1-RIPR, which link both complexes. This prevents production of *CER3*-derived siRNAs and triggering PTGS of *CER3* expression. The *CER3* transcript levels ensure optimal production of CER3 enzyme, which – together with CER1 – controls synthesis of very long chain (VLC) alkanes from VLC acyl-coAs via decarbonylation. This allows for normal wax biosynthesis, resulting in white inflorescence stems. (b) In *cer7* mutant, wild-type SKIc and RST1-RIPR thread *CER3* mRNA excess to the inactive exosome, making it inaccessible to XRN4. As a consequence, *CER3*-derived siRNAs are generated by RNAi machinery, which triggers PTGS of *CER3* expression. Decreased CER3 levels preclude efficient wax biosynthesis, leading to

glossy green inflorescence stems. (c) In *rst1* or *ripr* mutants, wild-type SKIc pulls *CER3* mRNA away from XRN4, but is unable to deliver it to the exosome. Unbalanced *CER3* transcript levels lead to elevated siRNA production, PTGS, and defect in wax biosynthesis, which phenocopies *cer7* mutation. (d) In *ski* mutants, *CER3* mRNA could not be targeted to the exosome-mediated 3'-5' decay due to SKIc dysfunction, but the excess of transcript pool is eliminated by undisturbed activity of XRN4. Therefore, *ski* mutations exert suppressor effect in the background of *cer7*, restoring nearly normal wax biosynthesis.

5.4 SKIc functions in the regulation of developmental processes in animals

The repertoire of biological functions of SKIc and associated factors has been recently expanded by demonstrating its involvement in the regulation of different developmental transitions in model animals.

Drosophila SKI2W ortholog, known as Twister or Tst, was shown to be expressed as two alternative isoforms, both at the mRNA and protein level. These isoforms are differentially expressed during fly development, starting from early embryos, through larval and pupal stages, to adulthood (Seago et al., 2001). This early study pointed to the potential role of the regulation of SKIc expression in shaping the transcriptome at particular developmental stages.

Two decades later SKIc involvement in the regulated degradation of a fraction of transcripts expressed during initial stages of *Drosophila* oogenesis was demonstrated (Blatt et al., 2021). During germ cell-to-maternal transition (GMT) some mRNAs, including oogenesis-specific transcripts, must be eliminated prior to embryogenesis, to ensure that only the appropriate mRNAs are contributed to the fertilized egg on the maternal side. Interestingly, *tst* mutation or germline-specific RNAi-mediated Tst depletion resulted in the failure of the egg chambers to grow in ovarioles, most likely due to their apoptosis. Similar phenotypes were observed upon *ski3* or *ski8* mutation or downregulation in the germline, suggesting that the entire SKIc is indispensable for the completion of oogenesis and fertility

(Blatt et al., 2021). Given the established SKIc role as a factor controlling mRNA metabolism, transcriptomic analyses were performed for ovaries of *tst* mutant and flies subjected to RNAi, which identified >200 genes upregulated specifically as a consequence of SKIc dysfunction. If SKIc is active, this set of mRNAs undergoes degradation in the course of oocyte specification – regulated transcripts are present in the undifferentiated germline stem cells and in early cyst stages, but significantly underrepresented at later cyst stages and virtually nonexistent in the eggs. Regulation of these mRNAs occurs most likely via NGD pathway, since *pelo* mutation phenocopies effects of SKIc dysfunction, and an overlap between transcripts, the levels of which are increased at least 2 times in both *pelo* and *tst* mutants, is 75%. Furthermore, based on the ribosome profiling data, mRNAs co-regulated by SKIc and Pelota display an increased association with the stalled ribosomes, which normally stimulates their elimination by NGD, unless SKIc and Pelota are non-functional (Blatt et al., 2021). While no evidence was found for the elevated content of sub-optimal codons in the ORFs of the regulated transcripts, which could lead to increased ribosome stalling, in more than a half of these mRNAs a motif rich in interspaced cytidines was identified. Moreover, Hfp protein, homologous to human PUF60 polypyrimidine tract binding protein, was demonstrated to bind to several Tst targets and thus proposed to recognize the C-rich motif and modulate ribosome association with a cohort of SKIc-regulated mRNAs during *Drosophila* oogenesis. In support, trilateral interaction between Tst, Pelota, and Hfp was confirmed by co-immunoprecipitation, and a significantly overlapping set of transcripts was regulated by Hfp compared to Tst and Pelota (Blatt et al., 2021). Further functional studies showed that while expression of at least some of these transcripts, including *e.g.* those coding

for actin cytoskeleton components, is indispensable in the undifferentiated stages, correct progression to subsequent steps of oogenesis requires their meticulous removal. A failure of SKIc and associated factors to eliminate these mRNAs is detrimental to the oocyte fate, resulting in the apoptotic death of the egg chambers and female infertility (Blatt et al., 2021).

Although the exosome function in the elimination of specific transcripts during oocyte maturation in *Drosophila* remains to be demonstrated, this is most probably the case, even though the loss of the exosome components results in a distinct phenotype, *i.e.* complete loss of the germline (Blatt et al., 2021). However, this is presumably due to broader functions of the exosome in RNA metabolism in both the cytoplasm and the nucleus. Concerning Ski7, it was claimed that Hbs1 protein fulfills its functions in *Drosophila*, but female *hbs1* mutants were fertile, contrary to animals with SKIc dysfunction (Blatt et al., 2021). In agreement, an analysis of transcriptomic datasets for different Eukaryotes revealed that the genuine *Drosophila* Ski7 protein is encoded by a separate, yet uncharacterized gene (Marshall et al., 2018). Interestingly, Ski7 has been implicated in an oocyte-to-embryo transition (OET) in zebrafish (Cabrera-Quio et al., 2021). Similar to *D. melanogaster* Tst, Ski7 in *Danio rerio* is required for the maternal transcriptome remodeling during early development. Like in humans, zebrafish Ski7 is synthesized from an alternatively spliced variant of a single *HBS1/SKI7* gene, and interacts with the exosome (Brunkard & Baker, 2018; Cabrera-Quio et al., 2021). Importantly, the levels of Ski7-coding transcript are much higher in the mature eggs compared to early phases of oogenesis and larval stages. The major developmental phenotypes of *ski7* null mutation included production of low quality eggs and decreased number of embryos developing beyond the

one-cell stage. Interestingly, later phases of embryogenesis seemed to be unaffected by the lack of functional Ski7, since embryos that underwent the first division developed into morphologically normal animals (Cabrera-Quio et al., 2021). Ski7 deficiency resulted in a deregulation of hundreds of genes during all OET stages, from oogenesis through eggs to embryogenesis, with little overlap of differentially expressed genes between these periods. Genes with enhanced expression in *ski7* mutants were generally expressed at lower levels in wild-type fish, indicating that the major physiological Ski7 role is to maintain amounts of the respective transcripts low, most likely by targeting them to exosome-mediated 3'-5' degradation, as suggested by biased accumulation of RNA-seq reads for upregulated genes towards 3'-ends of encoded transcripts (Cabrera-Quio et al., 2021). mRNAs accumulating upon *ski7* mutation shared some characteristics, *e.g.* short 3'-UTRs and enrichment of suboptimal codons, which may collectively contribute to their decreased stability in wild-type animals. At the proteome level, several proteins linked to the regulation of stress response and redox processes were upregulated in *ski7* mutant compared to wild-type, and this was supported by gene ontology analysis of differentially expressed genes, which retrieved terms such as redox-related processes, cellular respiration, and response to stress. As a consequence, *ski7* mutant embryos were less susceptible to reductive stress than wild-type counterparts (Cabrera-Quio et al., 2021). Strikingly, this is in contrast to yeast, where Ski7 and SKIc cooperate with Dom34-Hbs1 to overcome oxidative stress (Jamar et al., 2017).

6. CONCLUSIONS AND FUTURE DIRECTIONS

Multiple lines of evidence presented in this review and based on studies in different models indicate that SKI complex linked to the exosome plays vital roles in different aspects of cytoplasmic mRNA metabolism. Noticeably, SKIc functions in transcript degradation during co-translational mRNA surveillance usually converge with Dom34-Hbs1 contribution to ribosome splitting into subunits. These two interdependent processes occur whenever the ribosome stalls at the 3'-end of mRNA lacking termination codon, which could result from premature polyadenylation, mutations or transcript cleavage by enzymes such as NGD endonucleases (Cue2 or NONU-1) and Ire1 or Ago2 during UPR or RNAi, respectively. However, mechanistic details of interconnection between these phenomena vary considerably between distinct Eukaryotes. This is mainly due to various proteins, which interact with SKIc in different species. Yeast Ski7 was suggested to act not merely as a bridging factor between SKIc and the exosome, but also actively participate in ribosome dissociation. Nevertheless, the potential of Ski7 to enter the empty ribosomal A-site has never been structurally demonstrated. Furthermore, it is catalytically inert, unlike other translational GTPases that strictly rely on GTP hydrolysis, and it does not interact with eRF1-like protein. Even if confirmed, this putative Ski7 function is apparently not conserved in higher Eukaryotes. Its functional homolog in human cells – HBS1LV3 – has completely divergent structure and is entirely devoid of eRF3-like domain. On the other hand, human SKIc is able to physically associate not only with HBS1LV3-exosome, but also with HBS1LV1-PELOTA, most likely coupling mRNA decay to ribosome rescue, but detailed structural and functional insights into the mode of such cooperation are yet to be provided. In turn, SKIc functions in mESCs are supported by AVEN-FOCAD dimer, whereby AVEN acts as an anti-stalling

factor upon ribosome arrest during translation. In contrast, there is no evidence for the involvement of PELOTA-HBS1 in ribosome disassembly in mESCs, which is unique in the light of broad conservation of its function across eukaryotic organisms. Whether AVEN-FOCAD and HBS1L variants co-exist in this or other cell types and what is the nature of interplay between them remains to be further examined.

While considerable progress has been already achieved in the field of structural characterization of the SKI complex mechanism of action and its collaboration with the exosome and ribosome, some aspects still need to be addressed from structural viewpoint. In particular, the putative role of SKIc catalytic core and Ski2/SKI2W enzymatic (ATPase and RNA helicase) activities in remodeling of RNA structure or its interactions with proteins during mRNA degradation awaits deeper investigation, since no changes in the RecA domain conformation have been observed and thus the terms 'open'-'closed' states are not relevant for description of SKIc activation resulting from interactions with RNA substrate. This is puzzling, because mobility of RecA domains is characteristic of SF2 helicases. Instead, RNA access to Ski2 channel in the context of entire SKIc is presumably modulated by substrate-induced repositioning of structural elements outside of the core, namely Ski3 N-terminal fragment and the Ski2 Arch/insertion domain. This allows for transition from default auto-inhibited state to active/substrate-bound state, but has not been formally demonstrated, since in all available yeast and human Ski2 and SKIc structures Arch/insertion domain is in the same arrangement. However, this can be inferred from structural analyses of homologous MTR4 helicase – a component of multiple nuclear exosome co-factors – in which Arch/insertion movements are solely

responsible for oscillating between the so-called 'open' and 'closed' alternative conformations. Switching back and forth from auto-inhibited to active SKI complex state in yeast is additionally controlled by its interaction with ribosome. The picture emerging from studies of this experimental model is that SKIc delivers mRNA from the ribosome to the exosome via a common continuous channel. It would be desirable to continue the structural attempts towards demonstrating if a larger ribosome-SKIc-Ski7-exosome super-complex is formed in the course of mRNA transfer between these factors, what is the order of its assembly, and whether it is conserved in other Eukaryotes, including humans.

In parallel to characterization of SKIc participation in mRNA metabolism through studies in yeast and animal cellular models, an increasing number of current investigations focus on elucidation of connections between its molecular functions and different processes at the tissue and organismal levels. These efforts have already significantly expanded knowledge about versatile roles that SKIc plays in plant and animal development, antiviral defense, signaling pathways, and disease etiology. However, in the context of THES, for most mutations, especially missense ones, even the consequences for SKIc function and assembly remain largely unknown. Moreover, our understanding of links between the impairment of SKIc-mediated regulation of mRNA decay and quality control and diversified symptoms observed in patients is still in its infancy. Recently developed knock-out mice have shed new light on the molecular mechanism behind some clinical signs in the affected individuals, associated with SKIc dysfunction, such as hair abnormalities or immunodeficiency, and

certainly paved the way towards construction of subsequent models, which will likely allow to address the full spectrum of disease manifestation.

Tables

TABLE 1 Comparison of yeast and mammalian SKIc structural features.

SKIc subunits						
name (alternative name)	Uniprot ID	length (amino acids)	molecular weight (kDa)	copies in the complex	function	structural building blocks
yeast Ski2 (ySki2)	P35207	1287	146.1	1	catalytic (ATPase; RNA	• N-terminus: inner+wedge+outer segments

human SKI2W (SKI2; hSKI2)	Q15477	1246	137.8		helicase)	• central domain with two RecA subdomains • C-terminus: Arch/insertion domain between two winged helices (WH)+helical bundle (HB)
yeast Ski3 (ySki3)	P17883	1432	163.7	1	scaffolding	33 tetratricopeptide repeats (TPRs) *N-terminal arm (Ski3N): 10 TPRs* *C-terminal arm (Ski3C): 23 TPRs*
human TTC37 (SKI3; hSKI3)	Q6PGP7	1564	175.5			40 tetratricopeptide repeats (TPRs) *N-terminal arm (SKI3N): 8 TPRs* *C-terminal arm (SKI3C): 32 TPRs*
yeast Ski8 (ySki8)	Q02793	397	44.2	2 (designated $Ski8_{IN}$ and $Ski8_{OUT}$)	regulatory	7 WD40 repeats
human WDR61 (SKI8; hSKI8)	Q9GZS3	305	33.6			

major sites of contact between subunits within the complex	
yeast	**human**
I. Ski2-Ski3	**I. SKI2-SKI3**
1. Ski2N-Ski3C (TPRs 12-33)	1. SKI2N-SKI3C
– Ski2N inner segment-Ski3C TPRs 15-18 and 26-33	– SKI2N inner segment-SKI3C (multiple sites across TPRs 9-40)
– Ski2N wedge segment-Ski3C TPRs 17-18 and 22-23	– SKI2N wedge segment-SKI3C TPRs 17-24
– Ski2N outer segment-Ski3C TPR 12-15 and 21-24	– SKI2N outer segment-SKI3C TPRs 9-16 and 17-24
2. Ski2 RecA1-Ski3C TPRs 16-17	2. SKI2 enzymatic core-SKI3C TPRs 9-16 and 17-24
3. Ski2 HB-Ski3C TPRs 23-24	**II. SKI2-SKI8**
II. Ski2-Ski8	1. SKI2 enzymatic core-$SKI8_{IN}$
1. Ski2N inner segment-$Ski8_{IN}$	2. SKI2 enzymatic core-$SKI8_{OUT}$
2. Ski2 RecA1-$Ski8_{IN}$	**III. SKI3-SKI8**
3. Ski2 HB-$Ski8_{IN}$	1. SKI3C (TPRs 25-32)-$SKI8_{OUT}$
4. Ski2 HB-$Ski8_{OUT}$	2. SKI3C (TPRs 25-32)-$SKI8_{IN}$
III. Ski3-Ski8	
1. Ski3C (Q-R-x-x-ϕ motif in TPR 31)-$Ski8_{OUT}$ (hydrophobic patch on top surface of the protein)	
2. Ski3C (Q-R-x-x-ϕ motif in TPR 33)-$Ski8_{IN}$ (hydrophobic patch on top surface of the protein)	

major regulatory elements	
yeast	**human**
1. Ski3N	1. SKI3N
2. Ski2 Arch/insertion	2. SKI2 Arch/insertion

	3. SKI2N wedge segment	
sites of contact between SKIc and 40S ribosomal subunit		
yeast 1. Ski2 RecA2-rRNA helix 16, proteins eS10+uS3 2. Ski2 Arch/insertion-rRNA helix 41, proteins uS3+uS10 3. Ski8$_{OUT}$-proteins uS2+uS5+eS21	**human** 1. SKI2 RecA2-rRNA helix 16, proteins uS3+uS12+eS10 2. SKI2 Arch/insertion-rRNA helix 41, proteins uS3+uS10	
linker between SKIc and the exosome		
yeast: Ski7 • aa 1-105 interact with SKIc (precise site unknown) • aa 116-235 interact with the exosome (mainly Csl4 cap subunit+Rrp43 and Mtr3 subunits)	**human**: HBS1LV3 • aa 1-145 interact with SKIc (precise site unknown) • aa 546-572 and 609-625 interact with the exosome (*i.a.* with RRP43 subunit)	
other SKIc interactors		
yeast: Ska1	**human**: HBS1LV1	**mouse (ESCs)**: AVEN-FOCAD

TABLE 2 A compilation of available structures of Ski2/SKI2W (alone and within SKIc and larger assemblies) and homologous MTR4 helicase, which are referred to in this review.

protein or complex	accession number, method	species	RNA helicase enzymatic state	SKI complex state	area of best resolution	regions not determined in the structure	reference
Structures of Ski2/SKI2W and the SKI complex							
SKI complex	PDB: 4BUJ, X-ray	*S. cerevisiae*	closed[a]	auto-inhibited[b]	entire complex	-	(Halbach et al., 2013)
Ski2	PDB: 4A4Z, X-ray	*S. cerevisiae*	closed[a] (AMPPNP-bound)	-	Ski2 enzymatic core with Arch/insertion domain	Ski2N	(Halbach et al., 2012)
SKI complex bound to ribosome	PDB: 5MC6, cryo-EM	*S. cerevisiae*	open[a]	active/substrate-bound[b]	entire complex	-	(Schmidt et al., 2016)
SKI complex	PDB: 7QDR, cryo-EM	*Homo sapiens*	closed[a] (apo)	auto-inhibited[b]	SKI2 enzymatic core, SKI3C, SKI8$_{IN}$, SKI8$_{OUT}$	SKI2 Arch/insertion domain, SKI3C	(Kogel et al., 2022)
SKI complex	PDB: 7QDY, cryo-EM	*Homo sapiens*	closed[a]	active/substrate-bound[b]	SKI2 enzymatic core, SKI3C, SKI8$_{IN}$, SKI8$_{OUT}$	SKI2 Arch/insertion domain, SKI3C	(Kogel et al., 2022)

SKI complex bound to ribosome	PDB: 7QDZ, cryo-EM	*Homo sapiens*	closed[a]	active/substrate-bound[b]	SKI2 enzymatic core, SKI3C, $SKI8_{IN}$, $SKI8_{OUT}$	SKI2 Arch/insertion domain, SKI3C	(Kogel et al., 2022)
SKI2 in SKI complex bound to ribosome	PDB: 7QE0, cryo-EM	*Homo sapiens*	open[a]	-	SKI2 enzymatic core with Arch/insertion domain	SKI2C, SKI3, $SKI8_{IN}$, $SKI8_{OUT}$	(Kogel et al., 2022)
Structures of MTR4							
MTR4-NVL complex	PDB: 6RO1, X-ray	*Homo sapiens*	open[c]	-	enzymatic core with Arch/insertion domain	-	(Lingaraju et al., 2019)
MTR4	PDB: 6IEG, X-ray	*Homo sapiens*	closed[c]	-	enzymatic core with Arch/insertion domain	-	(J. Wang et al., 2019)
MTR4-NRDE2 complex	PDB: 6IEH, X-ray	*Homo sapiens*	closed[c]	-	enzymatic core with Arch/insertion domain	-	(J. Wang et al., 2019)
MTR4 bound to exosome	EMDB: 7818, cryo-EM	*Homo sapiens*	open[c]	-	entire exosome and MTR4 with Arch/insertion domain	-	(Weick et al., 2018)
MTR4 bound to exosome	EMDB: 7819, cryo-EM	*Homo sapiens*	closed[c]	-	entire exosome and MTR4 with Arch/insertion domain	-	(Weick et al., 2018)

[a]differentiation between 'open' and 'closed' conformations is emphasized in respective references, although no variability in RecA domains' spatial arrangement could be observed when comparing these two alternative states

[b]auto-inhibited and active/substrate-bound conformations represent distinct states of SKIc, differing in relative positioning of Ski2 Arch-insertion domain and Ski3 N-terminus

[c]according to authors' nomenclature used in the respective reference, but 'open' and 'closed' conformations refer to alternative positions of MTR4 Arch/insertion domain

TABLE 3 THES-associated mutations in *SKIV2L* gene. Mutations are numbered 1-41 in the leftmost column, in the order of appearance, and referred to as such in Figures 10-12. Recurring mutations are marked in italics.

***SKIV2L* mutations**					
I. Homozygous nonsense and frameshift mutations resulting in the rapid emergence of stop codon					
mutation (alleles 1 and 2)	location and effect	no. of families	no. of individuals	ethnicity - world region or country	reference
mut 1 c.12_13 delAG p.Glu5Ala fs*37	Exon 1; out-of-frame deletion → frameshift → stop codon	I	1	Asian (Chinese)	(M. Yang et al., 2022)
mut 2 c.235 C>T p.Arg79*	Exon 3; nonsense	I	1	American	(Dyment et al., 2021)[a]
mut 3 c.1434 delT p.Ser479Ala fs*3	Exon 14; out-of-frame deletion → frameshift → stop codon	II	I - 1 II - 1	Middle-Eastern (Turkish) Middle-Eastern (Turkish)	(Bourgeois et al., 2018; Fabre et al., 2012)
mut 4 c. 1635_1636 insA p.Gly546Arg fs*35	Exon 15; out-of-frame insertion → frameshift → stop codon	I	1	North African	(Fabre et al., 2012)
mut 5 c.2479 C>T p.Arg827*	Exon 21; nonsense	I	1	Middle-Eastern (Saudi Arabia)	(Alsaleem et al., 2022)
mut 6 c.2572 delG p.Val858*	Exon 21; out-of-frame deletion → frameshift → stop codon	I	1	Middle-Eastern (Turkish)	(Fabre et al., 2012)
mut 7 c.2662_2663 delAG p.Arg888Gly fs*12	Exon 22; out-of-frame deletion → frameshift → stop codon	II	I - 1 II - 1	Middle-Eastern (Turkish) Caucasian (Australian)	(Fabre et al., 2012; Hosking et al., 2018)
mut 8 c.3112_3140 del p.Glu1038Val fs*7	Exon 25; out-of-frame deletion → frameshift → stop codon	II	I - 1 II - 1	European European (Balkan)	(Bourgeois et al., 2018; Xinias et al., 2018; Q. Zhang et al., 2021)[b]
mut 9 c.3172 C>T p.Arg1058*	Exon 25; nonsense	I	2	Middle-Eastern	(Bourgeois et al., 2018)
mut 10 c.3187 C>T p. *	Exon 26; nonsense	I	1	European	(Bourgeois et al., 2018)
mut 11 c.3391 delC p.Leu1131Ser fs*5	Exon 26; out-of-frame deletion → frameshift → stop codon	I	1	Asian (Pakistani)	(Morgan et al., 2013)[c]

II. Compound heterozygous nonsense and frameshift mutations resulting in the rapid emergence of stop codon							
mutation (allele 1)	mutation (allele 2)	location and effect (mutation 1)	location and effect (mutation 2)	no. of families	no. of individuals	ethnicity - world region or country	reference
mut 12	*mut 7*	Exon 9;	Exon 22;	I	1	Australian	(Poulton

c.904 C>T p.Gln302*	*c.2662_2663 delAG* *p.Arg888Gly fs*12*	nonsense	out-of-frame deletion → frameshift → stop codon			(English/ Polish)	et al., 2019)
mut 13 c.1420 C>T p.Gln474*	mut 14 c.3262 G>T p.Glu1088*	Exon 14; nonsense	Exon 26; nonsense	I	1	Asian (Japanese)	(Hiejima et al., 2017)
mut 15 c.1452 delC p.Val485Cys fs*45	mut 16 c.2498_2499 delTG p.Val833Glu fs*45	Exon 14; out-of-frame deletion → frameshift → stop codon	Exon 21; out-of-frame deletion → frameshift → stop codon	I	1	European	(Bourgeois et al., 2018)
mut 17 c.2266 C>T p.Arg756*	mut 18 c.2442 G>A p.Trp814*	Exon 19; nonsense	Exon 20; nonsense	I	1	European	(Fabre et al., 2012)

III. Nonsense mutations in one allele only resulting in the rapid emergence of stop codon

mutation (allele 1)	mutation (allele 2)	location and effect (mutation 1)	location and effect (mutation 2)	no. of families	no. of individuals	ethnicity - world region or country	reference
mut 19 c.1528 C>T p.Arg510*	-	Exon 14; nonsense	-	I	2	South American	(Bourgeois et al., 2018)
mut 10 *c.3187 C>T* *p.Arg1063**	-	Exon 26; nonsense	-	I	1	European	(Bourgeois et al., 2018)

IV. Homozygous missense mutations

mutation (alleles 1 and 2)	location and effect	no. of families	no. of individuals	ethnicity - world region or country	reference
mut 20 c.1201 G>A p.Glu401Lys	Exon 11; missense	II	I - 1	I – Middle-Eastern (Arabic)	(Albar et al., 2021; Alsaleem et al., 2022)[d]
			II - 1	II – Middle-Eastern (Saudi Arabia)	
mut 21 c.1211 G>A p.Arg404His	Exon 11; missense	I	1	American	(Klee et al., 2021)
mut 22 c.1297 C>T p.Arg433Cys	Exon 13; missense	II	I - 1	I – Middle-Eastern (Arabic)	(Alsaleem et al., 2022; Taher et al. 2020)[d]
			II - 1	II – Middle-Eastern (Saudi Arabia)	
mut 23 c.1312 G>A p.Glu438Lys	Exon 13; missense	I	1	African	(Bourgeois et al., 2018)
mut 24 c.1396 T>G p.Trp466Gly	Exon 13; missense	I	1	African	(Bourgeois et al., 2018)
mut 25 c.1447 C>T p.Arg483Cys	Exon 14; missense	I	1	African	(Bourgeois et al., 2018)
mut 26 c.1891 G>A p.Gly631Ser	Exon 17; missense	I	1	Middle-Eastern (Arabic)	(Vardi et al., 2018)

V. Compound heterozygous nonsense or frameshift mutations resulting in the rapid emergence of stop codon + missense mutations

mutation (allele 1)	mutation (allele 2)	location and effect (mutation 1)	location and effect (mutation 2)	no. of families	no. of individuals	ethnicity - world region or country	reference
mut 27 c.848 G>A	mut 28 c.1022 T>G	Exon 9; nonsense	Exon 10; missense	I	1	European	(Fabre et al., 2012)

p.Trp283*	p.Val341Gly						
mut 29 c.1120 C>T p.Arg374*	*mut 26* *c.1891 G>A* *p.Gly631Ser*	Exon 11; nonsense	Exon 17; missense	I	1	Asian (Chinese)	(B. Zheng et al., 2016)
mut 10 *c.3187 C>T* *p.Arg1063**	*mut 26* *c.1891 G>A* *p.Gly631Ser*	Exon 26; nonsense	Exon 17; missense	I	2	Asian (Chinese)	(W. S. Lee et al., 2016)
mut 30 c.3602_3609 delAGCGCCTG p.Gln1201Arg fs*2	mut 31 c.1990 A>G p.Thr664Ala	Exon 28; out-of-frame deletion → frameshift → stop codon	Exon 18; missense	I	1	Asian (Chinese)	(Q. Zhang et al., 2021)

VI. Other homozygous mutations

mutation (alleles 1 and 2)	location and effect	no. of families	no. of individuals	ethnicity - world region or country	reference
mut 32 c.3561_3581del p.Ser1189_Leu1195del	Exon 28 In-frame deletion	XX	I - 1 II - 1 III - 3 IV - 1 V - 2 VI-XX - 1	I - European II - European III-XX - Middle-Eastern (Saudi Arabia)	(Alsaleem et al., 2022; Bourgeois et al., 2018; Fabre et al., 2013; Monies et al., 2015)[e]
mut 33 c.355-2 A>C p.?	Intron 4/5; 3' splice site mutation (skip of exon 5?)	I	1	Asian	(Kammermeier et al., 2014)

VII. Other compound heterozygous mutations

mutation (allele 1)	mutation (allele 2)	location and effect (mutation 1)	location and effect (mutation 2)	no. of families	no. of individuals	ethnicity - world region or country	reference
mut 34 c.919-1 G>A p.?	mut 35 c.2341-2 A>G p.?	Intron 9/10; 3' splice site mutation	Intron 19/20; 3' splice site mutation	I	1	European	(Bourgeois et al., 2018)
mut 36 c.994 G>C p.Ala332Pro	mut 37 c.3103_3105delAAG p.Lys1035del	Exon 10; missense	Exon 25; In-frame deletion	I	1	European	(Bourgeois et al., 2018; Q. Zhang et al., 2021)[f]
mut 38 c.1404-2 A > G p.?	mut 39 c.1647+1 G > A p.?	Intron 13/14; 3' splice site mutation	Intron 15/16; 5' splice site mutation	I	1	Asian	(Fung et al., 2020)
mut 15 *c.1452delC* *p.Val485Cys fs*45*	mut 40 c.3541-2 A>G p.?	Exon 14; out-of-frame deletion → frameshift → stop codon	Intron 27/28; 3' splice site mutation	I	1	*unknown*	(K. Yang, Han, Asada, et al., 2022; K. Yang, Han, Gill, et al., 2022)
mut 41 c.2203–1 G>C p.?	*mut 10* *c.3187 C>T* *p.Arg1063**	Intron 18/19; 3' splice site mutation	Exon 26; nonsense	II	I - 1 II - 1	I - North American II - European	(Bick et al., 2017; Rudilla et al., 2019)
mut 5 *c.2479C>T* *p.Arg827**	*mut 32* *c.3561_3581del* *p.Ser1189_Leu1195del*	Exon 21; nonsense	Exon 28 In-frame deletion	I	1	Middle-Eastern (Saudi Arabia)	(Alsaleem et al., 2022)

[a]patient diagnosed with Dubowitz syndrome

[b]alternatively described as c.3113_3141del, resulting in the same change at the amino acid sequence level (p.Glu1038Val fs*7)

[c]additional mutation in in the *AKR1D1* gene (c.587delG) identified in parallel

[d]it is possible that the two independent patients presented here represent in fact the same single case

[e]sometimes described as c.3559_3579del, also leading to an in-frame deletion

[f]mut 37 alternatively described as c.3101_3103delAGA, resulting in the same change at the amino acid sequence level (p.Lys1035del)

TABLE 4 THES-associated mutations in *TTC37* gene. Mutations are named with A-BL letter symbols in the leftmost column, in the order of appearance, and referred to as such in Figures 10-12. Recurring mutations are marked in italics.

***TTC37* mutations**					
I. Homozygous nonsense and frameshift mutations resulting in the rapid emergence of stop codon					
mutation (alleles 1 and 2)	location and effect	no. of families	no. of individuals	ethnicity - world region or country	reference
mut A c.287_291 delTGCCT p.Leu96Trp fs*11	Exon 6; out-of-frame deletion → frameshift → stop codon	I	2	Middle-Eastern	(Fabre et al., 2011)
mut B c.409 C>T p.Arg137*	Exon 8; nonsense	I	1	North American	(Bourgeois et al., 2018)
mut C c.751 G>A p.Phe215Glu fs*14	Exon 10; predicted as missense (p.Gly251Arg), but leads to an exon skipping and frameshift	I	1	Asian (Pakistani)	(Hartley et al., 2010)
mut D c.786 T>A p.Cys262*	Exon 11; nonsense	I	1	European	(Bourgeois et al., 2018)
mut E c.1632+1 delG p.Glu545Phe fs*40	Intron 17/18; 5′ splice site mutation with exon skipping	I	1	Middle-Eastern (Kurdish)	(Hartley et al., 2010)
mut F c.1708 C>T p.Arg570*	Exon 18; nonsense	I	1	African	(Bourgeois et al., 2018; Fabre et al., 2013)
mut G c.2181_2182 delGT p.Tyr728Cys fs*6	Exon 21; out-of-frame deletion → frameshift → stop codon	II	I - 1	I – Middle-Eastern (Saudi Arabia)	(Alsaleem et al., 2022; Kristal et al., 2022)
			II - 1	II – Middle-Eastern (Arabic - Bedouin)	
mut H c.2515+1 G>C p.Cys813Val fs*56	Intron 23/24; 5′ splice site mutation with exon skipping	I	1	North African	(Fabre et al., 2011)
mut I c.2779-2 A>G p.Glu974Gly fs*19	Intron 27/28; 3′ splice site mutation with exon skipping	II	I - 1	I - Asian (Pakistani)	(Hartley et al., 2010)
			II - 1	II - Asian (Pakistani)	
mut J c.2808 G>A p.Trp936*	Exon 28; nonsense	VI	I - 2	I - Asian (Indian)	(Bourgeois et al., 2018; Hartley et al., 2010; Kotecha et al., 2012)
			II - 1	II - Asian (Pakistani)	
			III - 1	III - Asian (Pakistani)	
			IV - 1	IV - Asian (Indian)	
			V - 1	V - Asian (Indian)	
			VI - 1	VI - North American	
mut K c.3426 insA p.Ala1143Ser fs*4	Exon 33; out-of-frame insertion → frameshift → stop codon	I	1	Asian (Chinese)	(W. S. Lee et al.,

					2016)[a]
mut L c.3464_3465 delAA p.Lys1155Arg fs*3	Exon 33; out-of-frame deletion → frameshift → stop codon	I	1	Asian (Taiwanese)	(W. I. Lee et al., 2016)[b]
mut M c.3960 C>A p.Tyr1320*	Exon 38; nonsense	I	1	North African	(Fabre et al., 2011)
mut N c.4102 C>T p.Gln1368*	Exon 39; nonsense	I	1	Middle-Eastern (Saudi Arabia)	(Monies et al., 2015)
mut O c. 4175_4176 insCA p.Val1393Gln fs*24	Exon 39; out-of-frame insertion → frameshift → stop codon	I	1	Middle-Eastern (Saudi Arabia)	(Alsalee m et al., 2022)[c]
mut P c.4572 G>A p.Trp1524*	Exon 42; nonsense	V	I - 4	I - Middle-Eastern (Turkish)	(Bourgeo is et al., 2018; Fabre et al., 2018)
			II - 1	II - Middle-Eastern (Turkish)	
			III - 1	III - Middle-Eastern (Turkish)	
			IV - 1	IV - Middle-Eastern (Turkish)	
			V - 1	V - European	

II. Compound heterozygous nonsense and frameshift mutations resulting in the rapid emergence of stop codon

mutation (allele 1)	mutation (allele 2)	location and effect (mutation 1)	location and effect (mutation 2)	no. of families	no. of individuals	ethnicity - world region or country	reference
mut Q c.52 delA p.Arg18Glu fs*9	mut R c.828 delT p.Ile276Met fs*3	Exon 4; out-of-frame deletion → frameshift → stop codon	Exon 11; out-of-frame deletion → frameshift → stop codon	I	1	African	(Bourgeo is et al., 2018)
mut S c.154 G>T p.Glu52*	mut T c.3507 T>G p.Tyr1169*	Exon 5; nonsense	Exon 33; nonsense	I	1	Asian (Cambodian)	(Chong et al., 2015)
mut U c.439 C>T p.Gln147*	mut V c.2251 C>T p.Gln751*	Exon 8; nonsense	Exon 21; nonsense	I	1	European (Italian)	(Hartley et al., 2010)
mut W c.1168 delG p.Val390Phe fs*30	mut X c.3564-2 A>G p.Ser1188Arg fs*4	Exon 14; out-of-frame deletion → frameshift → stop codon	Intron 33/34; 3' splice site mutation with exon skipping	I	1	European (French)	(Fabre et al., 2011)[d]
mut Y c.1307_1308 delAT p.Tyr436Ser fs*12	mut Z c.1374 C>G p.Tyr458*	Exon 15; out-of-frame deletion → frameshift → stop codon	Exon 16; nonsense	I	1	Australian	(Bourgeo is et al., 2018)
mut F *c.1708 C>T* *p.Arg570**	mut AA c.3185_3201dup p.Lys1068Ser fs*2	Exon 18; nonsense	Exon 31; out-of-frame duplication → frameshift → stop codon	I	1	*unknown*	(Bourgeo is et al., 2018; Vely et al., 2018)
mut AB c.3051_3052 insA p.Thr1018Asn fs*18	mut AC c.3364 delA p.Thr1122Gln fs*10	Exon 30; out-of-frame insertion → frameshift → stop codon	Exon 33; out-of-frame deletion → frameshift → stop codon	I	1	European	(Bourgeo is et al., 2018)
mut AD c.4059 delA	mut AE c.4575 C>G	Exon 39; out-of-frame	Exon 42; nonsense	I	1	South American	(Busoni et al.,

p.Ser1355Val fs*12	p.Tyr1525*	deletion → frameshift → stop codon					2017)
mut K *c.3426 insA* *p.Ala1143Ser fs*4*	*mut T* *c.3507 T>G* *p.Tyr1169**	Exon 33; out-of-frame insertion → frameshift → stop codon	Exon 33; nonsense	I	1	Asian (Taiwanese)	(W. I. Lee et al., 2016)
mut T *c.3507 T>G* *p.Tyr1169**	mut AF c.3601 C>T p.Arg1201*	Exon 33; nonsense	Exon 34; nonsense	I	1	Asian (Chinese)	(Chong et al., 2015)

III. Nonsense or frameshift mutations in one allele only resulting in the rapid emergence of stop codon

mutation (allele 1)	mutation (allele 2)	location and effect (mutation 1)	location and effect (mutation 2)	no. of families	no. of individuals	ethnicity - world region or country	reference
mut AG c.2990_3031 delinsC p.Lys997Thr fs*25	-	Exon 29-Intron 29/30-Exon 30; indel → frameshift → stop codon	-	I	1	Asian	(Bourgeois et al., 2018)

IV. Homozygous missense mutations

mutation (alleles 1 and 2)	location and effect	no. of families	no. of individuals	ethnicity - world region or country	reference
mut AH c.2210 T>C p.Val737Ala	Exon 21; missense	I	1	Middle-Eastern (Turkish)	(Karaca Edeer et al., 2019)
mut AI c.2282 T>C p.Leu761Pro	Exon 21; missense	I	1	Middle-Eastern (Arabic)	(Oz-Levi et al., 2015)
mut AJ c.3808 C>G p.Pro1270Ala	Exon 37; missense	I	1	North African	(Fabre et al., 2011)
mut AK c.4507 C>T p.Arg1503Cys	Exon 42; missense	I	2	South African (Somalian)	(Kinnear et al., 2017)

V. Compound heterozygous missense mutations

mutation (allele 1)	mutation (allele 2)	location and effect (mutation 1)	location and effect (mutation 2)	no. of families	no. of individuals	ethnicity - world region or country	reference
mut AL c.1499 G>T p.Gly500Val	mut AM c.2161 G>A p.Gly721Arg	Exon 17; missense	Exon 21; missense	I	2	European	(Bourgeois et al., 2018)
mut AN c.3583 C>G p.Leu1195Val	mut AO c3940 G>A p.Glu1314Lys	Exon 34; missense	Exon 38; missense	I	1	North American	(Lorant & Kua, 2021)

VI. Missense mutations in one allele only

mutation (allele 1)	mutation (allele 2)	location and effect (mutation 1)	location and effect (mutation 2)	no. of families	no. of individuals	ethnicity - world region or country	reference
mut AP c.3847 G>A p.Asp1283Asn	-	Exon 37; missense	-	II	I - 1 II - 1	I - European (Dutch) II - European (Flemish)	(Hartley et al., 2010)
mut AQ c.4514 T>C p.Leu1505Ser	-	Exon 42; missense	-	I	1	European	(Bourgeois et al., 2018; Fabre et al., 2013)

VII. Compound heterozygous nonsense or frameshift mutations resulting in the rapid emergence of stop codon + missense mutations							
mutation (allele 1)	mutation (allele 2)	location and effect (mutation 1)	location and effect (mutation 2)	no. of families	no. of individuals	ethnicity - world region or country	reference
mut AR c.1300_1301 delAA p.Lys434Gly fs*14	*mut AQ* *c.4514 T>C* *p.Leu1505Ser*	Exon 15; out-of-frame deletion → frameshift → stop codon	Exon 42; missense	I	1	European (English)	(Hartley et al., 2010)
mut AS c.2018 G>A p.Gly673Asp	*mut J* *c.2808 G>A* *p.Trp936**	Exon 20; missense	Exon 28; nonsense	I	1	Asian	(Kammermeier et al., 2014)
mut AT c.3230 C>A p.Ala1077Asp	mut AU c.3613 C>T p.Gln1205*	Exon 32; missense	Exon 34; nonsense	I	1	European	(Fabre et al., 2011)
mut AV c.3 G>A p.Met1Ile	*mut P* *c.4572 G>A* *p.Trp1524**	Exon 4; missense → loss of start codon	Exon 42; nonsense	I	1	Middle-Eastern (Turkish)	(Bourgeois et al., 2018)

VIII. Other mutations in one allele only							
mutation (allele 1)	mutation (allele 2)	location and effect (mutation 1)	location and effect (mutation 2)	no. of families	no. of individuals	ethnicity - world region or country	reference
mut AW c.1757+2 T>G p.?	-	Intron 18/19; 5' splice site mutation	-	I	1	European	(Bourgeois et al., 2018)

IX. Other homozygous mutations					
mutation (alleles 1 and 2)	location and effect	no. of families	no. of individuals	ethnicity - world region or country	reference
mut AX c.91-1 G>C p.?	Intron 4/5; 3' splice site mutation	I	1	Middle Eastern	(Bourgeois et al., 2018)
mut AY c.643-2 A>G p.?	Intron 9/10; 3' splice site mutation	I	1	*unknown*	(Bourgeois et al., 2018)
mut AZ c.2114+5 G>A p.?	Intron 20/21; 5' splice site mutation	II	I - 1 II - 1	I – European II - Middle-Eastern (Turkish)	(Bourgeois et al., 2018; Dorum & Gorukmez, 2021)
mut BA c.2921-2 A>G p.Ile976_1005Arg	Intron 28/29; 3' splice site mutation with exon skipping	II	I - 1 II - 1	I - European (Italian) II - European	(Bourgeois et al., 2018; Bozzetti et al., 2013; Fabre et al., 2013)

X. Other compound heterozygous mutations							
mutation (allele 1)	mutation (allele 2)	location and effect (mutation 1)	location and effect (mutation 2)	no. of families	no. of individuals	ethnicity - world region or country	reference
mut BB c.402+2 T>G p.?	mut BC c.994+1 G>A p.?	Intron 7/8; 5' splice site mutation	Intron 12/13; 5' splice site mutation	I	1	North American	(Bourgeois et al., 2018)
mut BD c.1453-1 G>C p.?	*mut AQ* *c.4514 T>C* *p.Leu1505Ser*	Intron 16/17; 3' splice site mutation	Exon 42; missense	I	1	European	(Bourgeois et al., 2018; Fabre et al., 2013)
mut BE c.2128 C>T p.Arg710*	mut BF c.4338_4339 insCTA p.Leu1446_Ala1447 InsLeu	Exon 21; nonsense	Exon 40; in-frame insertion	I	1	European; Caucasian (USA)	(Rider et al., 2015)[e]
mut BG c.2578-7_2578-3 delTTTTT p.Asn860_878Glu Del	mut BH c.4620+1 G>C p.Trp1524_1564 DelIns61	Intron 24/25; splice mutation with exon skipping	Intron 42/43; 5' splice site mutation with indel	I	1	European (French)	(Fabre et al., 2011)
mut BI c.3015-1 G>A p.?	mut BJ c.4454 T>G p.Leu1485Arg	Intron 29/30; 3' splice site mutation	Exon 41; missense	I	1	European (French)	(Fabre et al., 2011)
mut BK c.4130 C>G p.Ser1377*	mut BL Exon11-13del (in-frame)	Exon 39; nonsense	Exons 11-13; large in-frame deletion	I	1	Chinese	(Gao et al., 2022)

[a]referred to as c.3426dupA

[b]effect at the amino acid sequence level incorrectly described as DelK1155H fs*2

[c]referred to as c. 4175_4176 dupCA

[d]effect of c.3564-2 A>G mutation at the protein level uncertain; described as Ser1288Arg substitution in ref. (W. I. Lee et al., 2016), but leucine is present at position 1288. of TTC37, instead of serine; on the other hand, serine is present at position 1188., encoded by AGC triplet at the junction of exons 33 and 34 (nucleotides 3562-3564 of *TTC37* ORF)

[e]incorrectly described as c.4337_4338 insCTA (which would result in Ala1447*), based on Sanger sequencing chromatogram evidence

Funding Information

Narodowe Centrum Nauki, Grant/Award Numbers: UMO-2017/26/E/NZ1/00724, UMO-2022/45/B/NZ1/02654

References

Albar, R. F., Alghamdi, M. S., Alsulimani, E. F., Almasrahi, A. M., & Alsalmi, K. A. (2021). A Case of Mild Trichohepatoenteric Syndrome With New Variant Mutation in SKIV2L Gene: Case Report. *Cureus, 13*(11), e19404. https://doi.org/10.7759/cureus.19404

Alsaleem, B. M., Hasosah, M., Ahmed, A. B. M., Al Hatlani, M. M., Alanazi, A. H., Al-Hussaini, A., Asery, A. T., Alghamdi, K. A., AlRuwaithi, M. M., Khormi, M. A. M., Al Sarkhy, A., & Alshamrani, A. S. (2022). Tricho-hepato-enteric syndrome: Retrospective multicenter experience in Saudi Arabia. *The Saudi Journal of Gastroenterology, 28*(2), 135-142. https://doi.org/10.4103/sjg.sjg_200_21

Aly, H. H., Suzuki, J., Watashi, K., Chayama, K., Hoshino, S., Hijikata, M., Kato, T., & Wakita, T. (2016). RNA Exosome Complex Regulates Stability of the Hepatitis B Virus X-mRNA Transcript in a Non-stop-mediated (NSD) RNA Quality Control Mechanism. *Journal of Biological Chemistry, 291*(31), 15958-15974. https://doi.org/10.1074/jbc.M116.724641

Anderson, J. S., & Parker, R. P. (1998). The 3' to 5' degradation of yeast mRNAs is a general mechanism for mRNA turnover that requires the SKI2 DEVH box protein and 3' to 5' exonucleases of the exosome complex. *EMBO Journal, 17*(5), 1497-1506. https://doi.org/10.1093/emboj/17.5.1497

Araki, Y., Takahashi, S., Kobayashi, T., Kajiho, H., Hoshino, S., & Katada, T. (2001). Ski7p G protein interacts with the exosome and the Ski complex for 3'-to-5' mRNA decay in yeast. *EMBO Journal, 20*(17), 4684-4693. https://doi.org/10.1093/emboj/20.17.4684

Arribere, J. A., & Fire, A. Z. (2018). Nonsense mRNA suppression via nonstop decay. *eLife, 7,* e33292. https://doi.org/10.7554/eLife.33292

Ashton, J. J., Andreoletti, G., Coelho, T., Haggarty, R., Batra, A., Afzal, N. A., Beattie, R. M., & Ennis, S. (2016). Identification of Variants in Genes Associated with Single-gene Inflammatory Bowel Disease by Whole-exome Sequencing. *Inflammatory Bowel Diseases, 22*(10), 2317-2327. https://doi.org/10.1097/MIB.0000000000000890

Atkinson, G. C., Baldauf, S. L., & Hauryliuk, V. (2008). Evolution of nonstop, no-go and nonsense-mediated mRNA decay and their termination factor-derived components. *BMC Evolutionary Biology, 8*, 290. https://doi.org/10.1186/1471-2148-8-290

Auth, M., Nyiko, T., Auber, A., & Silhavy, D. (2021). The role of RST1 and RIPR proteins in plant RNA quality control systems. *Plant Molecular Biology, 106*(3), 271-284. https://doi.org/10.1007/s11103-021-01145-9

Basu, U., Meng, F. L., Keim, C., Grinstein, V., Pefanis, E., Eccleston, J., Zhang, T., Myers, D., Wasserman, C. R., Wesemann, D. R., Januszyk, K., Gregory, R. I., Deng, H., Lima, C. D., & Alt, F. W. (2011). The RNA exosome targets the AID cytidine deaminase to both strands of transcribed duplex DNA substrates. *Cell, 144*(3), 353-363. https://doi.org/10.1016/j.cell.2011.01.001

Benard, L., Carroll, K., Valle, R. C., Masison, D. C., & Wickner, R. B. (1999). The ski7 antiviral protein is an EF1-alpha homolog that blocks expression of non-Poly(A) mRNA in Saccharomyces cerevisiae. *Journal of Virology, 73*(4), 2893-2900. https://doi.org/10.1128/JVI.73.4.2893-2900.1999

Bernard, A., Domergue, F., Pascal, S., Jetter, R., Renne, C., Faure, J. D., Haslam, R. P., Napier, J. A., Lessire, R., & Joubes, J. (2012). Reconstitution of plant alkane biosynthesis in yeast demonstrates that Arabidopsis ECERIFERUM1 and ECERIFERUM3 are core components of a very-long-chain alkane synthesis complex. *Plant Cell, 24*(7), 3106-3118. https://doi.org/10.1105/tpc.112.099796

Bick, D., Fraser, P. C., Gutzeit, M. F., Harris, J. M., Hambuch, T. M., Helbling, D. C., Jacob, H. J., Kersten, J. N., Leuthner, S. R., May, T., North, P. E., Prisco, S. Z., Schuler, B. A, Shimoyama, M., Strong, K. A., Van Why S. K., Veith, R., Verbsky, J., Weborg Jr, A. M., … Dimmock, D. P. (2017). Successful Application of Whole Genome Sequencing in a Medical Genetics Clinic. *Journal of Pediatric Genetics, 6*(2), 61-76. https://doi.org/10.1055/s-0036-1593968

Blatch, G. L., & Lassle, M. (1999). The tetratricopeptide repeat: a structural motif mediating protein-protein interactions. *Bioessays, 21*(11), 932-939. https://doi.org/10.1002/(SICI)1521-1878(199911)21:11<932::AID-BIES5>3.0.CO;2-N

Blatt, P., Wong-Deyrup, S. W., McCarthy, A., Breznak, S., Hurton, M. D., Upadhyay, M., Bennink, B., Camacho, J., Lee, M. T., & Rangan, P. (2021). RNA degradation is required for the germ-cell to maternal transition in Drosophila. *Current Biology, 31*(14), 2984-2994.e7. https://doi.org/10.1016/j.cub.2021.04.052

Bourgeois, P., Esteve, C., Chaix, C., Beroud, C., Levy, N., THES clinical consortium, Fabre, A. & Badens, C. (2018). Tricho-Hepato-Enteric Syndrome mutation update: Mutations spectrum of TTC37 and SKIV2L, clinical analysis and future prospects. *Human Mutation, 39*(6), 774-789. https://doi.org/10.1002/humu.23418

Bousfiha, A., Jeddane, L., Picard, C., Ailal, F., Bobby Gaspar, H., Al-Herz, W., Chatila, T., Crow, Y. J., Cunningham-Rundles, C., Etzioni, A., Franco, J. L., Holland, S. M., Klein, C., Morio, T., Ochs, H. D., Oksenhendler, E., Puck, J., Tang, M. L. K., Tangye, S. G., … Sullivan, K. E. (2018). The 2017 IUIS Phenotypic Classification for Primary Immunodeficiencies. *Journal of Clinical Immunology, 38*(1), 129-143. https://doi.org/10.1007/s10875-017-0465-8

Bozzetti, V., Bovo, G., Vanzati, A., Roggero, P., & Tagliabue, P. E. (2013). A new genetic mutation in a patient with syndromic diarrhea and hepatoblastoma. *Journal of Pediatric Gastroenterology and Nutrition, 57*(3), e15. https://doi.org/10.1097/MPG.0b013e31825600c4

Branscheid, A., Marchais, A., Schott, G., Lange, H., Gagliardi, D., Andersen, S. U., Voinnet, O., & Brodersen, P. (2015). SKI2 mediates degradation of RISC 5'-cleavage fragments and prevents secondary siRNA production from miRNA targets in Arabidopsis. *Nucleic Acids Research, 43*(22), 10975-10988. https://doi.org/10.1093/nar/gkv1014

Brown, J. T., Bai, X., & Johnson, A. W. (2000). The yeast antiviral proteins Ski2p, Ski3p, and Ski8p exist as a complex in vivo. *RNA, 6*(3), 449-457. https://doi.org/10.1017/s1355838200991787

Brunkard, J. O., & Baker, B. (2018). A Two-Headed Monster to Avert Disaster: HBS1/SKI7 Is Alternatively Spliced to Build Eukaryotic RNA Surveillance Complexes. *Frontiers in Plant Science, 9*, 1333. https://doi.org/10.3389/fpls.2018.01333

Buhler, M., Spies, N., Bartel, D. P., & Moazed, D. (2008). TRAMP-mediated RNA surveillance prevents spurious entry of RNAs into the Schizosaccharomyces pombe siRNA pathway. *Nature Structural and Molecular Biology, 15*(10), 1015-1023. https://doi.org/10.1038/nsmb.1481

Busoni, V. B., Lemale, J., Dubern, B., Frangi, F., Bourgeois, P., Orsi, M., Badens, C., & Fabre, A. (2017). IBD-Like Features in Syndromic Diarrhea/Trichohepatoenteric Syndrome. *Journal of Pediatric Gastroenterology and Nutrition, 64*(1), 37-41. https://doi.org/10.1097/MPG.0000000000001218

Byrd, A. K., & Raney, K. D. (2012). Superfamily 2 helicases. *Frontiers in Bioscience (Landmark Edition), 17*(6), 2070-2088. https://doi.org/10.2741/4038

Cabrera-Quio, L. E., Schleiffer, A., Mechtler, K., & Pauli, A. (2021). Zebrafish Ski7 tunes RNA levels during the oocyte-to-embryo transition. *PLoS Genetics, 17*(2), e1009390. https://doi.org/10.1371/journal.pgen.1009390

Chen, C. Y., & Shyu, A. B. (2011). Mechanisms of deadenylation-dependent decay. *Wiley Interdisciplinary Reviews: RNA, 2*(2), 167-183. https://doi.org/10.1002/wrna.40

Cheng, Z., Liu, Y., Wang, C., Parker, R., & Song, H. (2004). Crystal structure of Ski8p, a WD-repeat protein with dual roles in mRNA metabolism and meiotic recombination. *Protein Science, 13*(10), 2673-2684. https://doi.org/10.1110/ps.04856504

Chiabudini, M., Tais, A., Zhang, Y., Hayashi, S., Wolfle, T., Fitzke, E., & Rospert, S. (2014). Release factor eRF3 mediates premature translation termination on polylysine-stalled ribosomes in Saccharomyces cerevisiae. *Molecular and Cellular Biology, 34*(21), 4062-4076. https://doi.org/10.1128/MCB.00799-14

Chong, J. H., Jamuar, S. S., Ong, C., Thoon, K. C., Tan, E. S., Lai, A., Aan, M. K. J., Tan, W. L. W., Foo, R., Tan, E. C., Lau, Y. L., & Liew, W. K. (2015). Tricho-hepato-enteric syndrome (THE-S): two cases and review of the literature. *European Journal of Pediatrics, 174*(10), 1405-

D'Orazio, K. N., & Green, R. (2021). Ribosome states signal RNA quality control. *Molecular Cell, 81*(7), 1372-1383. https://doi.org/10.1016/j.molcel.2021.02.022

D'Orazio, K. N., Wu, C. C., Sinha, N., Loll-Krippleber, R., Brown, G. W., & Green, R. (2019). The endonuclease Cue2 cleaves mRNAs at stalled ribosomes during No Go Decay. *eLife, 8*, e49117. https://doi.org/10.7554/eLife.49117

Das, M., Zattas, D., Zinder, J. C., Wasmuth, E. V., Henri, J., & Lima, C. D. (2021). Substrate discrimination and quality control require each catalytic activity of TRAMP and the nuclear RNA exosome. *Proceedings of the National Academy of Sciences of the United States of America, 118*(14), e2024846118. https://doi.org/10.1073/pnas.2024846118

Daszkowska-Golec, A. (2020). Degrade or Silence? - RNA Turnover Takes Control of Epicuticular Wax Synthesis. *Trends in Plant Science, 25*(10), 950-952. https://doi.org/10.1016/j.tplants.2020.06.009

De Bortoli, F., Espinosa, S., & Zhao, R. (2021). DEAH-Box RNA Helicases in Pre-mRNA Splicing. *Trends in Biochemical Sciences, 46*(3), 225-238. https://doi.org/10.1016/j.tibs.2020.10.006

Delan-Forino, C., Spanos, C., Rappsilber, J., & Tollervey, D. (2020). Substrate specificity of the TRAMP nuclear surveillance complexes. *Nature Communications, 11*(1), 3122. https://doi.org/10.1038/s41467-020-16965-4

Dobrev, N., Ahmed, Y. L., Sivadas, A., Soni, K., Fischer, T., & Sinning, I. (2021). The zinc-finger protein Red1 orchestrates MTREC submodules and binds the Mtl1 helicase arch domain. *Nature Communications, 12*(1), 3456. https://doi.org/10.1038/s41467-021-23565-3

Doitsh, G., & Shaul, Y. (2004). Enhancer I predominance in hepatitis B virus gene expression. *Molecular and Cellular Biology, 24*(4), 1799-1808. https://doi.org/10.1128/MCB.24.4.1799-1808.2004

Dorum, S., & Gorukmez, O. (2021). Expanding the clinical spectrum in trichohepatoenteric syndrome. *American Journal of Medical Genetics Part A, 185*(10), 2873-2877. https://doi.org/10.1002/ajmg.a.62354

Dyment, D. A., O'Donnell-Luria, A., Agrawal, P. B., Coban Akdemir, Z., Aleck, K. A., Antaki, D., Al Sharhan, H., Au, P. B., Aydin, H., Beggs, A. H., Bilguvar, K., Boerwinkle, E., Brand, H., Brownstein, C. A., Buyske, S., Chodirker, B., Choi, J., Chudley, A. E., Clericuzio, C. L., … Innes, A. M. (2021) Alternative genomic diagnoses for individuals with a clinical diagnosis of Dubowitz syndrome. *American Journal of Medical Genetics Part A, 185*(1), 119-133. https://doi.org/10.1002/ajmg.a.61926

Dziembowski, A., Lorentzen, E., Conti, E., & Seraphin, B. (2007). A single subunit, Dis3, is essentially responsible for yeast exosome core activity. *Nature Structural and Molecular Biology, 14*(1), 15-22. https://doi.org/10.1038/nsmb1184

Eberle, A. B., Lykke-Andersen, S., Muhlemann, O., & Jensen, T. H. (2009). SMG6 promotes endonucleolytic cleavage of nonsense mRNA in human cells. *Nature Structural and Molecular Biology, 16*(1), 49-55. https://doi.org/10.1038/nsmb.1530

Eckard, S. C., Rice, G. I., Fabre, A., Badens, C., Gray, E. E., Hartley, J. L., Crow, Y. J., & Stetson, D. B. (2014). The SKIV2L RNA exosome limits activation of the RIG-I-like receptors. *Nature Immunology, 15*(9), 839-845. https://doi.org/10.1038/ni.2948

Fabre, A., & Badens, C. (2014). Human Mendelian diseases related to abnormalities of the RNA exosome or its cofactors. *Intractable and Rare Diseases Research, 3*(1), 8-11. https://doi.org/10.5582/irdr.3.8

Fabre, A., Bourgeois, P., Coste, M. E., Roman, C., Barlogis, V., & Badens, C. (2017). Management of syndromic diarrhea/tricho-hepato-enteric syndrome: A review of the literature. *Intractable and Rare Diseases Research, 6*(3), 152-157. https://doi.org/10.5582/irdr.2017.01040

Fabre, A., Breton, A., Coste, M. E., Colomb, V., Dubern, B., Lachaux, A., Lemale, J., Mancini, J., Marinier, E., Martinez-Vinson, C., Peretti, N., Perry, A., Roquelaure, B., Venaille, A., Sarles, J., Goulet, O., & Badens, C. (2014). Syndromic (phenotypic) diarrhoea of infancy/tricho-hepato-enteric syndrome. Archives of Disease in Childhood, 99(1), 35-38. https://doi.org/10.1136/archdischild-2013-304016

Fabre, A., Charroux, B., Martinez-Vinson, C., Roquelaure, B., Odul, E., Sayar, E., Smith, H., Colomb, V., Andre, N., Hugot, J. P., Goulet, O., Lacoste, C., Sarles, J., Royet, J., Levy, N., & Badens, C. (2012). SKIV2L mutations cause syndromic diarrhea, or trichohepatoenteric syndrome. *The American Journal of Human Genetics, 90*(4), 689-692. https://doi.org/10.1016/j.ajhg.2012.02.009

Fabre, A., Martinez-Vinson, C., Goulet, O., & Badens, C. (2013). Syndromic diarrhea/Tricho-hepato-enteric syndrome. *Orphanet Journal of Rare Diseases, 8*, 5. https://doi.org/10.1186/1750-1172-8-5

Fabre, A., Martinez-Vinson, C., Roquelaure, B., Missirian, C., Andre, N., Breton, A., Lachaux, A., Odul, E., Colomb, V., Lemale, J., Cézard, J. P., Goulet, O., Sarles, J., Levy, N., & Badens, C. (2011). Novel mutations in TTC37 associated with tricho-hepato-enteric syndrome. *Human Mutation, 32*(3), 277-281. https://doi.org/10.1002/humu.21420

Fabre, A., Petit, L. M., Hansen, L. F., Wewer, A. V., Esteve, C., Chaix, C., Bourgeois, P., Badens, C., & Paerregaard, A. (2018). A new mutation in the C-terminal end of TTC37 leading to a mild form of syndromic diarrhea/tricho-hepato-enteric syndrome in seven patients from two families. *American Journal of Medical Genetics Part A, 176*(3), 727-732. https://doi.org/10.1002/ajmg.a.38618

Fairman-Williams, M. E., Guenther, U. P., & Jankowsky, E. (2010). SF1 and SF2 helicases: family matters. *Current Opinion in Structural Biology, 20*(3), 313-324. https://doi.org/10.1016/j.sbi.2010.03.011

Falk, S., Tants, J. N., Basquin, J., Thoms, M., Hurt, E., Sattler, M., & Conti, E. (2017). Structural insights into the interaction of the nuclear exosome helicase Mtr4 with the preribosomal protein Nop53. *RNA, 23*(12), 1780-1787. https://doi.org/10.1261/rna.062901.117

Falk, S., Weir, J. R., Hentschel, J., Reichelt, P., Bonneau, F., & Conti, E. (2014). The molecular architecture of the TRAMP complex reveals the organization and interplay of its two catalytic activities. *Molecular Cell, 55*(6), 856-867. https://doi.org/10.1016/j.molcel.2014.07.020

Fernando, M. M., Stevens, C. R., Sabeti, P. C., Walsh, E. C., McWhinnie, A. J., Shah, A., Green, T., Rioux, J. D, & Vyse, T. J. (2007). Identification of two independent risk factors for lupus within the MHC in United Kingdom families. *PLOS Genetics, 3*(11), e192. https://doi.org/10.1371/journal.pgen.0030192

Frischmeyer, P. A., van Hoof, A., O'Donnell, K., Guerrerio, A. L., Parker, R., & Dietz, H. C. (2002). An mRNA surveillance mechanism that eliminates transcripts lacking termination codons. *Science, 295*(5563), 2258-2261. https://doi.org/10.1126/science.1067338

Fung, J. L. F., Yu, M. H. C., Huang, S., Chung, C. C. Y., Chan, M. C. Y., Pajusalu, S., Mak, C. C. Y., Hui, V. C. C., Tsang, M. H. Y., Yeung, K. S., Lek, M., & Chung, B. H. Y. (2020). A three-year follow-up study evaluating clinical utility of exome sequencing and diagnostic potential of reanalysis. *NPJ Genomic Medicine, 5*(1), 37. https://doi.org/10.1038/s41525-020-00144-x

Gao, J., Hu, X., Hu, W., Sun, X., & Chen, L. (2022). Novel TTC37 mutations in a patient with Trichohepatoenteric syndrome: a case report and literature review. *Translational Pediatrics, 11*(6), 1050-1057. https://doi.org/10.21037/tp-21-574

Gerlach, P., Garland, W., Lingaraju, M., Salerno-Kochan, A., Bonneau, F., Basquin, J., Jensen, T. H., & Conti, E. (2022). Structure and regulation of the nuclear exosome targeting complex guides RNA substrates to the exosome. *Molecular Cell, 82*(13), 2505-2518.e7. https://doi.org/10.1016/j.molcel.2022.04.011

Gilman, B., Tijerina, P., & Russell, R. (2017). Distinct RNA-unwinding mechanisms of DEAD-box and DEAH-box RNA helicase proteins in remodeling structured RNAs and RNPs. *Biochemical Society Transactions, 45*(6), 1313-1321. https://doi.org/10.1042/BST20170095

Girault, D., Goulet, O., Le Deist, F., Brousse, N., Colomb, V., Cesarini, J. P., de Potter, S., Canioni, D., Griscelli, C., Fischer, A., & Ricour, C. (1994). Intractable infant diarrhea associated with phenotypic abnormalities and immunodeficiency. *Journal of Pediatrics, 125*(1), 36-42. https://doi.org/10.1016/s0022-3476(94)70118-0

Glover, M. L., Burroughs, A. M., Monem, P. C., Egelhofer, T. A., Pule, M. N., Aravind, L., & Arribere, J. A. (2020). NONU-1 Encodes a Conserved Endonuclease Required for mRNA Translation Surveillance. *Cell Reports, 30*(13), 4321-4331.e4. https://doi.org/10.1016/j.celrep.2020.03.023

Gonzalez, C., Tabernero, D., Cortese, M. F., Gregori, J., Casillas, R., Riveiro-Barciela, M., Godoy, C., Sopena, S., Rando, A., Yll, M., Lopez-Martinez, R., Quer, J., Esteban, R., Buti, M., & Rodriguez-Frias, F. (2018). Detection of hyper-conserved regions in hepatitis B virus X gene potentially useful for gene therapy. *World Journal of Gastroenterology, 24*(19), 2095-2107. https://doi.org/10.3748/wjg.v24.i19.2095

Goulet, O., Vinson, C., Roquelaure, B., Brousse, N., Bodemer, C., & Cezard, J. P. (2008). Syndromic (phenotypic) diarrhea in early infancy. *Orphanet Journal of Rare Diseases, 3*, 6. https://doi.org/10.1186/1750-1172-3-6

Greene, B. L., Kang, G., Cui, C., Bennati, M., Nocera, D. G., Drennan, C. L., & Stubbe, J. (2020). Ribonucleotide Reductases: Structure, Chemistry, and Metabolism Suggest New Therapeutic Targets. *Annual Review of Biochemistry, 89*, 45-75. https://doi.org/10.1146/annurev-biochem-013118-111843

Guydosh, N. R., & Green, R. (2017). Translation of poly(A) tails leads to precise mRNA cleavage. *RNA, 23*(5), 749-761. https://doi.org/10.1261/rna.060418.116

Guydosh, N. R., Kimmig, P., Walter, P., & Green, R. (2017). Regulated Ire1-dependent mRNA decay requires no-go mRNA degradation to maintain endoplasmic reticulum homeostasis in S. pombe. *eLife, 6*, e29216. https://doi.org/10.7554/eLife.29216

Halbach, F., Reichelt, P., Rode, M., & Conti, E. (2013). The yeast ski complex: crystal structure and RNA channeling to the exosome complex. *Cell, 154*(4), 814-826. https://doi.org/10.1016/j.cell.2013.07.017

Halbach, F., Rode, M., & Conti, E. (2012). The crystal structure of S. cerevisiae Ski2, a DExH helicase associated with the cytoplasmic functions of the exosome. *RNA, 18*(1), 124-134. https://doi.org/10.1261/rna.029553.111

Haller, O., Kochs, G., & Weber, F. (2006). The interferon response circuit: induction and suppression by pathogenic viruses. *Virology, 344*(1), 119-130. https://doi.org/10.1016/j.virol.2005.09.024

Hamann, F., Enders, M., & Ficner, R. (2019). Structural basis for RNA translocation by DEAH-box ATPases. *Nucleic Acids Research, 47*(8), 4349-4362. https://doi.org/10.1093/nar/gkz150

Hartley, J. L., Zachos, N. C., Dawood, B., Donowitz, M., Forman, J., Pollitt, R. J., Morgan, N. V., Tee, L., Gissen, P., Kahr, W. H. A., Knisely, A. S., Watson, S., Chitayat, D., Booth, I. W., Protheroe, S., Murphy, S., de Vries, E., Kelly, D. A., & Maher, E. R. (2010). Mutations in TTC37 cause trichohepatoenteric syndrome (phenotypic diarrhea of infancy). *Gastroenterology, 138*(7), 2388-2398, 2398.e1-2. https://doi.org/10.1053/j.gastro.2010.02.010

Hashimoto, Y., Takahashi, M., Sakota, E., & Nakamura, Y. (2017). Nonstop-mRNA decay machinery is involved in the clearance of mRNA 5'-fragments produced by RNAi and NMD in Drosophila melanogaster cells. *Biochemical and Biophysical Research Communications, 484*(1), 1-7. https://doi.org/10.1016/j.bbrc.2017.01.092

He, F., & Jacobson, A. (2015). Nonsense-Mediated mRNA Decay: Degradation of Defective Transcripts Is Only Part of the Story. *Annual Review of Genetics, 49*, 339-366. https://doi.org/10.1146/annurev-genet-112414-054639

Hetz, C., Zhang, K., & Kaufman, R. J. (2020). Mechanisms, regulation and functions of the unfolded protein response. *Nature Reviews Molecular Cell Biology, 21*(8), 421-438. https://doi.org/10.1038/s41580-020-0250-z

Hiejima, E., Yasumi, T., Nakase, H., Matsuura, M., Honzawa, Y., Higuchi, H., Okafuji, O., Yorifuji, T., Tanaka, T., Izawa, K., Kawai, T., Nishikomori, R., & Heike, T. (2017). Tricho-hepato-enteric syndrome with novel SKIV2L gene mutations: A case report. *Medicine (Baltimore), 96*(46), e8601. https://doi.org/10.1097/MD.0000000000008601

Hilbert, M., Karow, A. R., & Klostermeier, D. (2009). The mechanism of ATP-dependent RNA unwinding by DEAD box proteins. *Biological Chemistry, 390*(12), 1237-1250. https://doi.org/10.1515/BC.2009.135

Hooker, T. S., Lam, P., Zheng, H., & Kunst, L. (2007). A core subunit of the RNA-processing/degrading exosome specifically influences cuticular wax biosynthesis in Arabidopsis. *Plant Cell, 19*(3), 904-913. https://doi.org/10.1105/tpc.106.049304

Horikawa, W., Endo, K., Wada, M., & Ito, K. (2016). Mutations in the G-domain of Ski7 cause specific dysfunction in non-stop decay. *Scientific Reports, 6*, 29295. https://doi.org/10.1038/srep29295

Hosking, L. M., Bannister, E. G., Cook, M. C., Choo, S., Kumble, S., & Cole, T. S. (2018). Trichohepatoenteric Syndrome Presenting with Severe Infection and Later Onset Diarrhoea. *Journal of Clinical Immunology, 38*(1), 1-3. https://doi.org/10.1007/s10875-017-0460-0

Ikeuchi, K., Izawa, T., & Inada, T. (2018). Recent Progress on the Molecular Mechanism of Quality Controls Induced by Ribosome Stalling. *Frontiers in Genetics, 9*, 743. https://doi.org/10.3389/fgene.2018.00743

Inada, T. (2020). Quality controls induced by aberrant translation. *Nucleic Acids Research, 48*(3), 1084-1096. https://doi.org/10.1093/nar/gkz1201

Jamar, N. H., Kritsiligkou, P., & Grant, C. M. (2017). The non-stop decay mRNA surveillance pathway is required for oxidative stress tolerance. *Nucleic Acids Research, 45*(11), 6881-6893. https://doi.org/10.1093/nar/gkx306

Joazeiro, C. A. P. (2019). Mechanisms and functions of ribosome-associated protein quality control. *Nature Reviews Molecular Cell Biology, 20*(6), 368-383. https://doi.org/10.1038/s41580-019-0118-2

Johnson, A. W., & Kolodner, R. D. (1995). Synthetic lethality of sep1 (xrn1) ski2 and sep1 (xrn1) ski3 mutants of Saccharomyces cerevisiae is independent of killer virus and suggests a general role for these genes in translation control. *Molecular and Cellular Biology, 15*(5), 2719-2727. https://doi.org/10.1128/MCB.15.5.2719

Johnson, S. J., & Jackson, R. N. (2013). Ski2-like RNA helicase structures: common themes and complex assemblies. *RNA Biology, 10*(1), 33-43. https://doi.org/10.4161/rna.22101

Kalisiak, K., Kulinski, T. M., Tomecki, R., Cysewski, D., Pietras, Z., Chlebowski, A., Kowalska, K., & Dziembowski, A. (2017). A short splicing isoform of HBS1L links the cytoplasmic exosome and SKI complexes in humans. *Nucleic Acids Research, 45*(4), 2068-2080. https://doi.org/10.1093/nar/gkw862

Kammermeier, J., Drury, S., James, C. T., Dziubak, R., Ocaka, L., Elawad, M., Beales, P., Lench, N., Uhlig, H. H., Bacchelli, C., & Shah, N. (2014). Targeted gene panel sequencing in children with very early onset inflammatory bowel disease--evaluation and prospective analysis. *Journal of Medical Genetics, 51*(11), 748-755. https://doi.org/10.1136/jmedgenet-2014-102624

Karaca Edeer, N., Aykut, A., Pariltay, E., Aksu, G., Cogulu, O., & Kutukculer, N. (2019). A Novel TTC37 Mutation Causing Clinical Symptoms of Trichohepatoenteric Syndrome Such as Pyoderma Gangrenosum and Immunodeficiency Without Severe Diarrhea. *Journal of Investigational Allergology and Clinical Immunology, 29*(5), 396-398. https://doi.org/10.18176/jiaci.0418

Karamyshev, A. L., & Karamysheva, Z. N. (2018). Lost in Translation: Ribosome-Associated mRNA and Protein Quality Controls. *Frontiers in Genetics, 9*, 431. https://doi.org/10.3389/fgene.2018.00431

Karousis, E. D., & Muhlemann, O. (2019). Nonsense-Mediated mRNA Decay Begins Where Translation Ends. *Cold Spring Harbor Perspectives in Biology, 11*(2), a032862. https://doi.org/10.1101/cshperspect.a032862

Keller, C., Woolcock, K., Hess, D., & Buhler, M. (2010). Proteomic and functional analysis of the noncanonical poly(A) polymerase Cid14. *RNA, 16*(6), 1124-1129. https://doi.org/10.1261/rna.2053710

Kinnear, C., Glanzmann, B., Banda, E., Schlechter, N., Durrheim, G., Neethling, A., Nel, E., Schoeman, M., Johnson, G., van Helden, P. D., Hoal, E. G., Esser, M., Urban, M., & Moller, M. (2017). Exome sequencing identifies a novel TTC37 mutation in the first reported case of Trichohepatoenteric syndrome (THE-S) in South Africa. *BMC Medical Genetics, 18*(1), 26. https://doi.org/10.1186/s12881-017-0388-5

Klee, E. W., Cousin, M. A., Pinto E Vario F., Morales-Rosado, J. A., Macke, E. L., Jenkinson, W. G., Ferrer, A., Schultz-Rogers, L. E., Olson, R. J., Oliver, G. R., Sigafoos, A. N., Schwab, T. L., Zimmermann, M. T., Urrutia, R. A., Kaiwar, C., Gupta, A., Blackburn, P. R., Boczek, N. J., Prochnow, C. A., … Lazaridis, K. N. (2021). Impact of integrated translational research on clinical exome sequencing. *Genetics in Medicine, 23*(3), 498-507. https://doi.org/10.1038/s41436-020-01005-9

Kogel, A., Keidel, A., Bonneau, F., Schafer, I. B., & Conti, E. (2022). The human SKI complex regulates channeling of ribosome-bound RNA to the exosome via an intrinsic gatekeeping mechanism. *Molecular Cell, 82*(4), 756-769.e8. https://doi.org/10.1016/j.molcel.2022.01.009

Kotecha, U. H., Movva, S., Puri, R. D., & Verma, I. C. (2012). Trichohepatoenteric syndrome: founder mutation in asian indians. *Molecular Syndromology, 3*(2), 89-93. https://doi.org/10.1159/000339896

Kowalinski, E., Kogel, A., Ebert, J., Reichelt, P., Stegmann, E., Habermann, B., & Conti, E. (2016). Structure of a Cytoplasmic 11-Subunit RNA Exosome Complex. *Molecular Cell, 63*(1), 125-134. https://doi.org/10.1016/j.molcel.2016.05.028

Kowalinski, E., Schuller, A., Green, R., & Conti, E. (2015). Saccharomyces cerevisiae Ski7 Is a GTP-Binding Protein Adopting the Characteristic Conformation of Active Translational GTPases. *Structure, 23*(7), 1336-1343. https://doi.org/10.1016/j.str.2015.04.018

Kristal, E., Nahum, A., Ling, G., Broides, A., Shubinsky, G., Eskin-Schwartz, M., Hadar, N., Progador, O., & Birk, O. (2022). Hyper IgM in tricho-hepato-enteric syndrome due to TTC37 mutation. *Immunologic Research, 70*(6):775-780.. https://doi.org/10.1007/s12026-022-09305-9

Labno, A., Tomecki, R., & Dziembowski, A. (2016). Cytoplasmic RNA decay pathways - Enzymes and mechanisms. *Biochimica et Biophysica Acta, 1863*(12), 3125-3147. https://doi.org/10.1016/j.bbamcr.2016.09.023

Labno, A., Warkocki, Z., Kulinski, T., Krawczyk, P. S., Bijata, K., Tomecki, R., & Dziembowski, A. (2016). Perlman syndrome nuclease DIS3L2 controls cytoplasmic non-coding RNAs and provides surveillance pathway for maturing snRNAs. *Nucleic Acids Research, 44*(21), 10437-10453. https://doi.org/10.1093/nar/gkw649

LaCava, J., Houseley, J., Saveanu, C., Petfalski, E., Thompson, E., Jacquier, A., & Tollervey, D. (2005). RNA degradation by the exosome is promoted by a nuclear polyadenylation complex. *Cell, 121*(5), 713-724. https://doi.org/10.1016/j.cell.2005.04.029

Laffleur, B., Batista, C. R., Zhang, W., Lim, J., Yang, B., Rossille, D., Wu, L., Estrella, J., Rothschild, G., Pefanis, E., & Basu, U. (2022). RNA exosome drives early B cell development via noncoding RNA processing mechanisms. *Science Immunology, 7*(72), eabn2738. https://doi.org/10.1126/sciimmunol.abn2738

Laffleur, B., Lim, J., Zhang, W., Chen, Y., Pefanis, E., Bizarro, J., Batista, C. R., Wu, L., Economides, A. N., Wang, J., & Basu, U. (2021). Noncoding RNA processing by DIS3 regulates chromosomal architecture and somatic hypermutation in B cells. *Nature Genetics, 53*(2), 230-242. https://doi.org/10.1038/s41588-020-00772-0

Lam, P., Zhao, L., Eveleigh, N., Yu, Y., Chen, X., & Kunst, L. (2015). The exosome and trans-acting small interfering RNAs regulate cuticular wax biosynthesis during Arabidopsis inflorescence stem development. *Plant Physiology, 167*(2), 323-336. https://doi.org/10.1104/pp.114.252825

Lam, P., Zhao, L., McFarlane, H. E., Aiga, M., Lam, V., Hooker, T. S., & Kunst, L. (2012). RDR1 and SGS3, components of RNA-mediated gene silencing, are required for the regulation of cuticular wax biosynthesis in developing inflorescence stems of Arabidopsis. *Plant Physiology, 159*(4), 1385-1395. https://doi.org/10.1104/pp.112.199646

Lange, H., Ndecky, S. Y. A., Gomez-Diaz, C., Pflieger, D., Butel, N., Zumsteg, J., Kuhn, L., Piermaria, C., Chicher, J., Christie, M., Karaaslan, E. S., Lang, P. L. M., Weigel, D., Vaucheret, H., Hammann, P., & Gagliardi, D. (2019). RST1 and RIPR connect the cytosolic RNA exosome to the Ski complex in Arabidopsis. *Nature Communications, 10*(1), 3871. https://doi.org/10.1038/s41467-019-11807-4

Lassig, C., & Hopfner, K. P. (2017). Discrimination of cytosolic self and non-self RNA by RIG-I-like receptors. *Journal of Biological Chemistry, 292*(22), 9000-9009. https://doi.org/10.1074/jbc.R117.788398

Lee-Kirsch, M. A. (2022). Sensing of RNA stress by mTORC1 drives autoinflammation. *Journal of Clinical Investigation, 132*(2), e156119. https://doi.org/10.1172/JCI156119

Lee, N. N., Chalamcharla, V. R., Reyes-Turcu, F., Mehta, S., Zofall, M., Balachandran, V., Dhakshnamoorthy, J., Taneja, N., Yamanaka, S., Zhou, M., & Grewal, S. I. (2013). Mtr4-like protein coordinates nuclear RNA processing for heterochromatin assembly and for telomere maintenance. *Cell, 155*(5), 1061-1074. https://doi.org/10.1016/j.cell.2013.10.027

Lee, W. I., Huang, J. L., Chen, C. C., Lin, J. L., Wu, R. C., Jaing, T. H., & Ou, L. S. (2016). Identifying Mutations of the Tetratricopeptide Repeat Domain 37 (TTC37) Gene in Infants With Intractable Diarrhea and a Comparison of Asian and Non-Asian Phenotype and Genotype: A Global Case-report Study of a Well-Defined Syndrome With Immunodeficiency. *Medicine (Baltimore), 95*(9), e2918. https://doi.org/10.1097/MD.0000000000002918

Lee, W. S., Teo, K. M., Ng, R. T., Chong, S. Y., Kee, B. P., & Chua, K. H. (2016). Novel mutations in SKIV2L and TTC37 genes in Malaysian children with trichohepatoenteric syndrome. *Gene, 586*(1), 1-6. https://doi.org/10.1016/j.gene.2016.03.049

Lim, J., Giri, P. K., Kazadi, D., Laffleur, B., Zhang, W., Grinstein, V., Pefanis, E., Brown, L. M., Ladewig, E., Martin, O., Chen, Y., Rabadan, R., Boyer, F., Rothschild, G., Cogne, M., Pinaud, E., Deng, H., & Basu, U. (2017). Nuclear Proximity of Mtr4 to RNA Exosome Restricts DNA Mutational Asymmetry. *Cell, 169*(3), 523-537.e15. https://doi.org/10.1016/j.cell.2017.03.043

Linder, P., & Jankowsky, E. (2011). From unwinding to clamping - the DEAD box RNA helicase family. *Nature Reviews Molecular Cell Biology, 12*(8), 505-516. https://doi.org/10.1038/nrm3154

Lingaraju, M., Johnsen, D., Schlundt, A., Langer, L. M., Basquin, J., Sattler, M., Jensen, T. H., Falk, S., & Conti, E. (2019). The MTR4 helicase recruits nuclear adaptors of the human RNA exosome using distinct arch-interacting motifs. *Nature Communications, 10*(1), 3393. https://doi.org/10.1038/s41467-019-11339-x

Liu, J., Carmell, M. A., Rivas, F. V., Marsden, C. G., Thomson, J. M., Song, J. J., Hammond, S. M., Joshua-Tor, L., & Hannon, G. J. (2004). Argonaute2 is the catalytic engine of mammalian RNAi. *Science, 305*(5689), 1437-1441. https://doi.org/10.1126/science.1102513

Liu, J. J., Niu, C. Y., Wu, Y., Tan, D., Wang, Y., Ye, M. D., Liu, Y., Zhao, W., Zhou, K., Liu, Q. S., Dai, J., Yang, X., Dong , M. Q., Huang, N., & Wang, H. W. (2016). CryoEM structure of yeast cytoplasmic exosome complex. *Cell Research, 26*(7), 822-837. https://doi.org/10.1038/cr.2016.56

Liu, L., & Chen, X. (2016). RNA Quality Control as a Key to Suppressing RNA Silencing of Endogenous Genes in Plants. *Molecular Plant, 9*(6), 826-836. https://doi.org/10.1016/j.molp.2016.03.011

Liu, Q., Greimann, J. C., & Lima, C. D. (2006). Reconstitution, activities, and structure of the eukaryotic RNA exosome. *Cell, 127*(6), 1223-1237. https://doi.org/10.1016/j.cell.2006.10.037

Lorant, D. E., & Kua K.L. (2021). Enterocolitis with fulminate sepsis in a newborn with tricho-hepato-enteric syndrome: A case report. *Clinical Case Reports and Reviews, 7*, 1-4. https://doi.org/10.15761/CCRR.1000498

Lubas, M., Christensen, M. S., Kristiansen, M. S., Domanski, M., Falkenby, L. G., Lykke-Andersen, S., Andersen, J. S., Dziembowski, A., Jensen, T. H. (2011). Interaction profiling identifies the human nuclear exosome targeting complex. *Molecular Cell, 43*(4), 624-637. https://doi.org/10.1016/j.molcel.2011.06.028

Lykke-Andersen, S., Tomecki, R., Jensen, T. H., & Dziembowski, A. (2011). The eukaryotic RNA exosome: same scaffold but variable catalytic subunits. *RNA Biology, 8*(1), 61-66. https://doi.org/10.4161/rna.8.1.14237

MacFadden, A., O'Donoghue, Z., Silva, P., Chapman, E. G., Olsthoorn, R. C., Sterken, M. G., Pijlman, G. P., Bredenbeek, P. J., & Kieft, J. S. (2018). Mechanism and structural diversity of exoribonuclease-resistant RNA structures in flaviviral RNAs. *Nature Communications, 9*(1), 119. https://doi.org/10.1038/s41467-017-02604-y

Madrona, A. Y., & Wilson, D. K. (2004). The structure of Ski8p, a protein regulating mRNA degradation: Implications for WD protein structure. *Protein Science, 13*(6), 1557-1565. https://doi.org/10.1110/ps.04704704

Markiewicz, L., Drazkowska, K., & Sikorski, P. J. (2021). Tricks and threats of RNA viruses - towards understanding the fate of viral RNA. *RNA Biology, 18*(5), 669-687. https://doi.org/10.1080/15476286.2021.1875680

Marshall, A. N., Han, J., Kim, M., & van Hoof, A. (2018). Conservation of mRNA quality control factor Ski7 and its diversification through changes in alternative splicing and gene duplication. *Proceedings of the National Academy of Sciences of the United States of America, 115*(29), E6808-E6816. https://doi.org/10.1073/pnas.1801997115

Marshall, A. N., Montealegre, M. C., Jimenez-Lopez, C., Lorenz, M. C., & van Hoof, A. (2013). Alternative splicing and subfunctionalization generates functional diversity in fungal proteomes. *PLoS Genetics, 9*(3), e1003376. https://doi.org/10.1371/journal.pgen.1003376

Masison, D. C., Blanc, A., Ribas, J. C., Carroll, K., Sonenberg, N., & Wickner, R. B. (1995). Decoying the cap- mRNA degradation system by a double-stranded RNA virus and poly(A)- mRNA surveillance by a yeast antiviral system. *Molecular and Cellular Biology, 15*(5), 2763-2771. https://doi.org/10.1128/MCB.15.5.2763

Matsumoto, Y., Sarkar, G., Sommer, S. S., & Wickner, R. B. (1993). A yeast antiviral protein, SKI8, shares a repeated amino acid sequence pattern with beta-subunits of G proteins and several other proteins. *Yeast, 9*(1), 43-51. https://doi.org/10.1002/yea.320090106

Maurel, M., Chevet, E., Tavernier, J., & Gerlo, S. (2014). Getting RIDD of RNA: IRE1 in cell fate regulation. *Trends in Biochemical Sciences, 39*(5), 245-254. https://doi.org/10.1016/j.tibs.2014.02.008

McBride, R. C., Boucher, N., Park, D. S., Turner, P. E., & Townsend, J. P. (2013). Yeast response to LA virus indicates coadapted global gene expression during mycoviral infection. *FEMS Yeast Research, 13*(2), 162-179. https://doi.org/10.1111/1567-1364.12019

McKay, G. J., Silvestri, G., Patterson, C. C., Hogg, R. E., Chakravarthy, U., & Hughes, A. E. (2009). Further assessment of the complement component 2 and factor B region associated with age-related macular degeneration. *Investigative Ophthalmology and Visual Science, 50*(2), 533-539. https://doi.org/10.1167/iovs.08-2275

Meola, N., Domanski, M., Karadoulama, E., Chen, Y., Gentil, C., Pultz, D., Vitting-Seerup, K., Lykke-Andersen, S., Andersen, J. S., Sandelin, A., & Jensen, T. H. (2016). Identification of a Nuclear Exosome Decay Pathway for Processed Transcripts. *Molecular Cell, 64*(3), 520-533. https://doi.org/10.1016/j.molcel.2016.09.025

Mitchell, P., Petfalski, E., Shevchenko, A., Mann, M., & Tollervey, D. (1997). The exosome: a conserved eukaryotic RNA processing complex containing multiple 3'-->5' exoribonucleases. *Cell, 91*(4), 457-466. https://doi.org/10.1016/s0092-8674(00)80432-8

Mitchell, P., & Tollervey, D. (2003). An NMD pathway in yeast involving accelerated deadenylation and exosome-mediated 3'-->5' degradation. *Molecular Cell, 11*(5), 1405-1413. https://doi.org/10.1016/s1097-2765(03)00190-4

Miyao, S., Saito, K., Oshima, R., Kawahara, K., & Nagahama, M. (2022). MTR4 adaptor PICT1 functions in two distinct steps during pre-rRNA processing. *Biochemical and Biophysical Research Communications, 637*, 203-209. https://doi.org/10.1016/j.bbrc.2022.11.018

Monies, D. M., Rahbeeni, Z., Abouelhoda, M., Naim, E. A., Al-Younes, B., Meyer, B. F., & Al-Mehaidib, A. (2015). Expanding phenotypic and allelic heterogeneity of tricho-hepato-enteric syndrome. *Journal of Pediatric Gastroenterology and Nutrition, 60*(3), 352-356. https://doi.org/10.1097/MPG.0000000000000627

Morgan, N. V., Hartley, J. L., Setchell, K. D., Simpson, M. A., Brown, R., Tee, L., Kirkham, S., Pasha, S., Trembath, R. C., Maher, E. R., & Gissen, P., & Kelly, D. A. (2013). A combination of mutations in AKR1D1 and SKIV2L in a family with severe infantile liver disease. *Orphanet Journal of Rare Diseases, 8*, 74. https://doi.org/10.1186/1750-1172-8-74

Neves, J. F., Afonso, I., Borrego, L., Martins, C., Cordeiro, A. I., Neves, C., Lacoste, C., Badens, C., & Fabre, A. (2018). Missense mutation of TTC7A mimicking tricho-hepato-enteric (SD/THE) syndrome in a patient with very-early onset inflammatory bowel disease. *European Journal of Medical Genetics, 61*(4), 185-188. https://doi.org/10.1016/j.ejmg.2017.11.014

Ohnuma, K., Kishita, Y., Nyuzuki, H., Kohda, M., Ohtsu, Y., Takeo, S., Asano, T., Sato-Miyata, J., Ohtake, A., Murayama, K., Okazaki, Y., & Aigaki, T. (2020). Ski3/TTC37 deficiency associated with trichohepatoenteric syndrome causes mitochondrial dysfunction in Drosophila. *FEBS Letters, 594*(13), 2168-2181. https://doi.org/10.1002/1873-3468.13792

Olsen, K. J., & Johnson, S. J. (2021). Mtr4 RNA helicase structures and interactions. *Biological Chemistry, 402*(5), 605-616. https://doi.org/10.1515/hsz-2020-0329

Orban, T. I., & Izaurralde, E. (2005). Decay of mRNAs targeted by RISC requires XRN1, the Ski complex, and the exosome. *RNA, 11*(4), 459-469. https://doi.org/10.1261/rna.7231505

Orlando, L. J., Yim, M. K., Hallmark, T., Cotner, M., Johnson, S. J., & van Hoof, A. (2022). A yeast model for trichohepatoenteric syndrome suggests strong loss of Ski2 function in most causative mutations. *microPublication Biology, 2022*, 10.17912/micropub.biology.000575. https://doi.org/10.17912/micropub.biology.000575

Oz-Levi, D., Weiss, B., Lahad, A., Greenberger, S., Pode-Shakked, B., Somech, R., Olender, T., Tatarsky, P., Marek-Yagel, D., Pras, E., Anikster, Y., & Lancet, D. (2015). Exome sequencing as a differential diagnosis tool: resolving mild trichohepatoenteric syndrome. *Clinical Genetics, 87*(6), 602-603. https://doi.org/10.1111/cge.12494

Ozgur, S., Buchwald, G., Falk, S., Chakrabarti, S., Prabu, J. R., & Conti, E. (2015). The conformational plasticity of eukaryotic RNA-dependent ATPases. *FEBS Journal, 282*(5), 850-863. https://doi.org/10.1111/febs.13198

Passmore, L. A., & Coller, J. (2022). Roles of mRNA poly(A) tails in regulation of eukaryotic gene expression. *Nature Reviews Molecular Cell Biology, 23*(2), 93-106. https://doi.org/10.1038/s41580-021-00417-y

Pefanis, E., Wang, J., Rothschild, G., Lim, J., Chao, J., Rabadan, R., Economides, A. N., & Basu, U. (2014). Noncoding RNA transcription targets AID to divergently transcribed loci in B cells. *Nature, 514*(7522), 389-393. https://doi.org/10.1038/nature13580

Pisareva, V. P., Skabkin, M. A., Hellen, C. U., Pestova, T. V., & Pisarev, A. V. (2011). Dissociation by Pelota, Hbs1 and ABCE1 of mammalian vacant 80S ribosomes and stalled elongation complexes. *EMBO Journal, 30*(9), 1804-1817. https://doi.org/10.1038/emboj.2011.93

Poulton, C., Pathak, G., Mina, K., Lassman, T., Azmanov, D. N., McCormack, E., Broley, S., Dreyer, L., Gration, D., Taylor, E., OSullivan, M., Siafarikis, A., Ravikumara, M., Dawkins, H., Pachter, N., & Baynam, G. (2019). Tricho-hepatic-enteric syndrome (THES) without intractable diarrhoea. *Gene, 699*, 110-114. https://doi.org/10.1016/j.gene.2019.02.059

Powers, K. T., Szeto, J. A., & Schaffitzel, C. (2020). New insights into no-go, non-stop and nonsense-mediated mRNA decay complexes. *Current Opinion in Structural Biology, 65*, 110-118. https://doi.org/10.1016/j.sbi.2020.06.011

Pule, M. N., Glover, M. L., Fire, A. Z., & Arribere, J. A. (2019). Ribosome clearance during RNA interference. *RNA, 25*(8), 963-974. https://doi.org/10.1261/rna.070813.119

Puno, M. R., & Lima, C. D. (2018). Structural basis for MTR4-ZCCHC8 interactions that stimulate the MTR4 helicase in the nuclear exosome-targeting complex. *Proceedings of the National Academy of Sciences of the United States of America, 115*(24), E5506-E5515. https://doi.org/10.1073/pnas.1803530115

Puno, M. R., & Lima, C. D. (2022). Structural basis for RNA surveillance by the human nuclear exosome targeting (NEXT) complex. *Cell, 185*(12), 2132-2147.e26. https://doi.org/10.1016/j.cell.2022.04.016

Qu, X., Yang, Z., Zhang, S., Shen, L., Dangel, A. W., Hughes, J. H., Redman, K. L., Wu, L. C., & Yu, C. Y. (1998). The human DEVH-box protein Ski2w from the HLA is localized in nucleoli and ribosomes. *Nucleic Acids Research, 26*(17), 4068-4077. https://doi.org/10.1093/nar/26.17.4068

Rehwinkel, J., & Gack, M. U. (2020). RIG-I-like receptors: their regulation and roles in RNA sensing. *Nature Reviews Immunology, 20*(9), 537-551. https://doi.org/10.1038/s41577-020-0288-3

Rider, N. L., Boisson, B., Jyonouchi, S., Hanson, E. P., Rosenzweig, S. D., Cassanova, J. L., & Orange, J. S. (2015). Novel TTC37 Mutations in a Patient with Immunodeficiency without Diarrhea: Extending the Phenotype of Trichohepatoenteric Syndrome. *Frontiers in Pediatrics, 3*, 2. https://doi.org/10.3389/fped.2015.00002

Riley, L. G., Cowley, M. J., Gayevskiy, V., Minoche, A. E., Puttick, C., Thorburn, D. R., Rius, R., Compton, A. G., Menezes , M. J., Bhattacharya, K., Coman, D. , Ellaway, C., Alexander, I. E., Adams, L., Kava, M., Robinson, J., Sue, C. M., Balasubramaniam, S., & Christodoulou, J. (2020). The diagnostic utility of genome sequencing in a pediatric cohort with suspected mitochondrial disease. *Genetics in Medicine, 22*(7), 1254-1261. https://doi.org/10.1038/s41436-020-0793-6

Rudilla, F., Franco-Jarava, C., Martinez-Gallo, M., Garcia-Prat, M., Martin-Nalda, A., Riviere, J., Aguilo-Cucurull, A., Mongay, L., Vidal, F., Solanich, X., Irastorza, I., Santos-Perez, J. L., Sanchez, J. T., Cusco, I., Serra, C., Baz-Redon, N., Fernandez-Cancio, M., Carreras, C., Vagace, J. M., … Colobran, R. (2019). Expanding the Clinical and Genetic Spectra of Primary Immunodeficiency-Related Disorders With Clinical Exome Sequencing: Expected and Unexpected Findings. *Frontiers in Immunology, 10*, 2325. https://doi.org/10.3389/fimmu.2019.02325

Saito, S., Hosoda, N., & Hoshino, S. (2013). The Hbs1-Dom34 protein complex functions in non-stop mRNA decay in mammalian cells. *Journal of Biological Chemistry, 288*(24), 17832-17843. https://doi.org/10.1074/jbc.M112.448977

San Paolo, S., Vanacova, S., Schenk, L., Scherrer, T., Blank, D., Keller, W., & Gerber, A. P. (2009). Distinct roles of non-canonical poly(A) polymerases in RNA metabolism. *PLoS Genetics, 5*(7), e1000555. https://doi.org/10.1371/journal.pgen.1000555

Scheer, H., de Almeida, C., Ferrier, E., Simonnot, Q., Poirier, L., Pflieger, D., Sement, F. M., Koechler, S., Piermaria, C., Krawczyk, P., Mroczek, S., Chicher, J., Kuhn, L., Dziembowski, A., Hammann, P., Zuber, H., & Gagliardi, D. (2021). The TUTase URT1 connects decapping activators and prevents the accumulation of excessively deadenylated mRNAs to avoid siRNA biogenesis. *Nature Communications, 12*(1), 1298. https://doi.org/10.1038/s41467-021-21382-2

Schmidt, C., Kowalinski, E., Shanmuganathan, V., Defenouillere, Q., Braunger, K., Heuer, A., Pech, M., Namane, A., Berninghausen, O.,Fromont-Racine, M., Jacquier, A., Conti, E., Becker, T., & Beckmann, R. (2016). The cryo-EM structure of a ribosome-Ski2-Ski3-Ski8 helicase complex. *Science, 354*(6318), 1431-1433. https://doi.org/10.1126/science.aaf7520

Seago, J. E., Chernukhin, I. V., & Newbury, S. F. (2001). The Drosophila gene twister, an orthologue of the yeast helicase SKI2, is differentially expressed during development. *Mechanisms of Development, 106*(1-2), 137-141. https://doi.org/10.1016/s0925-4773(01)00429-4

Shichino, Y., Otsubo, Y., Yamamoto, M., & Yamashita, A. (2020). Meiotic gene silencing complex MTREC/NURS recruits the nuclear exosome to YTH-RNA-binding protein Mmi1. *PLoS Genetics, 16*(2), e1008598. https://doi.org/10.1371/journal.pgen.1008598

Shiromoto, F., Aly, H. H., Kudo, H., Watashi, K., Murayama, A., Watanabe, N., Zheng, X., Kato, T., Chayama, K., Muramatsu, M., & Wakita, T. (2018). IL-1beta/ATF3-mediated induction of Ski2 expression enhances hepatitis B virus x mRNA degradation. *Biochemical and Biophysical Research Communications, 503*(3), 1854-1860. https://doi.org/10.1016/j.bbrc.2018.07.126

Shoemaker, C. J., & Green, R. (2011). Kinetic analysis reveals the ordered coupling of translation termination and ribosome recycling in yeast. *Proceedings of the National Academy of Sciences of the United States of America, 108*(51), E1392-1398. https://doi.org/10.1073/pnas.1113956108

Sikorska, N., Zuber, H., Gobert, A., Lange, H., & Gagliardi, D. (2017). RNA degradation by the plant RNA exosome involves both phosphorolytic and hydrolytic activities. *Nature Communications, 8*(1), 2162. https://doi.org/10.1038/s41467-017-02066-2

Silla, T., Schmid, M., Dou, Y., Garland, W., Milek, M., Imami, K., Johnsen, D., Polak, P., Andersen, J. S., Selbach, M., Landthaler, M., & Jensen, T. H. (2020). The human ZC3H3 and RBM26/27 proteins are critical for PAXT-mediated nuclear RNA decay. *Nucleic Acids Research, 48*(5), 2518-2530. https://doi.org/10.1093/nar/gkz1238

Simms, C. L., Hudson, B. H., Mosior, J. W., Rangwala, A. S., & Zaher, H. S. (2014). An active role for the ribosome in determining the fate of oxidized mRNA. *Cell Reports, 9*(4), 1256-1264. https://doi.org/10.1016/j.celrep.2014.10.042

Sloan, K. E., & Bohnsack, M. T. (2018). Unravelling the Mechanisms of RNA Helicase Regulation. *Trends in Biochemical Sciences, 43*(4), 237-250. https://doi.org/10.1016/j.tibs.2018.02.001

Souret, F. F., Kastenmayer, J. P., & Green, P. J. (2004). AtXRN4 degrades mRNA in Arabidopsis and its substrates include selected miRNA targets. *Molecular Cell, 15*(2), 173-183. https://doi.org/10.1016/j.molcel.2004.06.006

Stadelmayer, B., Diederichs, A., Chapus, F., Rivoire, M., Neveu, G., Alam, A., Fraisse, L., Carter, K., Testoni, B., & Zoulim, F. (2020). Full-length 5'RACE identifies all major HBV transcripts in HBV-infected hepatocytes and patient serum. *Journal of Hepatology, 73*(1), 40-51. https://doi.org/10.1016/j.jhep.2020.01.028

Stankler, L., Lloyd, D., Pollitt, R. J., Gray, E. S., Thom, H., & Russell, G. (1982). Unexplained diarrhoea and failure to thrive in 2 siblings with unusual facies and abnormal scalp hair shafts: a new syndrome. *Archives of Disease in Childhood, 57*(3), 212-216. https://doi.org/10.1136/adc.57.3.212

Studer, M. K., Ivanovic, L., Weber, M. E., Marti, S., & Jonas, S. (2020). Structural basis for DEAH-helicase activation by G-patch proteins. *Proceedings of the National Academy of Sciences of the United States of America, 117*(13), 7159-7170. https://doi.org/10.1073/pnas.1913880117

Sudo, H., Nozaki, A., Uno, H., Ishida, Y., & Nagahama, M. (2016). Interaction properties of human TRAMP-like proteins and their role in pre-rRNA 5'ETS turnover. *FEBS Letters, 590*(17), 2963-2972. https://doi.org/10.1002/1873-3468.12314

Synowsky, S. A., & Heck, A. J. (2008). The yeast Ski complex is a hetero-tetramer. *Protein Science, 17*(1), 119-125. https://doi.org/10.1110/ps.073155908

Szadeczky-Kardoss, I., Csorba, T., Auber, A., Schamberger, A., Nyiko, T., Taller, J., Orban, T. I., Burgyan, J., & Silhavy, D. (2018). The nonstop decay and the RNA silencing systems operate cooperatively in plants. *Nucleic Acids Research, 46*(9), 4632-4648. https://doi.org/10.1093/nar/gky279

Szadeczky-Kardoss, I., Gal, L., Auber, A., Taller, J., & Silhavy, D. (2018). The No-go decay system degrades plant mRNAs that contain a long A-stretch in the coding region. *Plant Science, 275*, 19-27. https://doi.org/10.1016/j.plantsci.2018.07.008

Taher, Z. A., Alzahrani, S., Alsaghir, A., Nouh, F., & Alshumrani, M. (2020). A New Variant Mutation in SKIV2L Gene in Case of Trichohepatoenteric Syndrome. *Pediatric Reports, 12*(3), 93-97. https://doi.org/10.3390/pediatric12030021

Takahashi, S., Araki, Y., Sakuno, T., & Katada, T. (2003). Interaction between Ski7p and Upf1p is required for nonsense-mediated 3'-to-5' mRNA decay in yeast. *EMBO Journal, 22*(15), 3951-3959. https://doi.org/10.1093/emboj/cdg374

Tauchert, M. J., Fourmann, J. B., Luhrmann, R., & Ficner, R. (2017). Structural insights into the mechanism of the DEAH-box RNA helicase Prp43. *eLiife, 6*, e21510. https://doi.org/10.7554/eLife.21510

Thoms, M., Thomson, E., Bassler, J., Gnadig, M., Griesel, S., & Hurt, E. (2015). The Exosome Is Recruited to RNA Substrates through Specific Adaptor Proteins. *Cell, 162*(5), 1029-1038. https://doi.org/10.1016/j.cell.2015.07.060

Toh-E, A., Guerry, P., & Wickner, R. B. (1978). Chromosomal superkiller mutants of Saccharomyces cerevisiae. *Journal of Bacteriology, 136*(3), 1002-1007. https://doi.org/10.1128/jb.136.3.1002-1007.1978

Tomecki, R., Kristiansen, M. S., Lykke-Andersen, S., Chlebowski, A., Larsen, K. M., Szczesny, R. J., Drazkowska, K., Pastula, A., Andersen, J. S., Stepien, P. P., Dziembowski, A., & Jensen, T. H. (2010). The human core exosome interacts with differentially localized processive RNases: hDIS3 and hDIS3L. *EMBO Journal, 29*(14), 2342-2357. https://doi.org/10.1038/emboj.2010.121

Tuck, A. C., Rankova, A., Arpat, A. B., Liechti, L. A., Hess, D., Iesmantavicius, V., Castelo-Szekely, V., Gatfield, D., & Buhler, M. (2020). Mammalian RNA Decay Pathways Are Highly Specialized and Widely Linked to Translation. *Molecular Cell, 77*(6), 1222-1236.e13. https://doi.org/10.1016/j.molcel.2020.01.007

Tudek, A., Porrua, O., Kabzinski, T., Lidschreiber, M., Kubicek, K., Fortova, A., Lacroute, F., Vanacova, S., Cramer, P., Stefl, R., & Libri, D. (2014). Molecular basis for coordinating transcription termination with noncoding RNA degradation. *Molecular Cell, 55*(3), 467-481. https://doi.org/10.1016/j.molcel.2014.05.031

van Hoof, A., Frischmeyer, P. A., Dietz, H. C., & Parker, R. (2002). Exosome-mediated recognition and degradation of mRNAs lacking a termination codon. *Science, 295*(5563), 2262-2264. https://doi.org/10.1126/science.1067272

van Hoof, A., Lennertz, P., & Parker, R. (2000). Yeast exosome mutants accumulate 3'-extended polyadenylated forms of U4 small nuclear RNA and small nucleolar RNAs. *Molecular and Cellular Biology, 20*(2), 441-452. https://doi.org/10.1128/MCB.20.2.441-452.2000

van Hoof, A., Staples, R. R., Baker, R. E., & Parker, R. (2000). Function of the ski4p (Csl4p) and Ski7p proteins in 3'-to-5' degradation of mRNA. *Molecular and Cellular Biology, 20*(21), 8230-8243. https://doi.org/10.1128/MCB.20.21.8230-8243.2000

van Schouwenburg, P. A., Davenport, E. E., Kienzler, A. K., Marwah, I., Wright, B., Lucas, M., Malinauskas, T., Martin, H. C., WGS500 Consortium, Lockstone, H. E., Cazier, J. B., Chapel, H. M., Knight, J. C., & Patel, S. Y. (2015). Application of whole genome and RNA sequencing to investigate the genomic landscape of common variable immunodeficiency disorders. *Clinical Immunology, 160*(2), 301-314. https://doi.org/10.1016/j.clim.2015.05.020

Vanacova, S., Wolf, J., Martin, G., Blank, D., Dettwiler, S., Friedlein, A., Langen, H., Keith, G., & Keller, W. (2005). A new yeast poly(A) polymerase complex involved in RNA quality control. *PLoS Biology, 3*(6), e189. https://doi.org/10.1371/journal.pbio.0030189

Vardi, I., Barel, O., Sperber, M., Schvimer, M., Nunberg, M., Field, M., Ouahed, J., Marek-Yagel, D., Werner, L., Haberman, Y., Lahad, A., Anikster, Y., Rechavi, G., Barshack, I., McElwee, J. J., Maranville, J., Somech, R., Snapper, S. B., Weiss, B., & Shouval, D. S. (2018). Genetic and Structural Analysis of a SKIV2L Mutation Causing Tricho-hepato-enteric Syndrome. *Digestive Diseases and Sciences, 63*(5), 1192-1199. https://doi.org/10.1007/s10620-018-4983-x

Vely, F., Barlogis, V., Marinier, E., Coste, M. E., Dubern, B., Dugelay, E., Lemale, J., Martinez-Vinson, C., Peretti, N., Perry, A., Bourgeois, P., Badens, C., Goulet, O., Hugot, J. P., Farnarier, C., & Fabre, A. (2018). Combined Immunodeficiency in Patients With Trichohepatoenteric Syndrome. *Frontiers in Immunology, 9*, 1036. https://doi.org/10.3389/fimmu.2018.01036

Verloes, A., Lombet, J., Lambert, Y., Hubert, A. F., Deprez, M., Fridman, V., Gosseye, S., Rigo, J., & Sokal, E. (1997). Tricho-hepato-enteric syndrome: further delineation of a distinct syndrome with neonatal hemochromatosis phenotype, intractable diarrhea, and hair anomalies. *American Journal of Medical Genetics, 68*(4), 391-395. https://doi.org/10.1002/(sici)1096-8628(19970211)68:4<391::aid-ajmg3>3.0.co;2-p

Vicens, Q., Kieft, J. S., & Rissland, O. S. (2018). Revisiting the Closed-Loop Model and the Nature of mRNA 5'-3' Communication. *Molecular Cell, 72*(5), 805-812. https://doi.org/10.1016/j.molcel.2018.10.047

Wang, J., Chen, J., Wu, G., Zhang, H., Du, X., Chen, S., Zhang, L., Wang, K., Fan, J., Gao, S., Wu, X., Zhang, S., Kuai, B., Zhao, P., Chi, B., Wang, L., Li, G., Wong, C. C. L., Zhou, Y., … Cheng, H. (2019). NRDE2 negatively regulates exosome functions by inhibiting MTR4 recruitment and exosome interaction. *Genes and Development, 33*(9-10), 536-549. https://doi.org/10.1101/gad.322602.118

Wang, L., Lewis, M. S., & Johnson, A. W. (2005). Domain interactions within the Ski2/3/8 complex and between the Ski complex and Ski7p. *RNA, 11*(8), 1291-1302. https://doi.org/10.1261/rna.2060405

Wang, X., Kong, W., Wang, Y., Wang, J., Zhong, L., Lao, K., Dong, X.,Zhang, D., Huang, H., Mo, B., Yu, Y., & Ren, G. (2022). Uridylation and the SKI complex orchestrate the Calvin cycle of photosynthesis through RNA surveillance of TKL1 in Arabidopsis. *Proceedings of the National Academy of Sciences of the United States of America, 119*(38), e2205842119. https://doi.org/10.1073/pnas.2205842119

Weick, E. M., Puno, M. R., Januszyk, K., Zinder, J. C., DiMattia, M. A., & Lima, C. D. (2018). Helicase-Dependent RNA Decay Illuminated by a Cryo-EM Structure of a Human Nuclear RNA Exosome-MTR4 Complex. *Cell, 173*(7), 1663-1677.e21. https://doi.org/10.1016/j.cell.2018.05.041

Weir, J. R., Bonneau, F., Hentschel, J., & Conti, E. (2010). Structural analysis reveals the characteristic features of Mtr4, a DExH helicase involved in nuclear RNA processing and surveillance. *Proceedings of the National Academy of Sciences of the United States of America, 107*(27), 12139-12144. https://doi.org/10.1073/pnas.1004953107

Weston, S., Baracco, L., Keller, C., Matthews, K., McGrath, M. E., Logue, J., Liang, J., Dyall, J., Holbrook, M. R., Hensley, L. E., Jahrling, P. B., Yu, W., MacKerell Jr, A. D., & Frieman, M. B. (2020). The SKI complex is a broad-spectrum, host-directed antiviral drug target for

coronaviruses, influenza, and filoviruses. *Proceedings of the National Academy of Sciences of the United States of America, 117*(48), 30687-30698. https://doi.org/10.1073/pnas.2012939117

Wickner, R. B. (1992). Double-stranded and single-stranded RNA viruses of Saccharomyces cerevisiae. *Annual Review of Microbiology, 46*, 347-375. https://doi.org/10.1146/annurev.mi.46.100192.002023

Wickner, R. B. (1996a). Double-stranded RNA viruses of Saccharomyces cerevisiae. *Microbiology Reviews, 60*(1), 250-265. https://doi.org/10.1128/mr.60.1.250-265.1996

Wickner, R. B. (1996b). Prions and RNA viruses of Saccharomyces cerevisiae. *Annual Review of Genetics, 30*, 109-139. https://doi.org/10.1146/annurev.genet.30.1.109

Widner, W. R., & Wickner, R. B. (1993). Evidence that the SKI antiviral system of Saccharomyces cerevisiae acts by blocking expression of viral mRNA. *Molecular and Cellular Biology, 13*(7), 4331-4341. https://doi.org/10.1128/mcb.13.7.4331-4341.1993

Win, T. Z., Draper, S., Read, R. L., Pearce, J., Norbury, C. J., & Wang, S. W. (2006). Requirement of fission yeast Cid14 in polyadenylation of rRNAs. *Molecular and Cellular Biology, 26*(5), 1710-1721. https://doi.org/10.1128/MCB.26.5.1710-1721.2006

Wu, G., Schmid, M., Rib, L., Polak, P., Meola, N., Sandelin, A., & Jensen, T. H. (2020). A Two-Layered Targeting Mechanism Underlies Nuclear RNA Sorting by the Human Exosome. *Cell Reports, 30*(7), 2387-2401.e5. https://doi.org/10.1016/j.celrep.2020.01.068

Wurm, J. P., & Sprangers, R. (2019). Dcp2: an mRNA decapping enzyme that adopts many different shapes and forms. *Current Opinion in Structural Biology, 59*, 115-123. https://doi.org/10.1016/j.sbi.2019.07.009

Xinias, I., Mavroudi, A., Mouselimis, D., Tsarouchas, A., Vasilaki, K., Roilides, I., Lacaille, F., & Giouleme, O. (2018). Trichohepatoenteric syndrome: A rare mutation in SKIV2L gene in the first Balkan reported case. *SAGE Open Medical Case Reports, 6*, 2050313X18807795. https://doi.org/10.1177/2050313X18807795

Xu, C., & Min, J. (2011). Structure and function of WD40 domain proteins. *Protein and Cell, 2*(3), 202-214. https://doi.org/10.1007/s13238-011-1018-1

Yang, K., Han, J., Asada, M., Gill, J. G., Park, J. Y., Sathe, M. N., Gattineni, J., Wright, T., Wysocki, C. A., de la Morena. M. T., Garza, L. A., & Yan, N. (2022). Cytoplasmic RNA quality control failure engages mTORC1-mediated autoinflammatory disease. *Journal of Clinical Investigation, 132*(2), e146176. https://doi.org/10.1172/JCI146176

Yang, K., Han, J., Gill, J. G., Park, J. Y., Sathe, M. N., Gattineni, J., Wright, T., Wysocki, C., de la Morena, M. T., & Yan, N. (2022). The mammalian SKIV2L RNA exosome is essential for early B cell development. *Science Immunology, 7*(72), eabn2888. https://doi.org/10.1126/sciimmunol.abn2888

Yang, M., Jiang, Y., & Shao, X. (2022). Case Report: A Novel Homozygous Frameshift Mutation of the SKIV2L Gene in a Trichohepatoenteric Syndrome Patient Presenting With Short Stature, Premature Ovarian Failure, and Osteoporosis. *Frontiers in Genetics, 13*, 879899. https://doi.org/10.3389/fgene.2022.879899

Yoshikatsu, Y., Ishida, Y., Sudo, H., Yuasa, K., Tsuji, A., & Nagahama, M. (2015). NVL2, a nucleolar AAA-ATPase, is associated with the nuclear exosome and is involved in pre-rRNA processing. *Biochemical and Biophysical Research Communications, 464*(3), 780-786. https://doi.org/10.1016/j.bbrc.2015.07.032

Yu, A., Saudemont, B., Bouteiller, N., Elvira-Matelot, E., Lepere, G., Parent, J. S., Morel, J. B., Cao, J., Elmayan, T., & Vaucheret, H. (2015). Second-Site Mutagenesis of a Hypomorphic argonaute1 Allele Identifies SUPERKILLER3 as an Endogenous Suppressor of Transgene Posttranscriptional Gene Silencing. *Plant Physiology, 169*(2), 1266-1274. https://doi.org/10.1104/pp.15.00585

Zamore, P. D., Tuschl, T., Sharp, P. A., & Bartel, D. P. (2000). RNAi: double-stranded RNA directs the ATP-dependent cleavage of mRNA at 21 to 23 nucleotide intervals. *Cell, 101*(1), 25-33. https://doi.org/10.1016/S0092-8674(00)80620-0

Zeytuni, N., & Zarivach, R. (2012). Structural and functional discussion of the tetra-trico-peptide repeat, a protein interaction module. *Structure, 20*(3), 397-405. https://doi.org/10.1016/j.str.2012.01.006

Zhang, E., Khanna, V., Dacheux, E., Namane, A., Doyen, A., Gomard, M., Turcotte, B., Jacquier, A., & Fromont-Racine, M. (2019). A specialised SKI complex assists the cytoplasmic RNA exosome in the absence of direct association with ribosomes. *EMBO Journal, 38*(14), e100640. https://doi.org/10.15252/embj.2018100640

Zhang, Q., Qian, X., Zhou, J., Han, L., Zhou, S., & Wang, Z. (2021). Case Report: Novel Compound-Heterozygous Variants of SKIV2L Gene that Cause Trichohepatoenteric Syndrome 2. *Frontiers in Genetics, 12*, 756451. https://doi.org/10.3389/fgene.2021.756451

Zhang, X., Zhu, Y., Liu, X., Hong, X., Xu, Y., Zhu, P., Shen, Y., Wu, H., Ji, Y., Wen, X., Zhang, C., Zhao, Q., Wang, Y., Lu, J., & Guo, H. (2015). Plant biology. Suppression of endogenous gene silencing by bidirectional cytoplasmic RNA decay in Arabidopsis. *Science, 348*(6230), 120-123. https://doi.org/10.1126/science.aaa2618

Zhao, L., & Kunst, L. (2016). SUPERKILLER Complex Components Are Required for the RNA Exosome-Mediated Control of Cuticular Wax Biosynthesis in Arabidopsis Inflorescence Stems. *Plant Physiology, 171*(2), 960-973. https://doi.org/10.1104/pp.16.00450

Zheng, B., Pan, J., Jin, Y., Wang, C., & Liu, Z. (2016). Targeted next-generation sequencing identification of a novel missense mutation of the SKIV2L gene in a patient with trichohepatoenteric syndrome. *Molecular Medicine Reports, 14*(3), 2107-2110. https://doi.org/10.3892/mmr.2016.5503

Zhou, D., Lai, M., Luo, A., & Yu, C. Y. (2019). An RNA Metabolism and Surveillance Quartet in the Major Histocompatibility Complex. *Cells, 8*(9). https://doi.org/10.3390/cells8091008

Zhou, Y., Zhu, J., Schermann, G., Ohle, C., Bendrin, K., Sugioka-Sugiyama, R., Sugiyama , T., & Fischer, T. (2015). The fission yeast MTREC complex targets CUTs and unspliced pre-mRNAs to the nuclear exosome. *Nature Communications, 6*, 7050. https://doi.org/10.1038/ncomms8050

Zinoviev, A., Ayupov, R. K., Abaeva, I. S., Hellen, C. U. T., & Pestova, T. V. (2020). Extraction of mRNA from Stalled Ribosomes by the Ski Complex. *Molecular Cell, 77*(6), 1340-1349.e6. https://doi.org/10.1016/j.molcel.2020.01.011

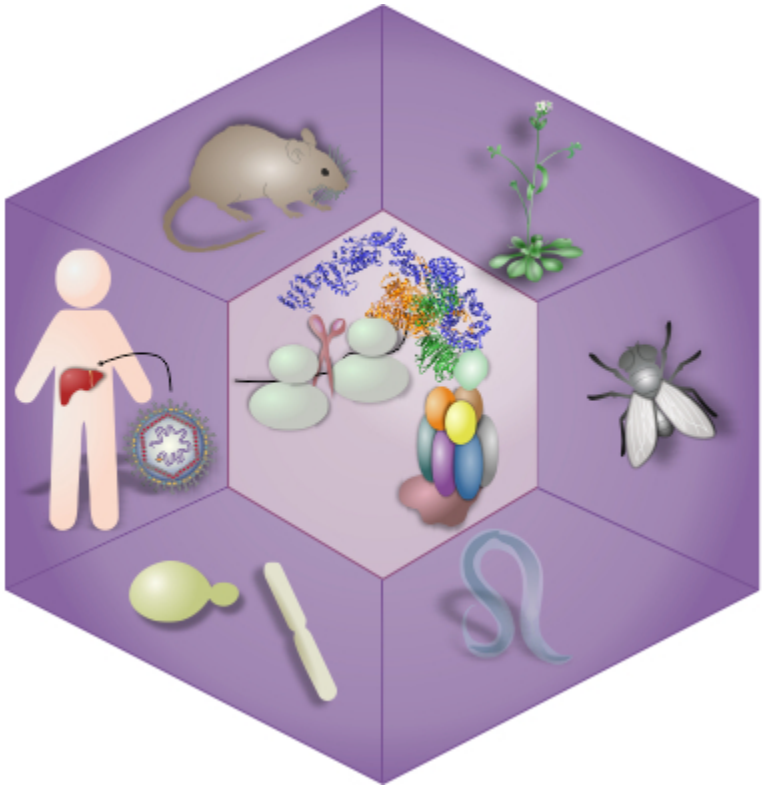

Structurally characterized SKI complex collaborates with the exosome and ribosome in translation-dependent mRNA decay and surveillance and plays versatile roles in disease, signaling pathways, antiviral responses, and developmental regulation across eukaryotic species.

32x33mm (300 x 300 DPI)

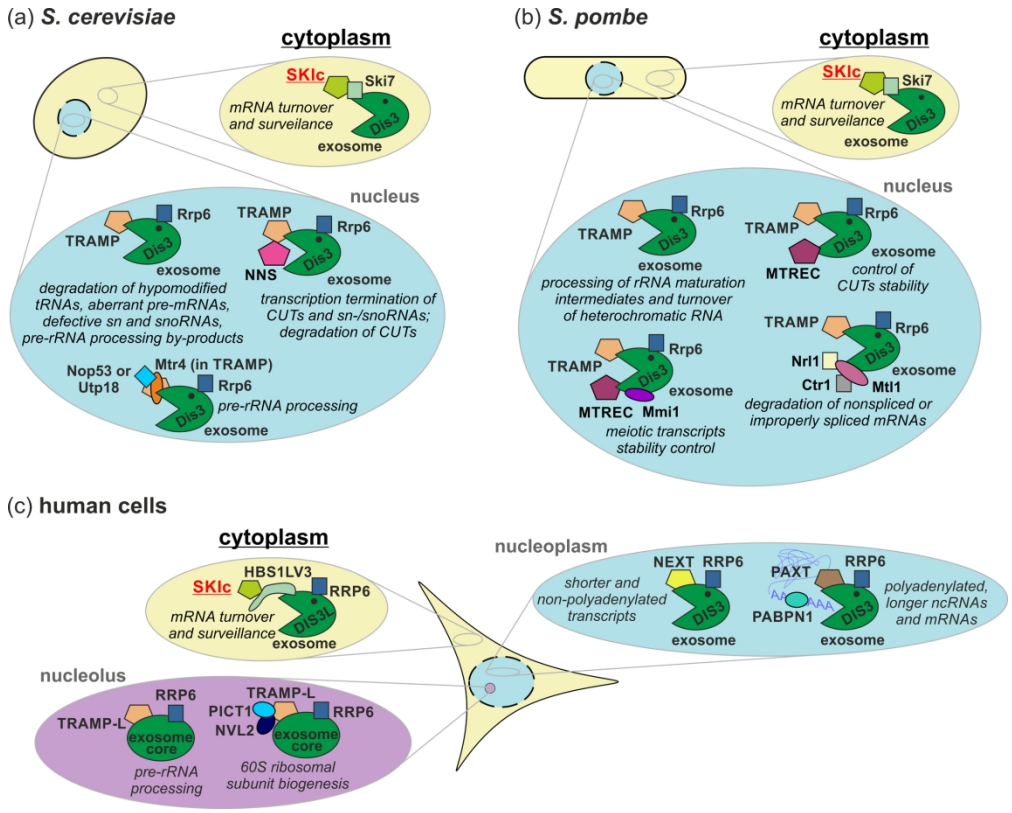

Nuclear exosome is accompanied by diverse accessory complexes containing different RNA helicases, whereas cytoplasmic exosome functions are supported exclusively by SKIc in different eukaryotic species (a-c). (a) In the nucleus of S. cerevisiae Mtr4 provides helicase activity to the TRAMP complex, containing also Trf4/5 non-canonical poly(A) polymerase (PAP), and the zinc-knuckle RNA-binding protein Air1/2; distinct TRAMP isoforms, formed by inclusion of Trf4 or Trf5 and Air1 or Air2 paralogs, enable degradation or precise trimming of ribosomal RNA precursors, pre-mRNAs, hypomodified tRNAs, sn- and snoRNAs, as well as cryptic unstable transcripts (CUTs), in the nucleolus or in the nucleoplasm; TRAMP-exosome recruitment to CUTs and sn-/snoRNAs is aided by interaction with Nrd1-Nab3-Sen1 (NNS) complex, which mediates transcription termination of those RNAs; Mtr4 in budding yeast can also associate via its arch domain with Nop53 or Utp18 for pre-rRNA processing or degradation of its by-products. (b) In Schizosaccharomyces pombe apart from TRAMP, encompassing Mtr4, Air1, and Cid14 (Trf4/5 ortholog), which partakes i.a. in the processing of rRNA maturation intermediates and heterochromatic RNA turnover, additional co-factors exist, either of which contains Mtr4 paralog, known as Mtl1; one of them, MTREC (or NURS), contains Red1 zinc-finger protein and controls stability of CUTs, and – together with additional partners, such as Mmi1 – meiotic transcripts; Mtl1 can alternatively interact with Nrl1 and Ctr1 to degrade un- or misspliced mRNAs. (c) In human cell nucleolus, besides TRAMP-like complex composed of MTR4/SKIV2L2, PAPD5 or PAPD7, and ZCCHC7 Zn-knuckle protein, MTR4 interacts with NVL2 and with Nop53 ortholog – PICT1, to ensure proper 60S ribosomal subunit biogenesis; in the nucleoplasm MTR4 forms complexes with either RBM7-ZCCHC8 or ZFC3H1, referred to as NEXT and PAXT, respectively; in addition, an important connection between the PAXT dimeric core and PABPN1 protein is mediated by RNA; significant functional specialization between NEXT and PAXT is apparent, with the former targeting shorter and non-polyadenylated transcripts, such as PROMPTs, upstream antisense RNAs, enhancer RNAs and the latter recruiting the exosome to longer ncRNAs and mRNAs, which are polyadenylated. (a-c) An exclusive partner of the cytoplasmic exosome in the regulation of mRNA turnover and surveillance, endowed with enzymatic activity of Ski2 RNA helicase and common for all species, is SKIc (marked in red and underlined). Interaction between SKIc and exosome is bridged by Ski7 in yeast (a,b) and HBS1LV3 in human cells (c).

190x152mm (300 x 300 DPI)

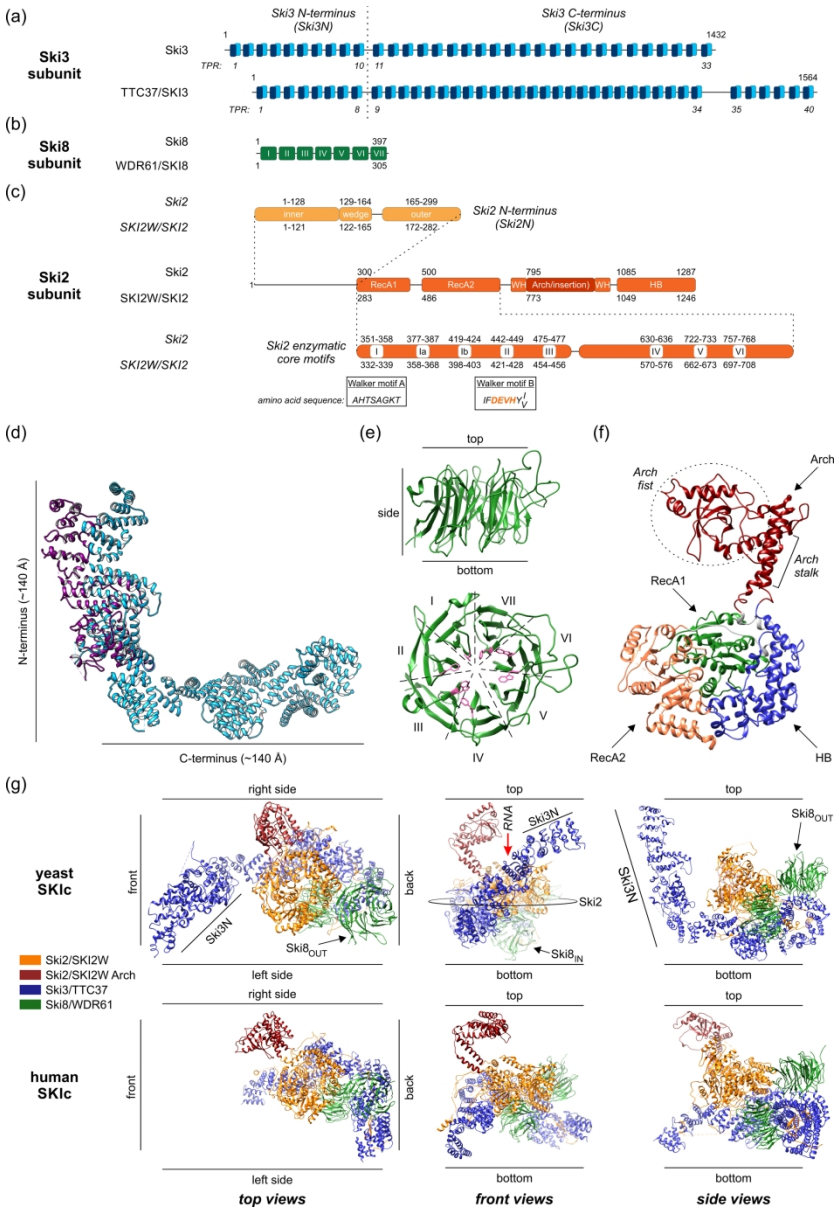

Structural features of SKIc subunits and the entire complex. (a) Comparison of TPR motifs distribution in yeast Ski3 and human TTC37; numbers above correspond to amino acids; numbering of TPR motifs is provided below, in italics; vertical dashed line indicates the boundary between TPRs building N-terminal (Ski3N) and C-terminal (Ski3C) parts of proteins. (b) Schematic presentation of Ski8/WDR61 secondary structure, with seven WD40 repeats indicated with roman numerals; numbers above and below correspond to amino acid positions in yeast Ski8 and human WDR61, respectively. (c) middle: domain organization of Ski2/SKI2W; WH – winged helix; HB – helical bundle; top: three segments of the Ski2 N-terminus (Ski2N); bottom: location of the eight enzymatic core motifs within Ski2 RecA domains; numbers above and below correspond to amino acid positions in yeast Ski2 and human SKI2W, respectively; amino acid sequences of motifs I and II (Walker motifs A and B) are provided in rectangular boxes; DExH signature in Walker motif B is indicated in orange. (d) Structure of the yeast Ski3 is shown in bright blue, with N- and C-terminal arms indicated. Purple ribbons visualize translocation of the N-terminal arm into position characteristic for substrate and ribosome binding. (e) Structure of the yeast Ski8 protein from the front (top panel) and top (bottom panel); dashed lines separate seven blades of the beta-propeller, indicated with roman numerals

and the residues important for Ski3 binding are highlighted in pink in the bottom panel. (f) Structure of the yeast Ski2 helicase with functional domains indicated with arrows and highlighted in separate colors (red – the Arch/insertion domain with the stalk and the fist additionally marked; blue – the HB domain; orange – the RecA1 domain; green – the RecA2 domain). (g) top: three distinct views of the yeast SKIc structure; positions of selected structural elements are indicated; the site where RNA substrate enters the channel is marked with red arrow; bottom: corresponding views of the human SKIc; the N-terminal part of TTC37 is missing in the human structure; structures of both complexes were compared using MatchMaker tool of UCSF Chimera package, based on the Ski2/SKI2W helicase structure.

197x285mm (300 x 300 DPI)

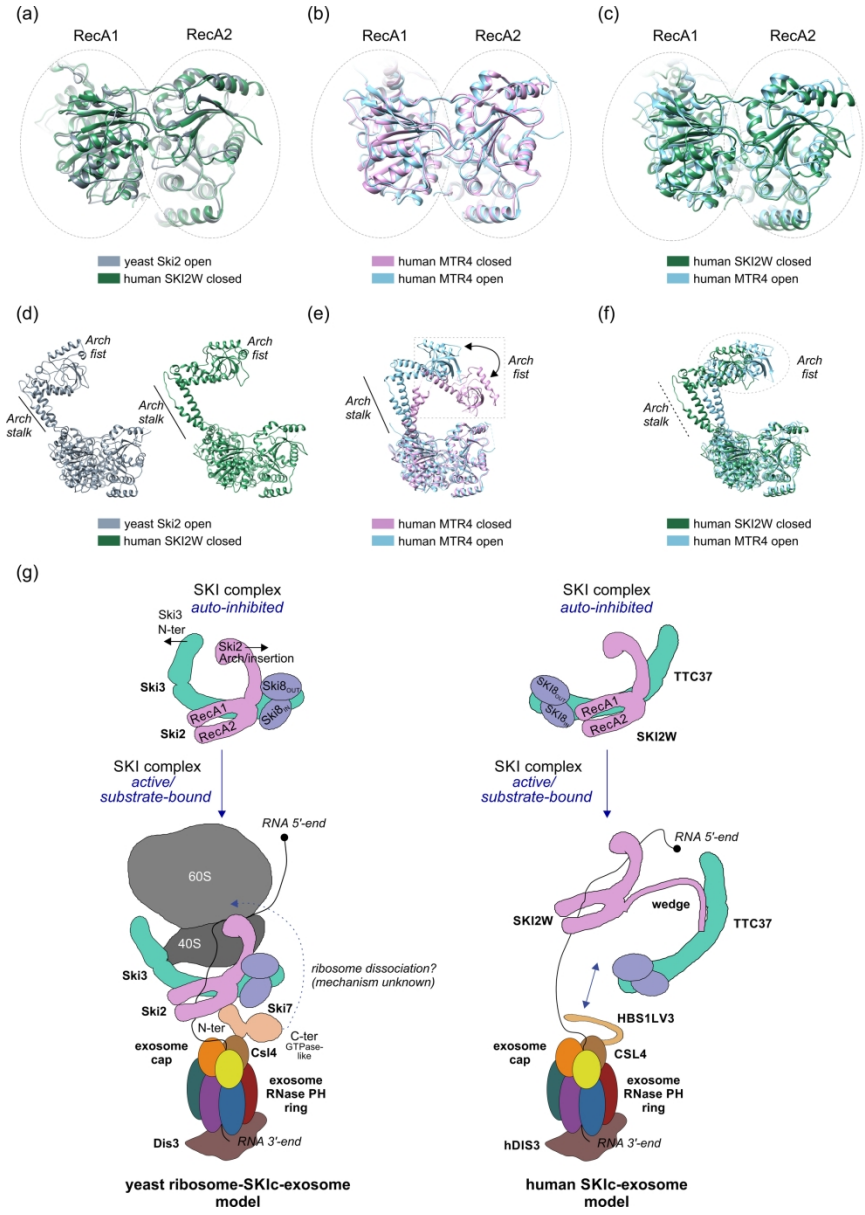

Regulation of SKIc activity is dependent on the flexibility of structural elements outside of the Ski2/SKI2W enzymatic core as well as interactions with RNA substrate and ribosome. (a-c) Superimpositions of RecA domain arrangement in Ski2 and SKI2W from yeast and humans (a), human MTR4 in the 'open' and 'closed' states (b), and human SKI2W and MTR4 in the 'open' conformation (c) demonstrate that they are rather immobile. (d) Side-by-side comparison of yeast Ski2 in the 'open' state and human SKI2W in the 'closed' state, showing that positioning of the Arch domain segments ('stalk' and 'fist') is similar. (e) Relocation of the Arch 'fist' (marked with an arrow) can be readily observed in superimposed MTR structures representing 'closed' and 'open' states. In the latter the Arch domain moves further away from the helicase enzymatic core. (f) Superimposed structures of the human SKI2W and MTR4 reveal that despite different states ('closed' and 'open', respectively) the spatial location of the Arch domains is comparable. (g) Schematic illustration of changes in domain arrangement between SKIc in the auto-inhibited and active/substrate-bound states in yeast (left) and human (right) complexes. In the auto-inhibited state of yeast SKIc Ski2 Arch/insertion domain and Ski3 N-terminal fragment are close to each other and form a lid, which limits RNA access to the catalytic core. These two structural elements have to move outward (black arrows) while

switching to the active/substrate-bound state. In yeast this occurs upon SKIc binding to the ribosome and the substrate and allows for RNA transfer to the exosome, linked to SKIc by the N-terminus of Ski7 protein. In the auto-inhibited state of human SKIc exit from the helicase channel is occluded, which blocks the RNA path towards exosome. This occlusion is removed by the movement of SKI2W 'wedge' segment, which induces partial dissociation of the helicase from TTC37:WDR61 scaffold.

197x275mm (300 x 300 DPI)

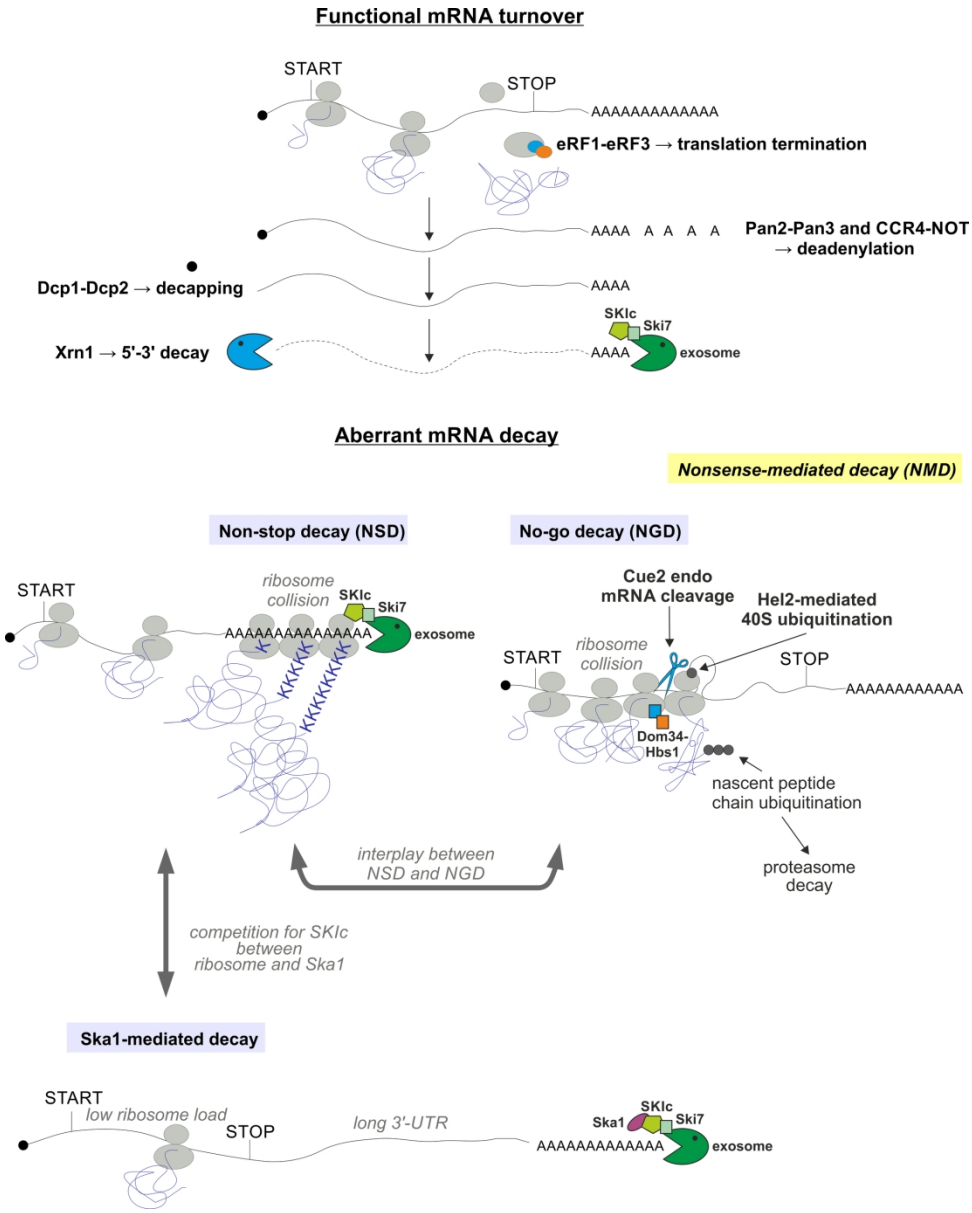

An overview of the canonical mRNA turnover pathway compared to NSD, NGD, and Ska1-mediated decay in S. cerevisiae. Functional mRNAs undergo several rounds of translation, which coincides with gradual 3'-end polyadenosine tail shortening, called deadenylation. This results in transcript decapping at the 5'-end by Dcp1-Dcp2, followed by degradation mediated by Xrn1 5'-3' exonuclease. Alternatively, mRNA can be degraded directly in the 3'-5' direction, by the exosome recruited to mRNAs by SKIc with Ski7. There are four cytoplasmic mRNA quality control pathways, which are functionally linked to the rate of transcript translation. Three of them rely considerably on the SKIc action, and are illustrated here. In turn, the involvement of SKIc-exosome in NMD (marked with yellow box) is less understood. NGD is triggered by ribosomes stalled within ORF; the main effector of this pathway is the Dom34-Hbs1 dimer, which structurally mimics the eRF1-eRF3 translation termination factor, and similarly interacts with the ribosomal A-site. Dom34-Hbs1 recruitment leads to endonucleolytic cleavage of the mRNA, coupled to proteolytic degradation of the defective nascent polypeptide in ribosome-associated quality control (RQC) pathway. NSD is triggered e.g. by the lack of a stop codon, when translation proceeds through the 3'-terminal poly(A)-tail. The third and relatively newly described pathway centers around the Ska1 protein, which also

interacts with SKIc. This pathway targets mRNAs with long 3'-UTRs, which have a low ribosome load. There is some redundancy between NSD, NGD, and Ska1-associated pathway, which ensures rapid removal of aberrant mRNAs from the cytoplasm. In particular, the line between NSD and NGD is not clear.

194x241mm (300 x 300 DPI)

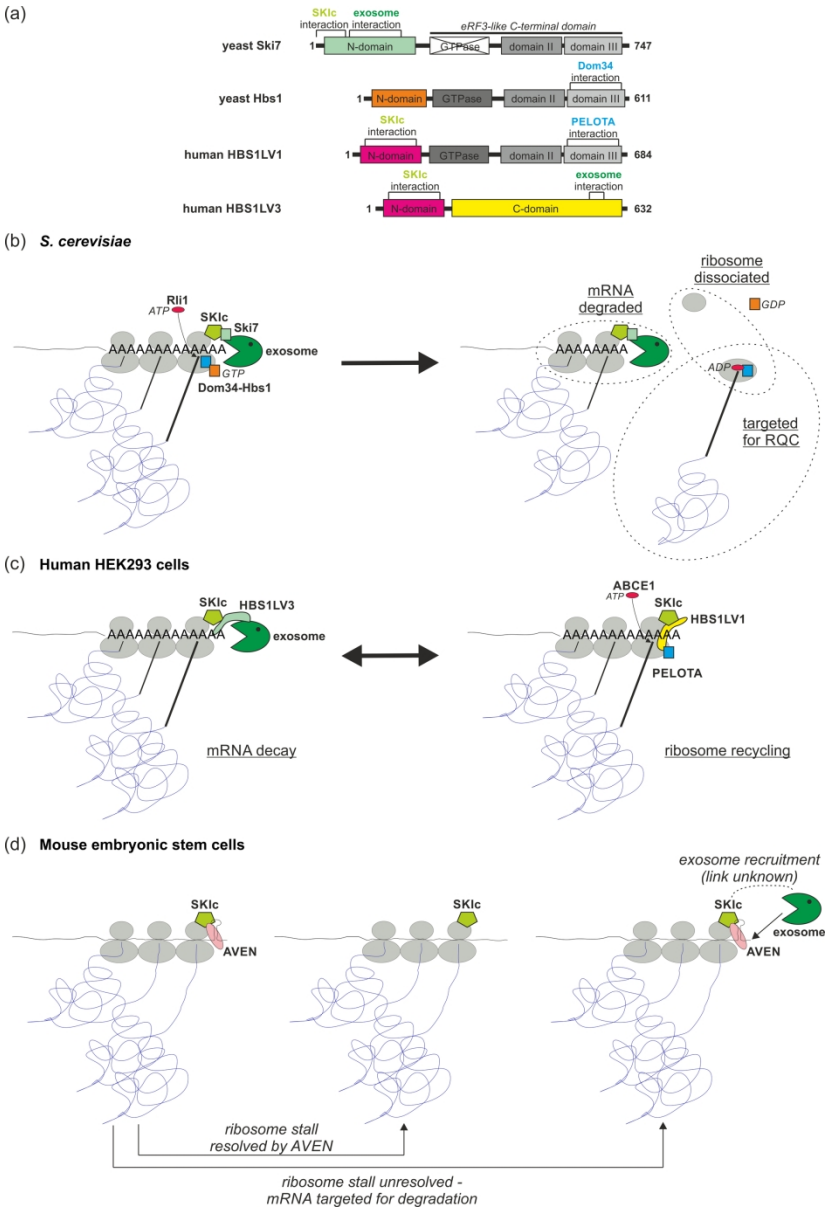

Different SKIc interactors in yeast and mammalian cells facilitate ribosome release and transcript degradation during translation-dependent mRNA surveillance. (a) Domain organization of yeast Ski7 and Hbs1 and two human HBS1L isoforms. Ski7, Hbs1, and HBS1LV1 contain conserved eRF3-like C-terminal region subdivided into segments (grey rectangles), including GTPase module, which is catalytically active only in Hbs1/HBS1LV1. The latter are able to interact with eRF1 homolog – Dom34/DOM34 (aka PELOTA in humans). Yeast Ski7 encompasses an N-terminal domain (pale green rectangle) different from Hbs1 (orange rectangle), with SKIc- and exosome-interacting motifs. HBS1LV1 and HBS1LV3 share an identical N-terminus (magenta rectangle), responsible for their competitive interactions with SKIc. Only the unique C-terminal region of HBS1LV3 (yellow rectangle) comprises motifs connecting it to the human exosome. (b) In S. cerevisiae, ribosome stalling at e.g. internal or terminal poly(A)-tracts during NGD or NSD leads to SKIc binding to the 40S subunit and exosome recruitment via Ski7. This triggers aberrant transcript degradation, although Ski7 may be also involved in ribosome release via unknown mechanism. The major ribosome rescue factor if Dom34-Hbs1, which co-operates with Rli1 ATPase. GTP and ATP hydrolysis by Hbs1 and Rli1, respectively, are required for ribosome dissociation into 40S subunit and 60S-peptidyl-tRNA complex,

subjected to RQC pathway. (c) In human cells, due to competition for SKIc between HBS1L variants, some equilibrium is probably established between SKIc functions in mRNA degradation, involving HBS1LV3 (left) and ribosome recycling (right), dependent on PELOTA-HBS1LV1 and ABCE1 (Rli1 homolog). (d) In mouse embryonic stem cells, SKIc does not interact with HBS1L isoforms, but rather with AVEN, which counteracts ribosome stalling. Otherwise, the exosome is recruited for mRNA degradation, but the physical link between SKIc and exosome in this cell-type remains elusive.

191x280mm (300 x 300 DPI)

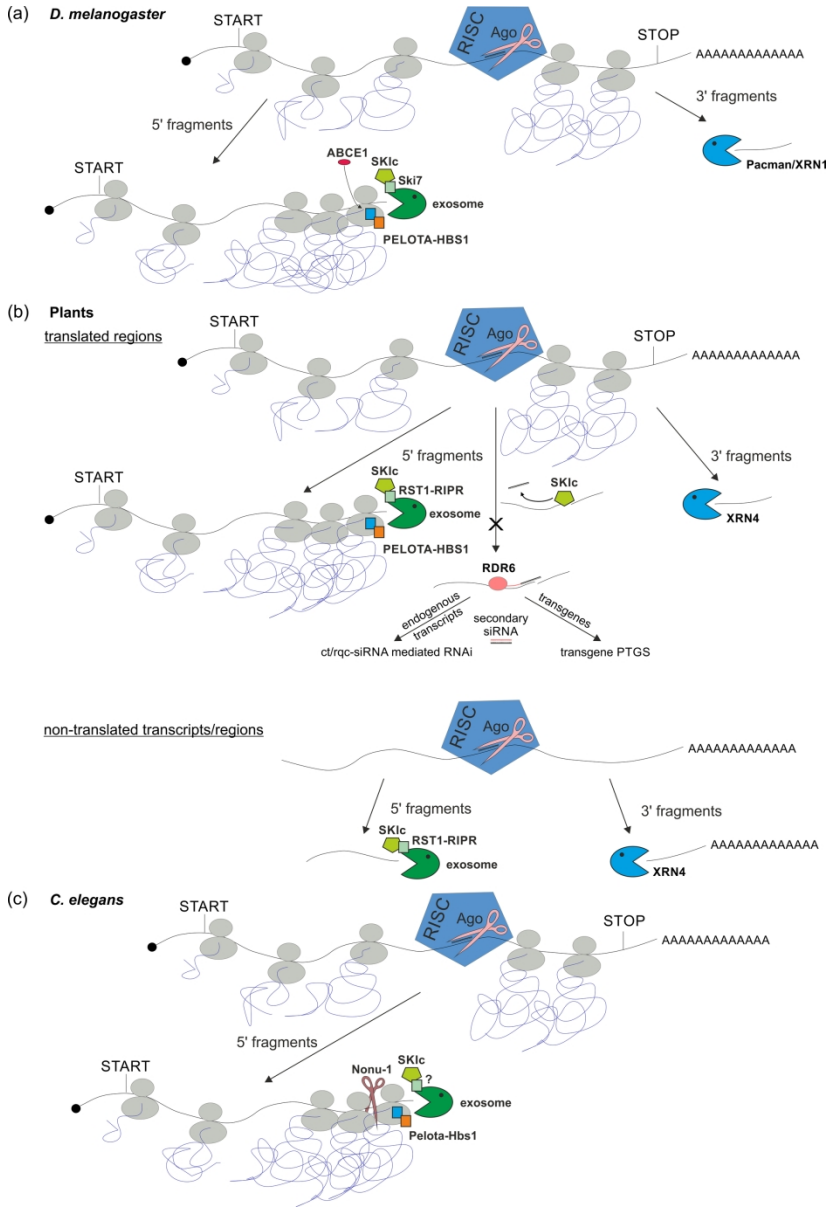

SKIc is engaged in RNAi across eukaryotic species. (a-c) RNAi-targeted transcripts undergo RISC-mediated endonucleolytic cleavage performed by Ago2 or its counterparts, depending on the species. Cleavage generates 5' fragments and 3' fragments upstream and downstream of the Ago action site, respectively. Both fragments become available to exoribonucleases. 3' fragments are degraded from 5' to 3' end by Xrn1 homologs – Pacman in fruit fly (a) and XRN4 in plants (b). 5' fragments are digested from 3' to 5' end by the exosome (a-c). Degradation of 5' fragments is translation-dependent, reminiscent of NSD. Ribosomes stalled on stop codon-less transcript fragments are released by PELOTA-HBS1 and ABCE1 rescue factors, with the involvement of SKIc. Ribosome dissociation is accompanied by transcript degradation by the exosome in assistance of SKIc, linked by Ski7 in fruit fly or via RST1-RIPR in plants (a,b); the identity of factor bridging SKIc with exosome in C. elegans is unknown (c). Additional SKIc role in plant RNAi, which concerns coding transcripts, is preventing RDR6 polymerase action. SKIc, taking advantage of its helicase activity, unwinds miRNA-mRNA duplexes and precludes using them for RDR6-catalyzed synthesis of secondary siRNAs: ct/rqc-siRNAs arising from endogenous mRNAs and transgene-derived siRNAs acting in PTGS (b, upper panel). Furthermore, Ago cleavage of non-translated transcripts or mRNA regions devoid of

ribosomes in plants generates 5' fragments with non-protected 3'-end, easily available for degradation mediated by exosome-RST1-RIPR-SKIc (b, lower panel). In C. elegans secondary cut between collided trailing and leading ribosomes is performed by NGD endonuclease, NONU-1 (c).

194x285mm (300 x 300 DPI)

SKIc involvement in S. pombe UPR. ER overload with proteins entails incorrect protein folding and activates UPR. One of the UPR pathways is RIDD, which leads to dedicated degradation of ER-associated mRNAs. Transmembrane endonuclease Ire1 cleaves RIDD targets, usually within UGC motifs. Most transcripts targeted by RIDD encode proteins with ER membrane-anchoring domains. mRNA incision by Ire1 results in ribosome stalling at newly generated 3'-end of transcripts, which are reminiscent of NGD substrates. No-go endonuclease Cue2 cleaves mRNAs upstream of the initial Ire1 cut, at the 5' side of leading stalled ribosome, and this process could be re-iterated. Eventually, SKIc and exosome linked by Ski7, as well as Dom34-Hbs1 cooperatively lead to mRNA degradation and release of stalled ribosomes, similar to NGD.

156x56mm (300 x 300 DPI)

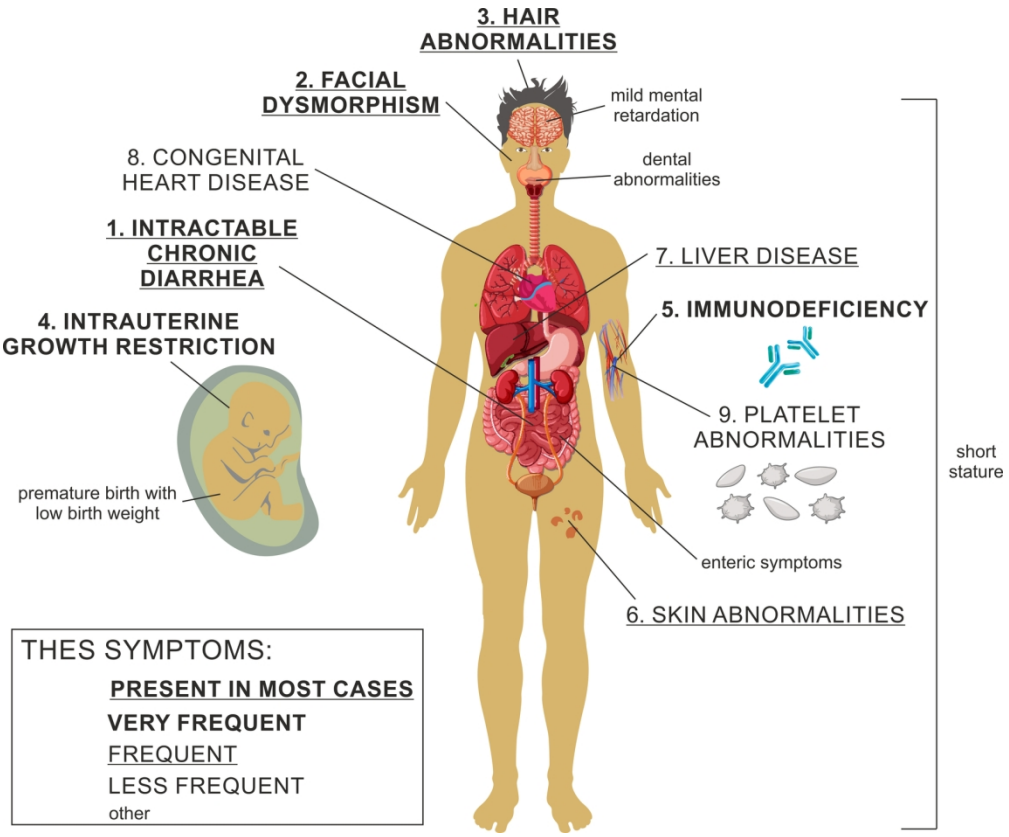

Broad spectrum of clinical symptoms, which affect multiple tissues and organs, is observed in THES patients. 9 major symptoms are numbered and highlighted with different fonts (see rectangular inset box for explanations) to illustrate the differences in the frequency, with which they are identified in different cases of the disease. Minor, less recurring symptoms are marked with lowercase. Assets freely available at freepik.com (human body and fetus images) were used for the preparation of this illustration.

156x129mm (300 x 300 DPI)

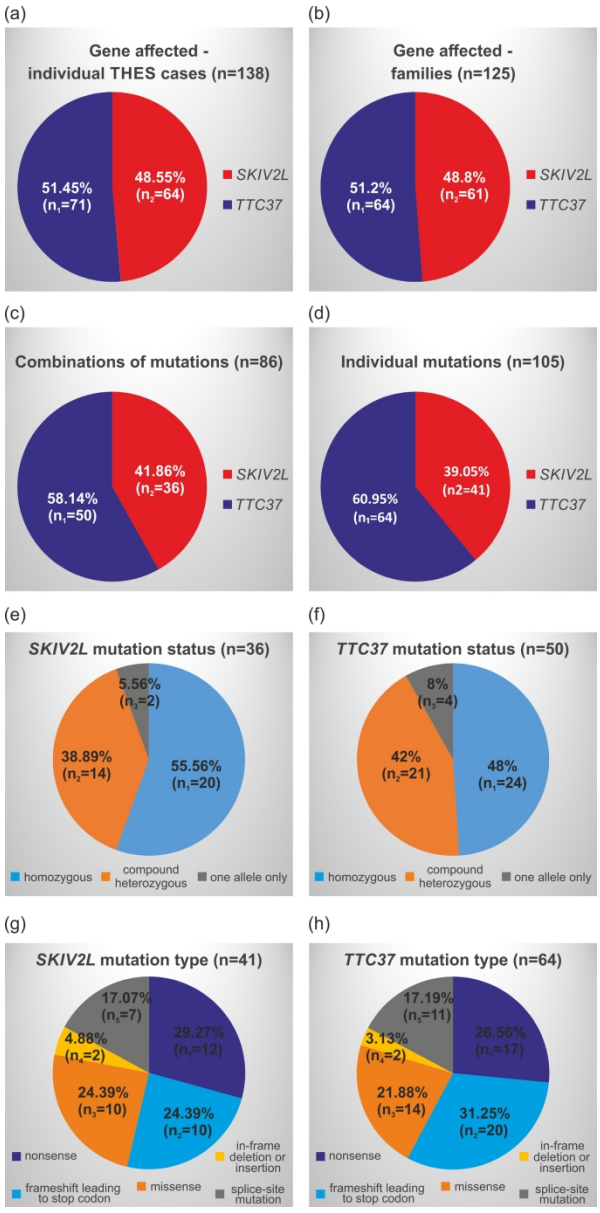

General THES-associated mutations statistics. (a-d) Percentage and number (in parentheses) of: (a) mutations in SKIV2L (red) and TTC37 (dark blue), identified in 138 individual THES cases; (b) mutations in SKIV2L and TTC37 in 125 families, where THES cases were identified; (c) different combinations of mutations in SKIV2L and TTC37 among 86 sets detected in total; (d) individual mutations in SKIV2L and TTC37 among 105 detected in total. (e-f) Percentage and number (in parentheses) of mutation sets identified as homozygous (blue), compound heterozygous (orange) or affecting one allele only (grey) in THES patients with impaired SKIV2L (e) or TTC37 (f) gene function. (g-h) Percentage and number (in parentheses) of mutation types (nonsense – dark blue; frameshift leading to the immediate appearance of the termination codon – blue; missense – orange; in-frame deletion/insertion – yellow; splice site mutation – grey) identified in THES patients with SKIV2L (g) or TTC37 (h) mutations.

138x280mm (300 x 300 DPI)

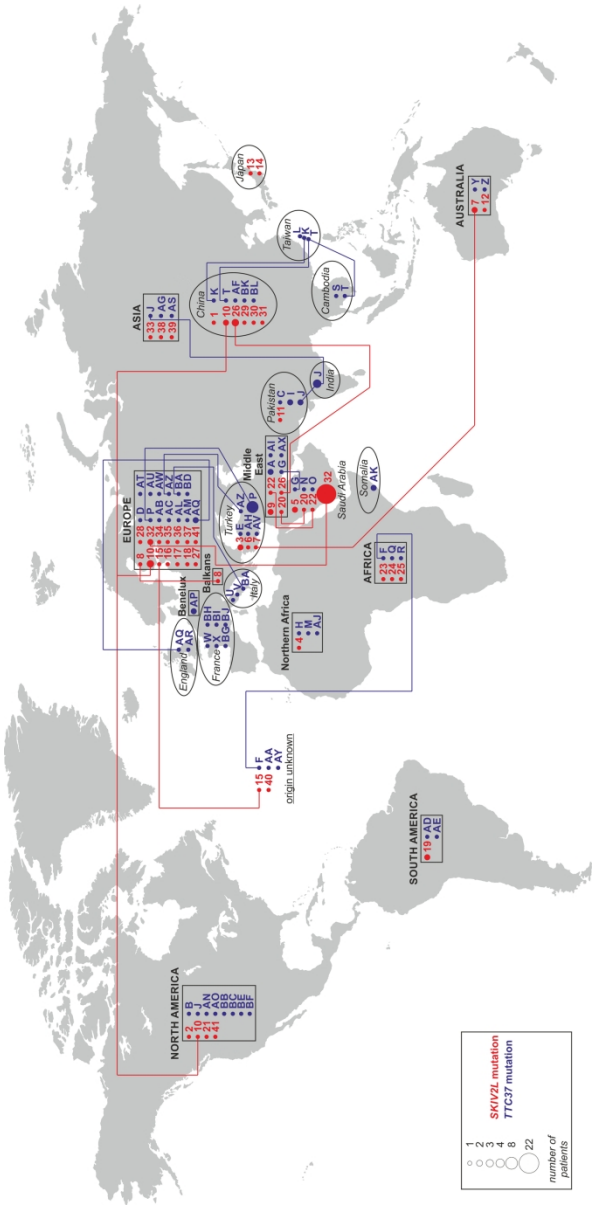

Global distribution of individual THES-associated mutations in SKIV2L (red) and TTC37 (dark blue). Unless precise information about the country (italicized), in which a given THES case was identified, was provided in the original publication (instances marked with ovals), mutations are categorized under the names of world regions (bolded capitalized case) or continents (bolded upper case) within rectangular boxes. Size of the filled circle next to the mutation name corresponds to the number of patients carrying the same mutation (see inset box in the bottom left corner). Red (SKIV2L) and dark blue (TTC37) lines connect identical mutations found in different world locations. Names of mutations (numerical symbols 1-41 for SKIV2L; letter symbols A-BL for TTC37) match the data presented in Tables 3 and 4. World contour freely available at freepik.com was used for the preparation of this illustration.

139x284mm (300 x 300 DPI)

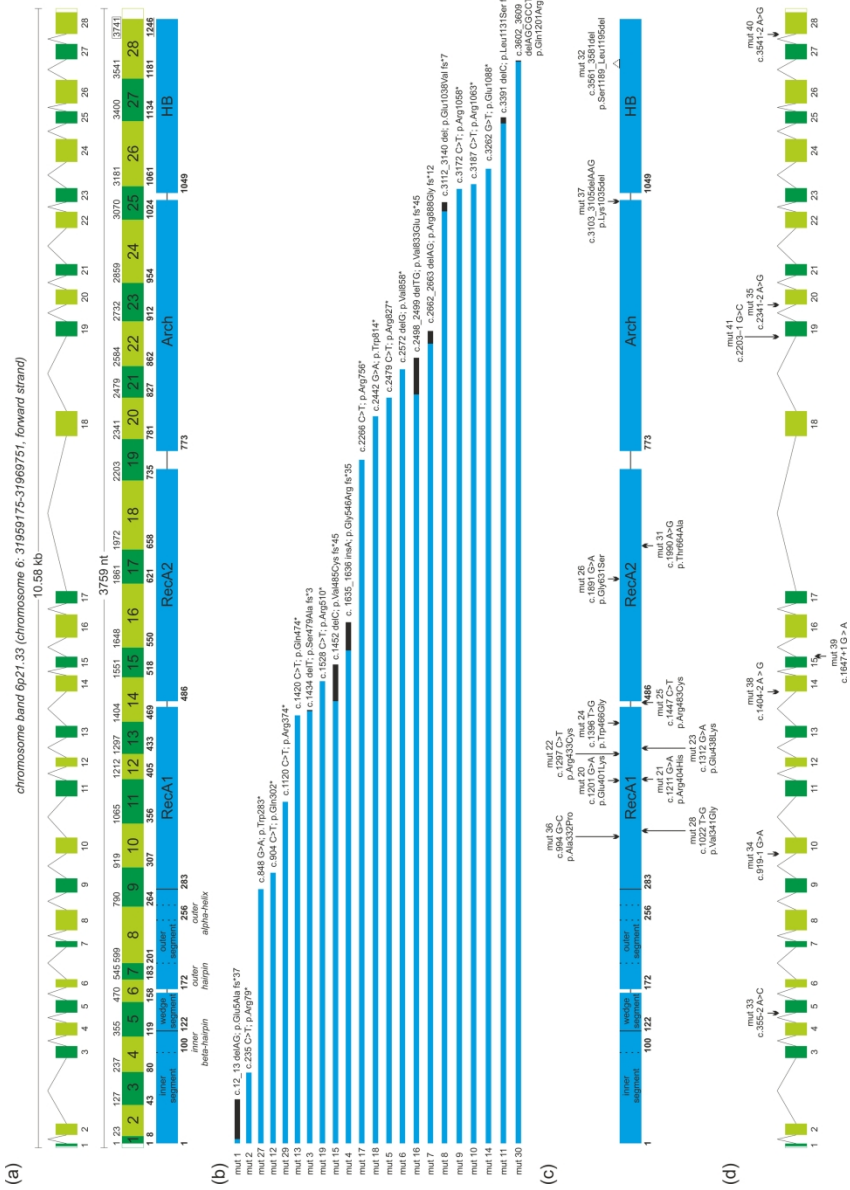

Distribution of THES-associated mutation in SKIV2L with regard to gene structure and protein domains. (a) Upper part: SKIV2L gene spans the region of 10.58 kb and comprises 28 exons (numbered 1-28 and marked as dark and light green rectangles) and 27 introns (represented by polylines); middle part: resulting transcript is 3759 nt-long and encodes SKI2W containing 1246 amino acids; larger numbers inside green rectangles indicate exons; small numbers above indicate positions of the exon-exon boundaries in mature SKIV2L transcript and are based on the numbering of the coding sequence; bolded numbers below indicate corresponding amino acid positions in SKI2W protein; bottom part (in blue): location of structural domains, crucial for SKI2W activity and interactions with other SKIc subunits; SKI2W N-terminal subdomains are further specified; numbers below indicate positions of the first amino acids in particular segments. (b) Schematic representation of truncated SKI2W variants, arising as a result of 22 mutations introducing PTC (13 nonsense and 9 frameshift), lined up from the most extreme at the top to the most benign at the bottom; blue segments correspond to natural SKI2W amino acid sequence; black segments represent divergent C-terminal extensions, generated due to out-of-frame insertions or deletions. (c) Location of 10 missense mutations and 2 in-frame deletions, with respect to protein domains. (d) Location of 7 splice site

mutations with respect to the gene structure (6 mutations affecting 3'ss are indicated above, and 1 mutation affecting 5'ss is shown below). Arbitrary names of SKIV2L mutations (numerical symbols 1-41) match the data presented in Table 3.

198x282mm (300 x 300 DPI)

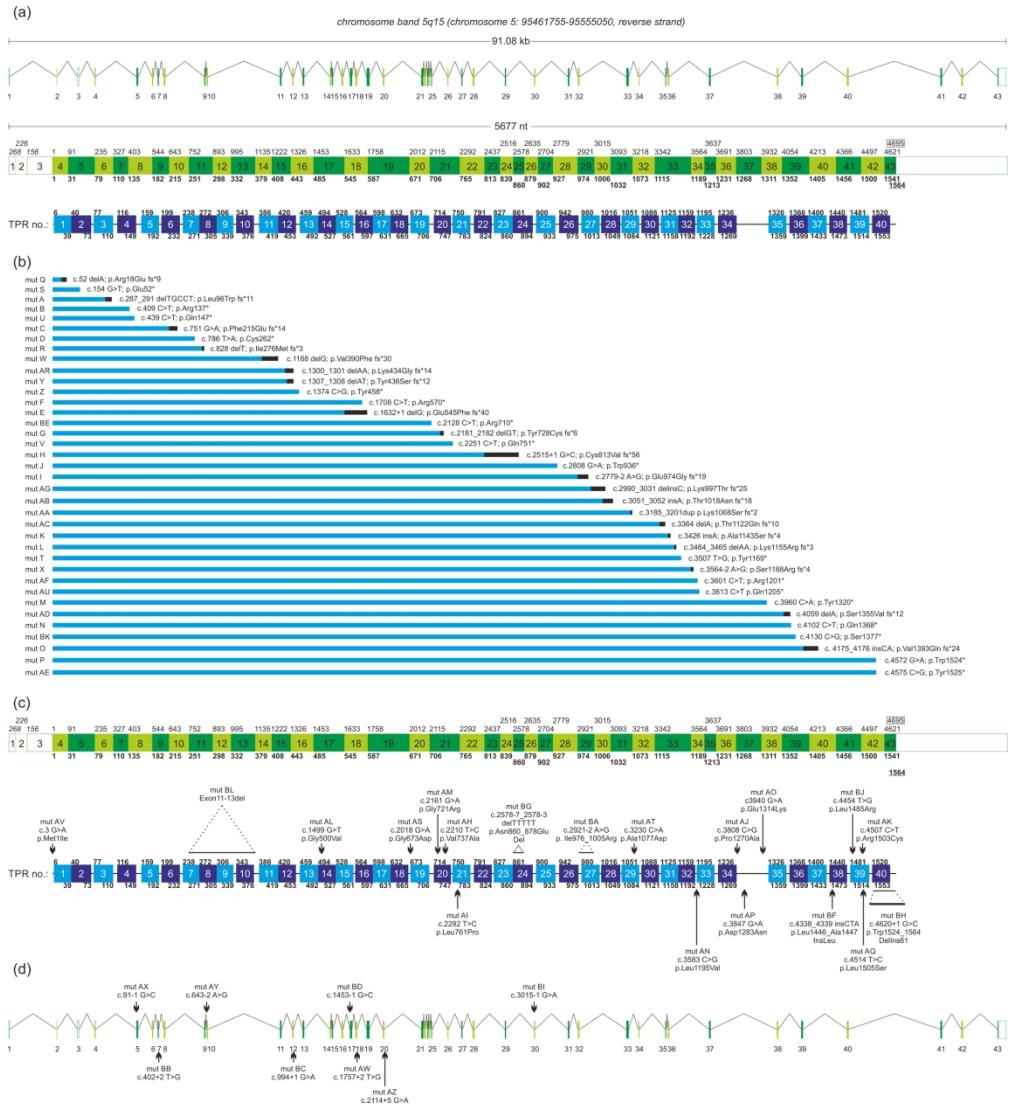

Distribution of THES-associated mutations in TTC37 with regard to gene structure and TTC37 TPRs. (a) Upper part: TTC37 gene spans the region of 91.08 kb and comprises 43 exons (numbered 1-43 and marked as dark and light green rectangles, except for exons 1-3, which are non-coding and thus marked as white rectangles) and 42 introns (represented by polylines); middle part: resulting transcript is 5677 nt-long and encodes TTC37 protein containing 1564 amino acids; larger numbers inside dark and light green rectangles indicate exons; small numbers above coding exons indicate positions of the exon-exon boundaries in mature TTC37 transcript and are based on the numbering of the coding sequence; italicized small numbers above non-coding exons 1-3 indicate the distance between their 5'-end and translation initiation codon present in exon 4; bolded numbers below indicate corresponding amino acid positions in TTC37 protein; bottom part: location of 40 TPR motifs (marked as light and dark blue rectangles), crucial for TTC37 scaffolding functions; numbers above and below each TPR indicate their boundaries. (b) Schematic representation of truncated TTC37 variants, arising as a result of 37 mutations introducing PTC (17 nonsense, 16 frameshift, and 4 splice site mutations), lined up from the most extreme at the top to the most benign at the bottom; blue segments correspond to natural TTC37 amino acid sequence; black segments represent divergent C-terminal extensions, generated due to out-of-frame insertions, deletions or splice site mutations. (c) Location of 14 missense mutations, and 5 other mutations: insertion, deletion, and 3 splice site mutations, which result in the in-frame changes at the protein level, with respect to TPRs. (d) Location of the remaining

8 splice site mutations with respect to the gene structure (4 mutations affecting 3'ss are indicated above and 4 other mutations, affecting 5'ss are shown below). Arbitrary names of TTC37 mutations (letter symbols A-BL) match the data presented in Table 4.

199x219mm (300 x 300 DPI)

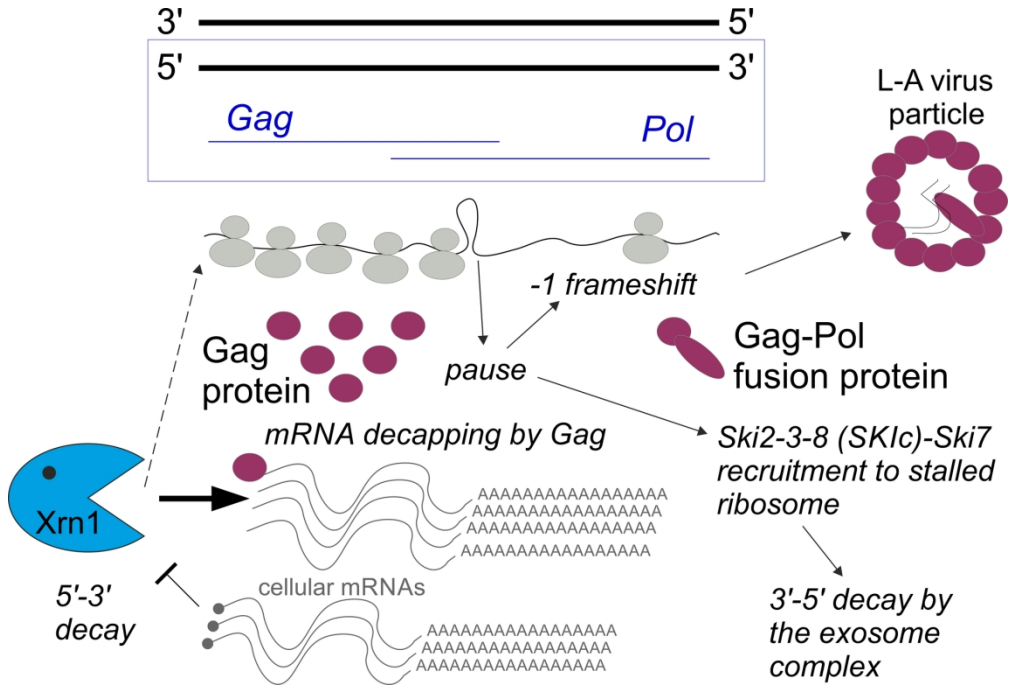

An overview of S. cerevisiae dsRNA L-A virus biogenesis, showing the role of cellular factors involved in RNA degradation in curbing virus propagation, and mechanisms used by the virus to counteract their activity. The double-stranded L-A RNA virus contains two ORFs under a single translation initiation signal. The first ORF serves as a template for the synthesis of the coat protein (Gag), the second encodes the RNA-dependent RNA polymerase (Pol). Production of Pol protein fused to Gag requires a -1 frameshift, which is facilitated by ribosome pausing at a strong secondary structure. Gag protein, aside from its structural role, triggers decapping of cellular mRNAs. This diverts Xrn1 5'-3' exonuclease activity from targeting viral transcripts, which are less effectively delivered to the major cytoplasmic decay pathway. However, the virus RNA levels are also controlled by the SKI and exosome complexes, which are effectors of mRNA quality control pathways triggered by ribosome stalling: NSD and NGD.

177x119mm (300 x 300 DPI)

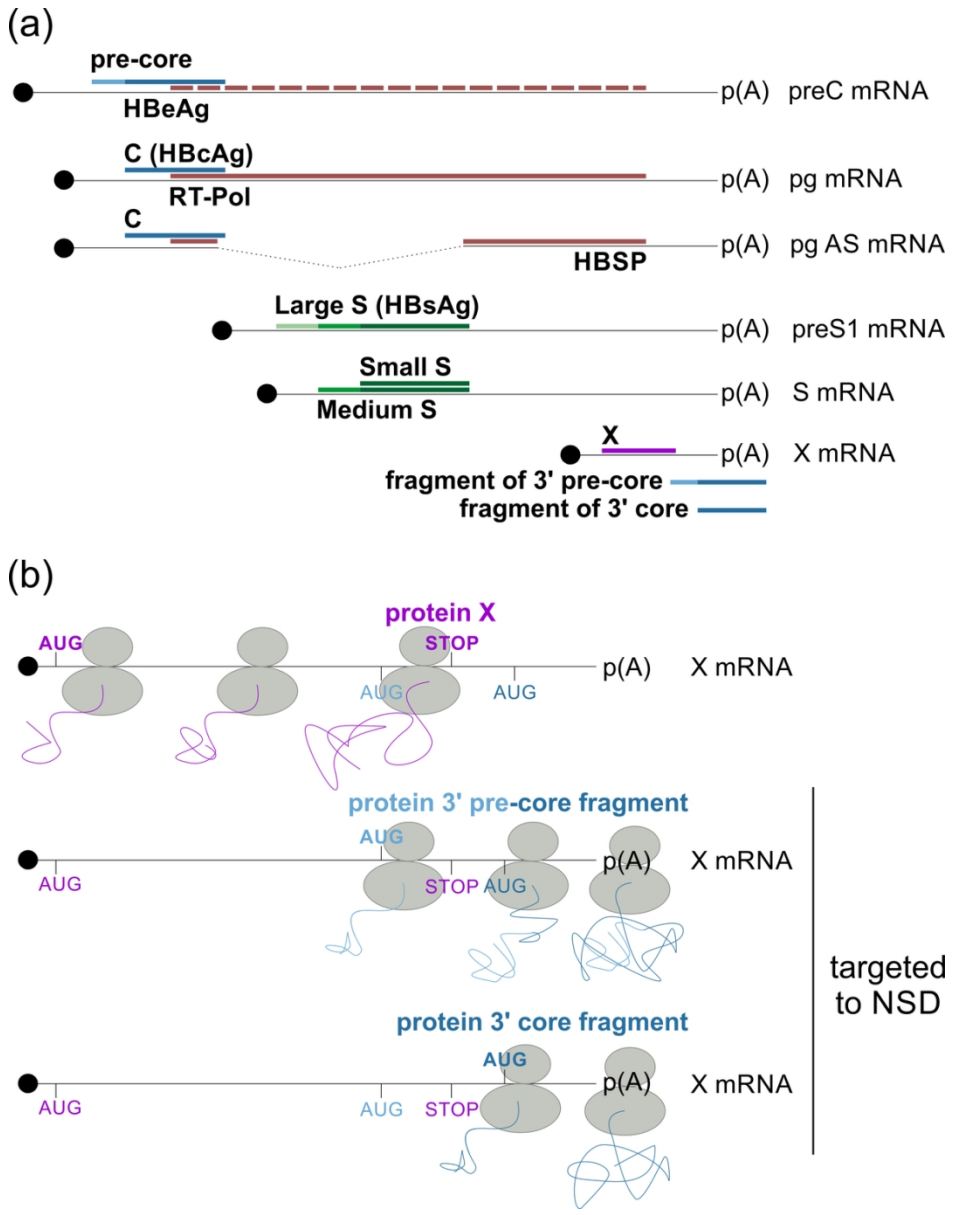

NSD helps to restrict HBV infection in human cells. (a) Six mRNAs, with the same polyadenylation signal and 3'-end, arise from HBV genome. preC mRNA encodes pre-core protein (light+dark blue), which undergoes proteolytic cleavages at N- and C-termini to generate envelope antigen HBeAg (dark blue); an overlapping ORF corresponds to RT-polymerase (burgundy, dashed line), which is not expressed from this transcript; pg mRNA gives rise to the core protein – HBcAg antigen (dark blue), and RT-polymerase (burgundy, solid line) from overlapping ORFs; pg AS (alternatively spliced) mRNA encodes core protein (dark blue) and HBSP (burgundy) in overlapping ORFs; preS1 and S (also named preS2) mRNAs encode three surface antigens (HBsAg), translated from overlapping ORFs: the former gives rise to large S (light+mid+dark green), and the latter – to medium (mid+dark green) and small (dark green) S proteins; X mRNA encodes transcriptional activator, protein X (purple), which is expressed only from this transcript due to its AUG situated in an ORF alternate to frame shared by all remaining HBV transcripts; likewise, exclusively X mRNA gives rise to fragmentary 3' pre-core and 3' core proteins (see panel b for further details). (b) Upper part: Protein X (purple) is synthesized in a standard manner, i.e. the first AUG (bolded purple) present at the X mRNA 5'-end and STOP codon (bolded purple) are used. Instead, one of two downstream out-of-frame AUGs

(light and dark blue) can be used for synthesis of fragmentary 3' (pre)-core proteins; middle part: when translation begins at the first of additional AUGs (bolded light blue), 3' pre-core protein fragment is synthesized; bottom part: alternatively, ribosomes start synthesis of the 3' core fragment (dark blue) from the downstream AUG (bolded dark blue). 3' pre-core and 3' core ORFs lack termination codon, which results in ribosome stalling during translation. In such case, X mRNAs are targeted to NSD. This in turn leads to decreased levels of HBV transcriptional activator and attenuation of protein X ability to promote replication of the virus in the cells.

103x132mm (300 x 300 DPI)

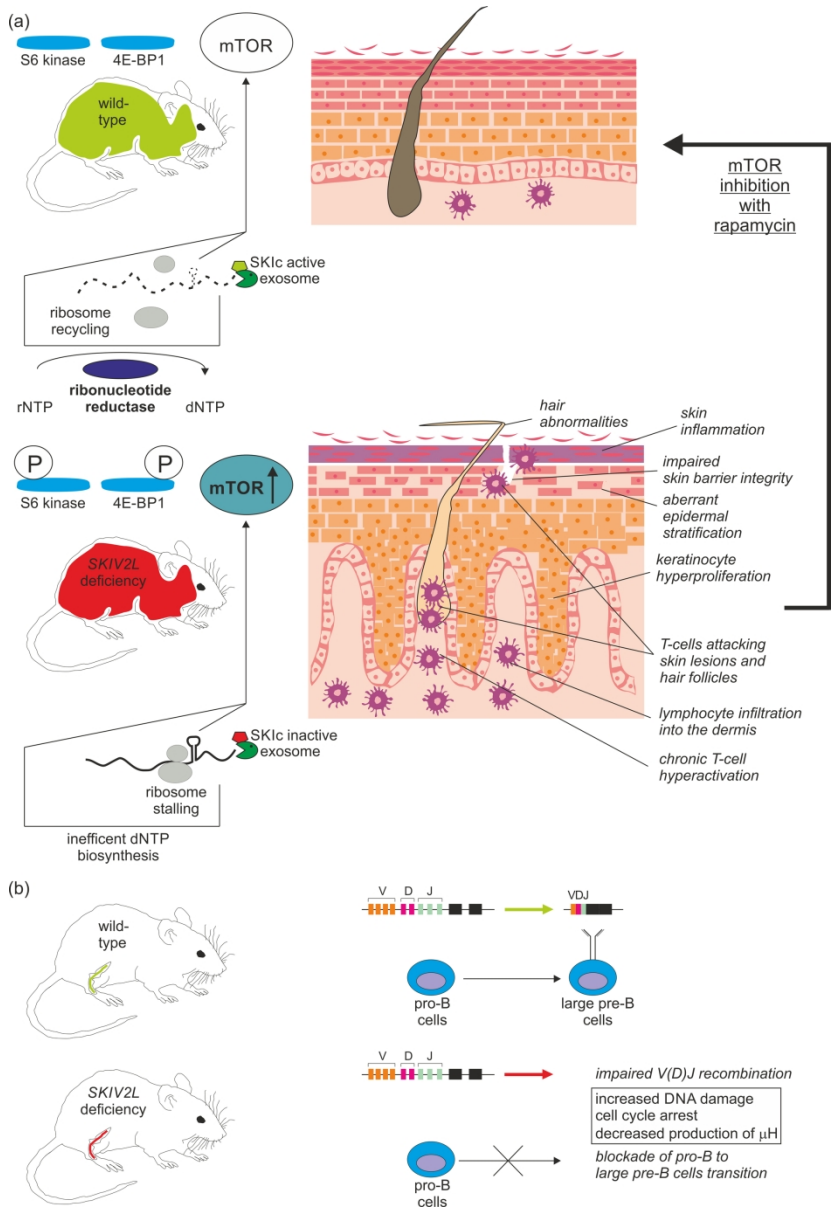

SKIV2L-deficient murine models reveal consequences of SKIc dysfunction at the organismal level. (a) Whole-body conditional SKIV2L knock-out resulted in skin inflammation and lesions due to aberrant stratification of the epidermis, hyperproliferation of keratinocytes, and loss of skin barrier function. In addition, T lymphocytes were chronically hyperactivated, infiltrated into the dermis, and attacked skin lesions and hair follicles, leading to hair abnormalities and progressive hair loss. These phenotypes likely stemmed from enhanced mTOR signaling, as documented by increased phosphorylation of S6 kinase and 4E-BP1. This might be due to e.g. reduced supply of dNTPs, produced by RNR from ribonucleotides, the pool of which is diminished upon SKIc inactivation resulting in inefficient RNA turnover. (b) SKIV2L knock-out specific to B cells precludes efficient transition from pro-B to large pre-B cell stage in the bone marrow, which is caused by impaired V(D)J recombination, leading to diminished synthesis of μ heavy chain (μH), and accompanied by elevated DNA damage response and cell cycle defects.

195x284mm (300 x 300 DPI)

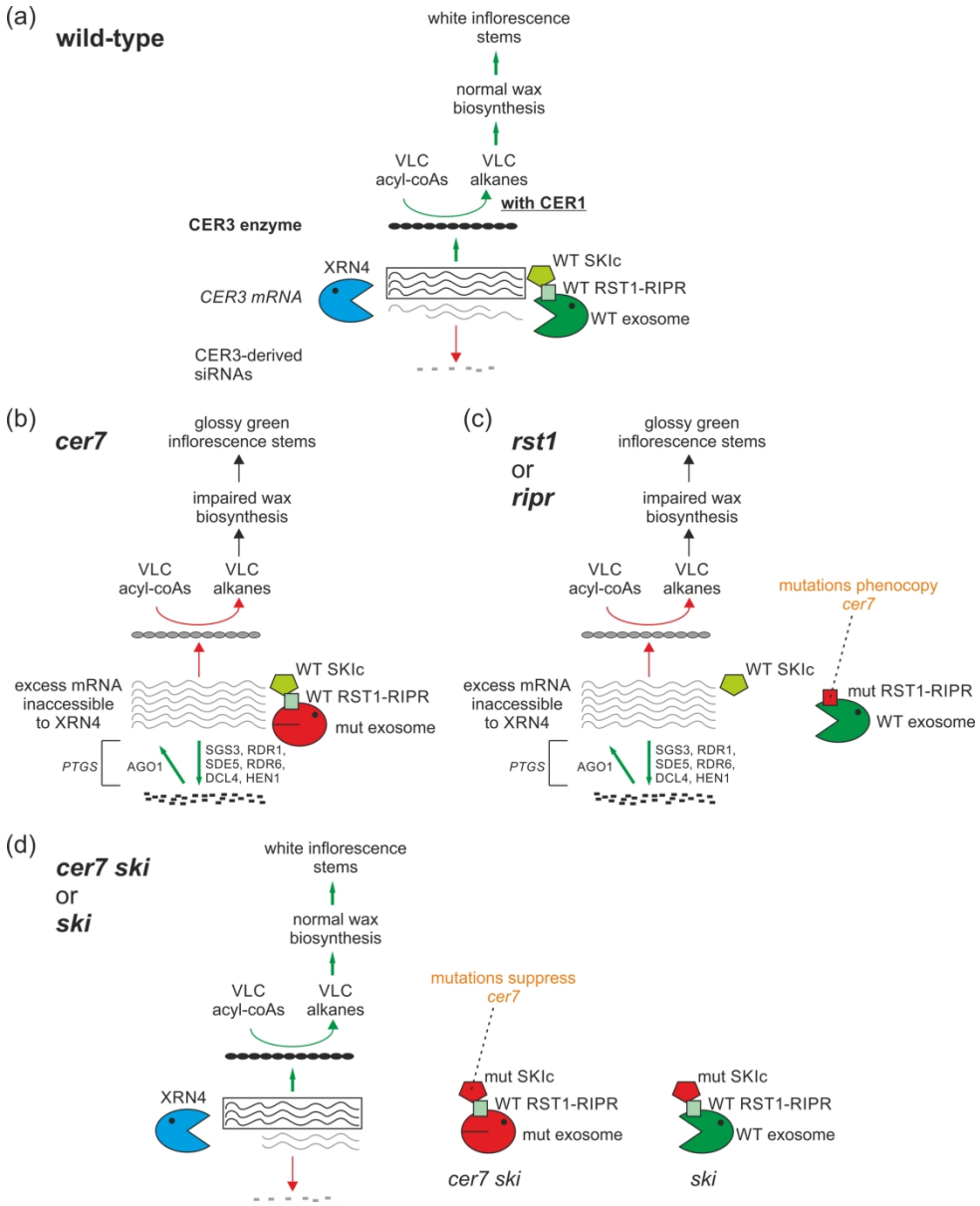

SKIc co-regulates wax biosynthesis in A. thaliana. (a) In wild-type plants the levels of CER3 mRNA are fine-tuned by both XRN4-mediated 5'-3' decay and 3'-5' degradation, carried out by the exosome in collaboration with SKIc and RST1-RIPR, which link both complexes. This prevents production of CER3-derived siRNAs and triggering PTGS of CER3 expression. The CER3 transcript levels ensure optimal production of CER3 enzyme, which – together with CER1 – controls synthesis of very long chain (VLC) alkanes from VLC acyl-coAs via decarbonylation. This allows for normal wax biosynthesis, resulting in white inflorescence stems. (b) In cer7 mutant, wild-type SKIc and RST1-RIPR thread CER3 mRNA excess to the inactive exosome, making it inaccessible to XRN4. As a consequence, CER3-derived siRNAs are generated by RNAi machinery, which triggers PTGS of CER3 expression. Decreased CER3 levels preclude efficient wax biosynthesis, leading to glossy green inflorescence stems. (c) In rst1 or ripr mutants, wild-type SKIc pulls CER3 mRNA away from XRN4, but is unable to deliver it to the exosome. Unbalanced CER3 transcript levels lead to elevated siRNA production, PTGS, and defect in wax biosynthesis, which phenocopies cer7 mutation. (d) In ski mutants, CER3 mRNA could not be targeted to the exosome-mediated 3'-5' decay due to SKIc dysfunction, but the excess of transcript pool is eliminated by undisturbed activity of XRN4. Therefore, ski mutations exert

suppressor effect in the background of cer7, restoring nearly normal wax biosynthesis.

163x201mm (300 x 300 DPI)